DIPARTIMENTO DI INGEGNERIA DELL'AMBIENTE, DEL TERRITORIO E DELLE INFRASTRUTTURE

CORSO DI LAUREA IN: RISCHI NATURALI E PROTEZIONE CIVILE

INVESTIGATING THE COUPLING BETWEEN STORMWATER AND FLOOD ROUTING MODELS
Quantifying the Role of Building Roofs in Urban Flood Dynamics

Studente:
Giulio Paradiso

Relatore:
PROF. DANIELE GANORA

Correlatore:
PROF. GIUSEPPE MASCARO

ANNO ACCADEMICO 2023-2024

ABSTRACT

Pluvial floods occur in small urban catchments when intense rainfall exceeds the stormwater drainage capacity. These events have been happening more frequently and with increasing impacts due to ongoing urbanization and the intensification of sub-daily precipitation extremes. Modeling these fast-evolving phenomena at high spatial resolutions (1-5 m) is crucial to understand their dynamics and mitigate the impacts. In this work, we focus on better quantifying the role of building rooftops in the rainfall-runoff transformation involved in pluvial flooding. We adopt a modeling framework based on the LISFLOOD-FP rain-on-grid hydrodynamic model forced with gridded net precipitation inputs, accounting for the roof effects. A significant challenge in incorporating roofs is accurately representing how the distinct effects of construction type, slope, surface material, and drainage systems affect rainfall losses, runoff delays, and, ultimately, water depths on the streets. We evaluate two methodologies inspired by recent research. The first involves categorizing buildings based on roof typology—such as flat or sloping roofs—and calculating the volume of water flowing from roofs to streets using variable runoff coefficients. In the second method, the distribution of downspouts is considered to account for the spatial variability and time delay in flood water discharged from the roofs. We test these methods in an urban catchment in New York City, where a wealth of high-resolution terrain, infrastructure, and building data is publicly available, along with distributed observations of street flooding. This work provides useful insights into the role of roof runoff in urban flooding, contributing to improved flood management strategies in highly urbanized areas like New York City facing similar challenges of increased pluvial flooding due to climate change.

CONTENTS

LIST OF TABLES

ACRONYMS AND ABBREVIATIONS

RC	Runoff coefficient
BIRR	Building induced rainfall redistribution

LIST OF FIGURES

INTRODUCTION

The continuous urban expansion that adds more impermeable surfaces and the growing increase of more frequent strong rainfall events due to climate change (Hammond et al., 2015) lead to even more diffuse pluvial flooding events, causing high economic and social losses.

Pluvial urban flooding events are characterized by the rapid flooding of streets and buildings because of the impossibility of the urban drainage system to manage all the stormwater runoff.

To understand the urban flooding dynamics and so to better prevent the effects of these types of events it is important to take into consideration the interference between stormwater runoff and urban infrastructure, like sewer, permeable areas and buildings.

In the last years the growing trend oh happening of these types of events induced a clear increase of research for the comprehension of the pluvial flooding phenomena dynamics and evolution.

Due to the complexity of the urban system, pluvial flooding modelling studies are even more diffuse and more accurate software is continuing developed.

What this thesis is focused on, is the modelling and analysis of the contribution of buildings, because they determine changes in the stormwater flow paths and in the runoff quantity of water that flows into the streets from the roofs.

To quantify this, the New York flood event that occurred on September 29, 2023, was studied and modelled, focusing on the effect on the Brooklyn borough, which was one of the most injured.

The two-dimensional hydrodynamic model LISFLOOD-FP was selected for this study due to its ability to manage high-resolution input data, such as the 1-meter resolution Digital Elevation Model (DEM) of the Brooklyn borough. High-resolution data like this are essential in modelling pluvial floods, as they enable the simulation of the complex flow paths of stormwater runoff.

To achieve the objective of this thesis two approaches were implemented to consider the building role in stormwater runoff dynamics, the “Runoff Coefficient Approach” (Farreny et

al., 2011a) and the “Building Induced Rainfall Redistribution Approach (BIRR)” (Xuejian et al., 2021).

For both the methods the data inputs implementation’s steps have requested the use of different processing and geoprocessing software like MATLAB, QGIS and AutoCAD to adapt the approaches cited before to the LISFLOOD-FP model.

The LISFLOOD-FP model inputs for both methods are a net precipitation file, a digital elevation model, a manning coefficients file and a boundary conditions file.

Finally, these inputs are combined by the software in a “Rain on grid” calculation method to obtain the results.

CHAPTER 1
PLUVIAL FLOOD MODELLING

According to the Sendai Framework for Disaster Risk Reduction 2015-2030 (Nations Office for Disaster Risk Reduction, n.d.) one of the possible strategies to reduce disaster risks is the creation of models to know better the consequences of a natural extreme event.

In this thesis, Pluvial flooding is the main risk that was considered because in the last twenty years extreme rainfall events that have damaged urban systems have become even more frequent. Figure 1 reports the graph that represents the trend of the Research and Review articles (Elsevier, ScienceDirect), published from 2001 to 2023, related to Pluvial and River Flood modelling.

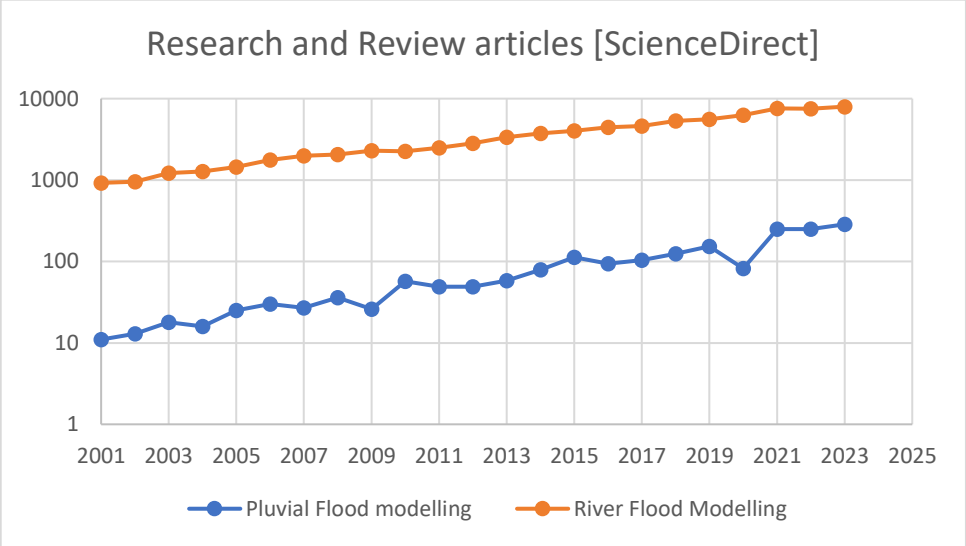

Figure 1: Analysis of Research and Review articles

Figure 1 demonstrates that there is a huge difference between the two topics but there is an increasing interest in Pluvial flooding.

To delve into this research field first this chapter provides an overview of different modelling approaches applicable to pluvial flooding events.

All the modelling types for pluvial flooding are numerical flood models, so a computer-based approach that uses mathematical and computational calculations to simulate water behaviour during a flood (Sañudo et al., 2022, Anees et al., 2016). Inside the numerical model can be distinguished three major groups depending on the spatial discretization of the rainfall-runoff module used. These are the Rapid flood spreading method (RFS) (Bulti et al., 2020), Semi-Distributed models (SD) and Fully- Distributed models (FD) (Pina et al., 2016).

1.1 **Rapid flood spreading (RFS)**

Rapid flood spreading is the simplest flood simulation method, and so the most used when necessary to understand the general flooding scenarios (Aksoy et al., 2016) and so a less specific risk assessment, because the only result of this method is the final state of the inundation. The RFS process is divided into two stages (Bulti et al., 2020):

- Pre-calculation phase: in this stage are defined the areas of accumulation of floodwater, known as impact zones (Figure 2), using a DEM (digital elevation model) and a grid cell to start the spreading of the floodwater

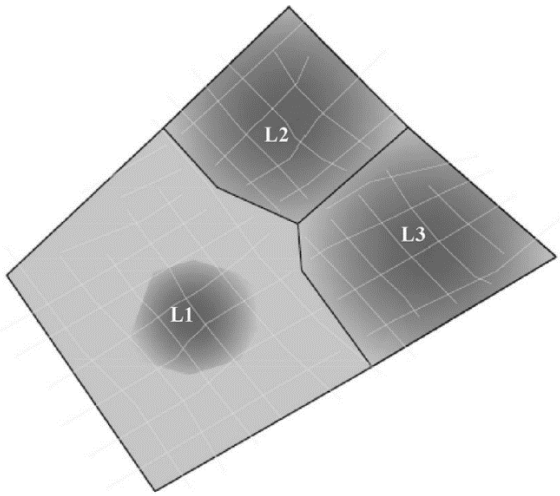

Figure 2: Impact zones delineated using a DEM (digital terrain model)

- Inundation phase: in this stage start the computation of the floodwater propagation. The calculation process is a loop procedure that starts by filling the lowest elevation cell adjacent to the input points and spilling the excess to the neighbouring cells.

1.2 **Semi-Distributed models (SD)**

SD models consider the studied area as divided into sub catchment units, where each one is defined by the percentage of land use cover (Figures 3-4). In these types of models, a known rainfall is applied to estimate runoff volumes. Then using empirical or physically based methods the runoff is converted into inflows hydrographs.

The main characteristics (Pina et al., 2016) are:

- The initial losses are typically defined as a constant value, function of the sub-catchment slope and surface types (*Urban Drainage, Third Edition*, 2010), that is initially subtracted from the rainfall
- The continuing infiltration losses are estimated and subtracted considering soil saturation to each sub-catchment before the model starts.
- SD models do not represent the real connection between impervious and pervious areas on the surface.

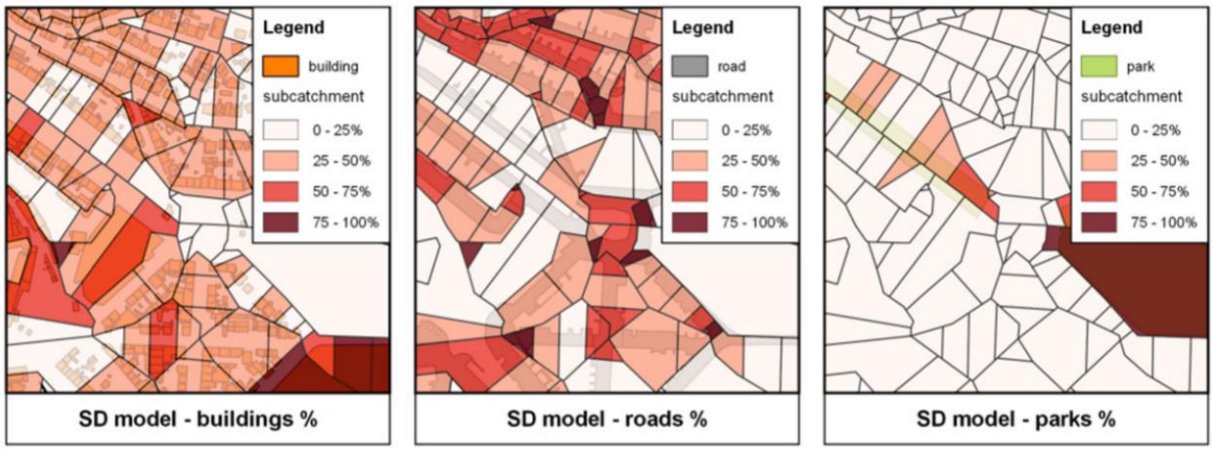

Figure 3: SD land use surface discretization (Pina et al., 2016)

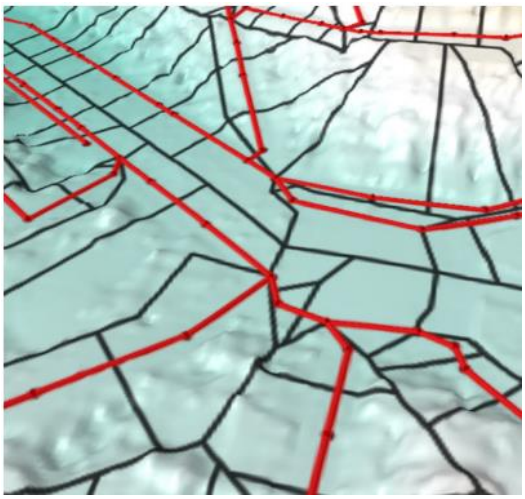

Figure 4: SD surface model (Pina et al., 2016)

1.2.1 *One-dimensional surface model (Overland flow modelling)*

The one-dimensional (1D) surface flow model represents major system flow in one dimension by discretizing the floodplain into linked nodes, with links as linear surface pathways and nodes as ponds and junctions, derived from DEMs (Bulti & Abebe, 2020; Leandro et al., 2009; Ochoa-Rodríguez et al., 2013).This method, requiring minimal input data (DEM and surface networks) and short run-time, effectively determines inundation characteristics when the flow is well-contained within the network (Ochoa-Rodríguez et al., 2013). However, it is time-consuming (Henonin et al., 2013) and its accuracy is affected by not considering minor drainage impacts and its inability to simulate multidirectional flow (tro et al., 2013).

1.2.2 *One-dimensional sewer model*

The one-dimensional (1D) sewer flow modelling approach simulates storm sewer flow and simplifies overflow situations by representing the system as links (conduits) and nodes (manholes or gullies) (Bulti & Abebe, 2020). Overflow is modelled as stagnant water in virtual storage above manholes (Figure 5), which returns when hydraulic conditions allow (Henonin et al., 2013). Saint-Venant equations are used: continuity (Eq. 1) and dynamic (Eq. 2). Its advantages include efficient stormwater drainage planning (Shaik & Agarwal, 2019; Walsh et al., 2014; Zhu et al., 2016) and suitability for rapid studies, real-time applications, emergency operations, and early warnings (Gharbi et al., 2016; Jiang et al., 2015).

$$\frac{\partial A}{\partial t} + \frac{\partial Q}{\partial x} = 0$$

(1)

$$\frac{\partial Q}{\partial t} + \frac{\partial (\frac{Q^2}{A})}{\partial x} + gA\frac{\partial y}{\partial x} - gA(S_0 - S_f) = 0$$

(2)

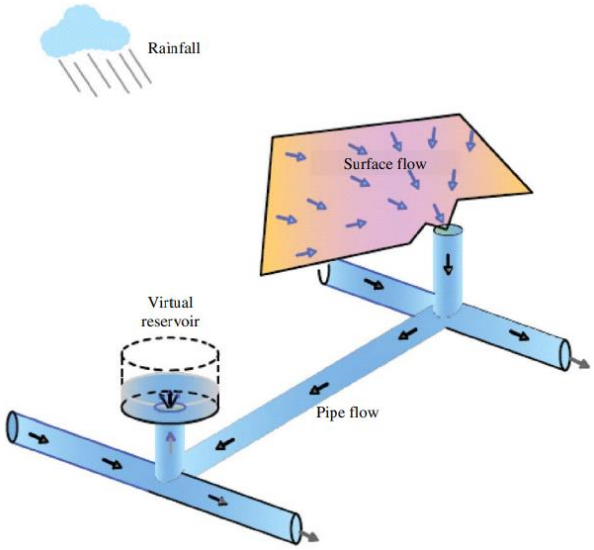

Figure 5: Scheme od One-dimensional sewer model

1.2.3 *Coupled sewer-surface 1D-1D model*

The 1D–1D (sewer-surface) coupling approach integrates a one-dimensional model for minor system flow with a one-dimensional surface flow representation, treating the floodplain as a custom network of open channels and ponds linked to the stormwater drainage system, thereby capturing the interaction between underground and surface flow (Mark et al., 2004), using surface networks, stormwater drainage networks, and DEM as main inputs. This method accurately determines overflow locations, flow depth, and velocity if surface flow paths are well-defined (Bisht et al., 2016; Henonin et al., 2013; Kourtis et al., 2017), but it fails to provide flood information when water exits the defined pathways.

1.2.4 *Coupled sewer-surface 1D-2D model*

This method is better suited for analysing complex systems and yields more accurate results than other approaches (Hankin et al., 2008), although it requires significant computational resources in terms of run-time and data needs (Kourtis et al., 2017; Leandro et al., 2009; Schlauß & Grottker, 2016). The flow interaction between the two systems occurs at gullies, manholes, and 2D grid cells (Jahanbazi & Egger, 2014), with the minor system modelled in one dimension and surface flow in two dimensions as represented in Figure 6.

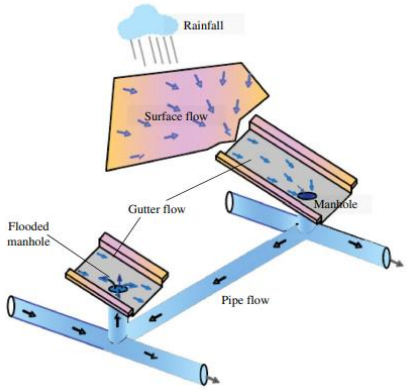

Figure 6: Scheme of coupled sewer-surface 1D-2D model

1.3 **Fully-Distributed models (FD)**

FD models consider the studied area with the real 2D elements, characterized by a specific land use type (Figures 7-8), in which using a grid cell the runoff is directly applied and routed.

The main characteristics (Pina et al., 2016) are:

- Rainfall is directly applied to the mesh grid and the infiltration is calculated for each cell depending on soil saturation and water depth
- FD models represent the real connection between impervious and pervious areas on the surface

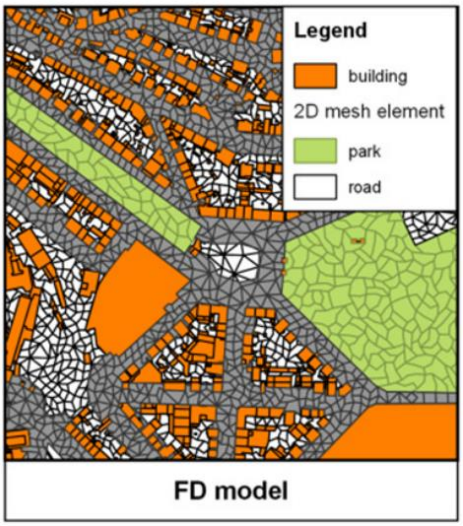

Figure 7: FD land use surface discretization (Pina et al., 2016)

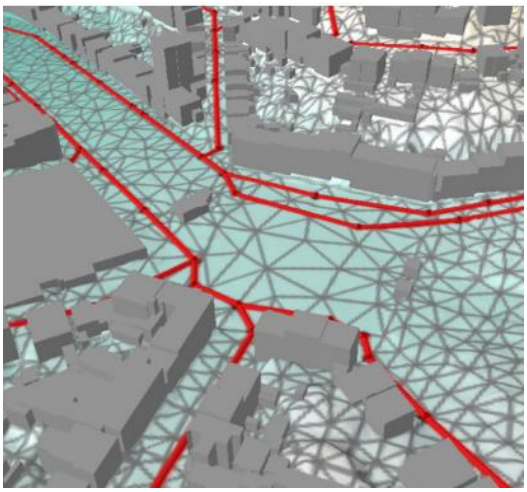

Figure 8: FD surface model (Pina et al., 2016)

1.3.1 *Two-dimensional surface models (Overland flow models)*

Two-dimensional (2D) modelling of surface flow simulates overland flow by considering both orthogonal components and dividing the catchment into structured or unstructured hydraulic grid cells (Kim et al., 2014), with each cell represented by coordinates (X, Y, Z) and assuming uniform catchment parameters and rainfall (Ochoa-Rodríguez et al., 2013). This approach effectively identifies maximum inundation extent and flow dynamics, such as depth and velocity (Liu & Pender, 2013), and is well-suited for urban areas due to its ability to model small topographic features (Hénonin et al., 2015; Nkwunonwo et al., 2020), but it requires fine grids (usually <5 m) and high-resolution topographic data (Mark et al., 2004), resulting in significant computational demands (Fewtrell et al., 2008; Liu and Pender, 2012)(Fewtrell et al., 2008; Gharbi et al., 2016; Shen et al., 2015) while also being limited in identifying

overflow locations and modelling in-channel flow, particularly in narrow waterways, and failing to account for minor drainage system influences, which can impact accuracy.

$$\frac{\partial h}{\partial t} + \frac{\partial (hu)}{\partial x} + \frac{\partial (hv)}{\partial y} = 0$$

(3)

$$\frac{\partial (hu)}{\partial t} + \frac{\partial (\mathrm{hu}^2 + 0.5\ \mathrm{gh}^2\ )}{\partial x} + \frac{\partial (huv)}{\partial y} = gh(S_{0x} - S_{fx})$$

(4)

$$\frac{\partial (hv)}{\partial t} + \frac{\partial (huv)}{\partial x} + \frac{\partial (\mathrm{hv}^2 + 0.5\ g\mathrm{h}^2)}{\partial y} = gh(S_{0y} - S_{fy})$$

(5)

CHAPTER 2
LISFLOOD-FP 8.1 MODEL

For this thesis many factors were considered to decide what was the best flood inundation model to use for Pluvial floods simulations.

In particular, the main checkpoints were:

- Open-source model
- Large spectrum of applications
- Complexity of the solving algorithm
- Precise outputs considering the importance in pluvial floods modelling to use complex and high-resolution DEM (Digital Elevation Model), to obtain relevant results, like acceptable water depth prevision or runoff directions.
- Fast processing times
- Possibility to use space and temporal dynamic rainfall

Considering these points LISFLOOD-FP hydraulic model was chosen. LISFLOOD-FP (Bates et al., 2013) is a two-dimensional raster-based hydrodynamic model designed for research purposes by the University of Bristol. The model includes several numerical schemes (solvers) that simulate the propagation of flood waves along channels and across floodplains using simplifications of the shallow water equations which can be written as (Sharifian et al., 2023):

$$\frac{\partial \mathrm{h}}{\partial t} + \frac{\partial q_x}{\partial x} + \frac{\partial q_y}{\partial y} = r \qquad \textit{(6)}$$

$$\frac{\partial \mathrm{q_x}}{\partial \mathrm{t}} + \frac{\partial \left(\frac{\mathrm{gh}^2}{2}\right)}{\partial \mathrm{x}} + \frac{\partial (\mathrm{q_x^2/h})}{\partial \mathrm{x}} + \frac{\partial \left(\frac{\mathrm{q_x q_y}}{\mathrm{h}}\right)}{\partial \mathrm{y}} + \mathrm{gh}\frac{\partial \mathrm{z}}{\partial \mathrm{x}} + \frac{\mathrm{gn_M^2 |q_x| q_x}}{\mathrm{h}^{\frac{7}{3}}} = 0 \qquad \textit{(7)}$$

$$\frac{\partial q_y}{\partial t} + \frac{\partial\left(\frac{gh^2}{2}\right)}{\partial x} + \frac{\partial(q_x^2/h)}{\partial y} + \frac{\partial\left(\frac{q_x q_y}{h}\right)}{\partial x} + gh\frac{\partial z}{\partial y} + \frac{gn_M^2|q_y|q_y}{h^{\frac{7}{3}}} = 0$$

(8)

where Eq. (6) is the mass conservation equation, and Eqs. (7) – (8) are the momentum conservation equations. In these equations, h [L] represents the water depth, and q_x = hu and q_y= hv [L^2T^{-1}] are the discharge per unit width in the x and y orthogonal directions, respectively, expressed involving the velocity components u and v [LT^{-1}]; r [LT^{-1}] is the prescribed rainfall rate, g [$L\ T^{-12}$] is the gravitational acceleration, z [L] is the two-dimensional topographic elevation and n_M is Manning's coefficient [$L^{1/6}$].

2.1 **Floodplain flow solvers**

The available LISFLOOD-FP model solvers for calculating floodplain flow are (Bates et al., 2013) :

- **Routing solver**: this is the simplest method for transferring water from one cell to another. It is applied only to cells containing very shallow water (less than 1 mm by default or user-defined) or where water slopes are very steep (greater than 1 in 10 or user-defined). It replaces the shallow water equations in cells with water depths below or slopes above a user-defined threshold. Water flows at a fixed velocity from the specified cell into the neighboring cell with the lowest elevation, following a pre-calculated flow direction map. The solver settings help reduce model runtime and enable water to flow over terrain discontinuities (such as off building roofs) without destabilizing the solution.
- **Flow limited model solver**: it is the least complex solver based on the shallow water equations. It uses an approximation of the diffusion wave equations, relying on Manning's equation. The flow between cells during a user-defined fixed time step is calculated as a function of the free surface and bed gradients (water slope) and the friction slope. Both local and convective acceleration terms are considered negligible. This method is rarely used due to its low accuracy.
- **Adaptive model solver**: it is a one-dimensional approximation of a diffusion wave based on a uniform flow formula, decoupled in the x and y directions to enable the simulation of 2D flows. Unlike the flow-limited solver, it employs a time step that varies in duration throughout the simulation. This method is rarely used for high-resolution simulations.

- **ACC solver (local inertial acceleration solver)**: this method is a simplified version of the shallow water equations, where only the convective acceleration term is disregarded. The flow between cells is determined by the friction and water slopes, along with local water acceleration.

  Like the adaptive solver, the time step changes throughout the simulation, but in this case, it adjusts according to the Courant-Friedrichs-Lewy condition (The_Courant_Friedrichs_Lewy_CFL_Conditio, 2012.) and depends on the cell size and water depth. This approach can greatly reduce computation time compared to the adaptive solver and is typically used for fluvial or pluvial flooding problems at catchment-scale resolutions.
- **Roe solver**: this solver is the most advanced, as it incorporates all terms from the complete shallow water equations. It has been evaluated on a limited range of scenarios and may not be as dependable as other, more frequently used solvers.
- **DG2 solver (Second-order discontinuous Galerkin solver):** this solver implements the DG2 formulation of Kesserwani et al., (2018) that adopts a simplified "slope-decoupled" stencil compatible with raster-based Godunov-type finite-volume solvers. It models topography, water depth, and discharge using average coefficients for each element, along with separate x-slope and y-slope coefficients. This approach ensures accurate results even with complex, piecewise-planar topography and conditions of wetting and drying. Additionally, before each time step, a piecewise-planar method is applied to handle friction, following the split implicit friction scheme from Liang & Marche, (2009); Shaw et al.,(2021).

  This solver is applicable to fluvial flooding, dam-breaks, tsunamis and flows around hydraulic structures problems.
- **FV1 solver (First-order finite volume solver):** this solver is obtained by simplifying the DG2 formulation to remove the slope coefficients and the spatial operators, yielding piecewise-constant representations of topography and flow variables.

  It uses a standard first order forward Euler time-stepping scheme and the well-balanced wetting and drying treatment necessitates a maximum stable Courant number of 0.5 (Kesserwani & Liang, 2012; Shaw et al., 2021).

  This solver is applicable to fluvial and pluvial flooding and dam-breaks.

2.2 **Floodplain flow solvers implemented with GPU**

Some floodplain solvers have been implemented with GPU to increase solver's performance.

The above-mentioned solvers are:

- **ACC:** this solver is implemented considering uniform grid and non-uniform grid. The last update was implemented in LISFLOOD-FP 8.1 version, released on the 23 of September of 2022. It includes a new GPU-accelerated solver, known as the non-uniform ACC solver.
- **Adaptive FV1/DG2:** LISFLOOD-FP 8.1 version include a GPU-parallelised adaptive FV1/DG2 solvers that run on an adaptive grid generated by the MRA of the Haar wavelets (HW)/ Multiwavelets (MW), respectively, whereby adaptive grid refers to a dynamic-in-time non-uniform grid that is generated every timestep.

2.3 **Model assumptions**

The last update of the manual of LISFLOOD-FP (Bates et al., 2013) define the sequent model assumptions:

- The code is designed for situations where there is enough information to clearly define the model's boundary conditions, especially the mass flux over time at all inflow points.
- The model uses standard SI units, like meters for measuring length, seconds for time, and cubic meters per second (m^3/s) for flow rates, among others.
- The solvers assume that the flow changes gradually, but with some some exceptions:
    - The routing solver works well for very shallow flows over steep slopes or when the terrain has abrupt changes.
    - The FV1 and DG2 solvers are flexible enough to handle all kinds of flow, including those in steep or uneven terrains, as well as rapidly changing flows.

2.4 **Key limitations of floodplain flow solver**

Floodplain flow solvers before described have the sequent limitations, as defined in the user manual (Bates et al., 2013):

- For out-of-bank flow we assume that flow can be treated using a series of storage cells discretised as a raster grid with flow in Cartesian coordinate directions only.
- There is no exchange of momentum between 1D channel solvers and floodplain flows, only mass.
- During floodplain flow lateral friction is assumed negligible and is neglected.
- The flow limited solver underestimates wave propagation speeds and can be a poor representation of flow dynamics and is left as an option for comparative experimentation only.
- Due to high computation cost the adaptive solver is rarely suitable for high resolution simulations.
- Wave propagation speed can be underestimated during flows in extremely low Manning's friction conditions and/or relatively high Froude number by all solvers except FV1, DG2, and Roe.
- Using the acceleration solver, low Manning's friction conditions can cause instabilities, and a numerical diffusion term must be included.
- The routing solver assumes that flow between cells occurs at a constant speed and that flow direction is controlled purely by DEM elevation. However, it also assumes that water will not flow between cells when the water elevation in the recipient cell is greater than the DEM elevation in the source cell.
- The routing solver assumes no knowledge of roof level drainage structures
- ACC solver is not recommended for supercritical flows, e.g., thin flows in pluvial flooding simulations at fine resolution
- FV1 solver might fail in capturing small-scale transients of flows
- DG2 solver is not recommended for high computational cost for large-scale applications and restrictive time-step for applications that involve thin flows

2.5 **Pros of LISFLOOD-FP pluvial floods modelling**

According to what discussed in the precedent paragraphs, here are reported what are the main points that makes LISFLOOD-FP the best choice for this case study.

- Open source
- Possibility of implement dynamic rainfall file that could represent rainfall changing in space and time, using NetCDF file extension (Network Common Data Form)

- Better performance in terms of inundation extent
- Faster and with no instabilities reported in different studies, thanks to the latest versions in which solvers were implemented with GPU
- Ability of the finer resolution models to capture more terrain details and route the flow in the right direction considering depressions and relief
- Complexity of the modelling schemes that permits a more efficient representation of the overall flood extent and water depth, also at the watermarks

CHAPTER 3
CASE STUDY
SEPTEMBER 2023 NEW YORK PLUVIAL FLOODS

In this chapter will be reported all the characteristics of the study area and the event that is analysed in this thesis.

Part of the assumptions about the area of study come from a precedent study of the event conducted by the Professor Giuseppe Mascaro and his work group for the seminar "New York City as a Lab to Advance Urban Flood Knowledge and Risk Mitigation". Giuseppe Mascaro is an Associate Professor in the School of Sustainable Engineering and the Built Environment (SSEBE) at Arizona State University and member of the Center for Hydrologic Innovations of the Arizona State University.

3.1 **General description of the September 2023 Storm**

On September 29, 2023, heavy rainfall led to flooding across portions of the New York City metropolitan area and surrounding areas in the United States (Figure 9).

The flooding inundated numerous highways and roads, and affecting all New York City subway service, suspending and delaying routes and services, and causing damages of about $100 million.

Figure 9: September 29, 2023 in the Brooklyn borough of New York City

The flood was caused by a low-pressure area that had absorbed the remnants of Tropical Storm Ophelia, which then stalled over the New York City area. Multiple rounds of heavy rainfall also moved through the region because of favourable precipitable water values, convective instability, and low-level winds. This induced high rainfall totals across northwestern New Jersey, southeastern New York, and southwestern Connecticut.

In figure 10 are reported all the complaints about flooding made in the day of the event.

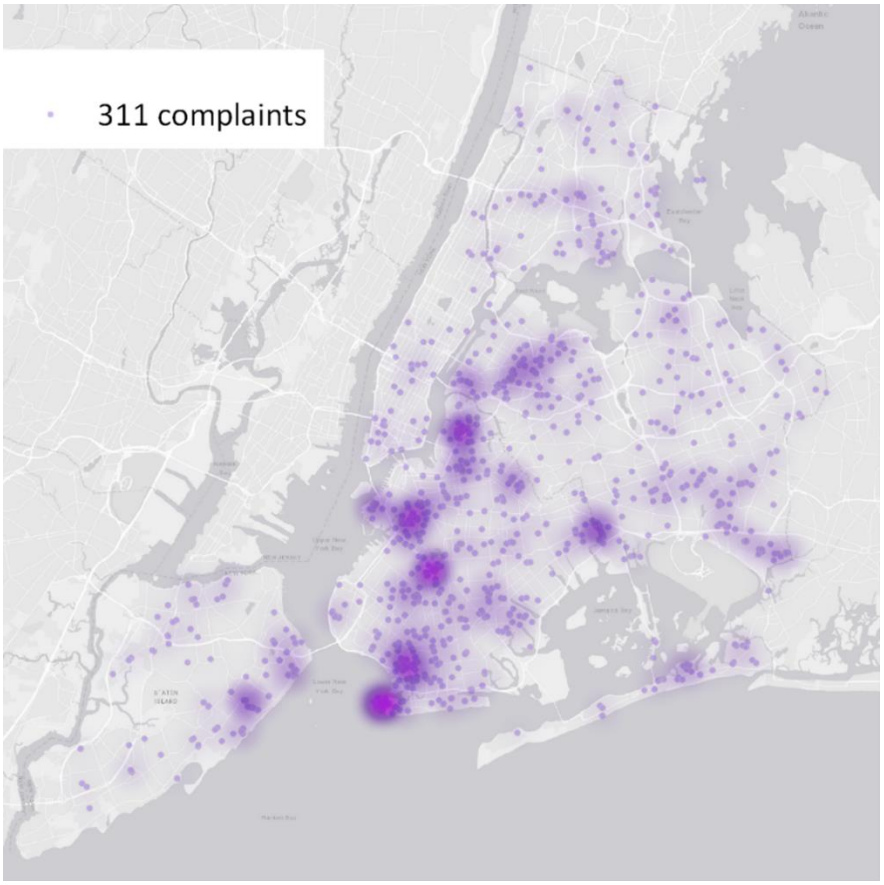

Figure 10: Map of 311 Complaints on September 29, Office of the NYC Controller

3.2 **Area of study**

The area that in this thesis is investigated is in the Brooklyn borough of New York City (Figure 11) that was one of the most injured and where the highest height of rainfall was registered. The Brooklyn area is one of the older urbanized boroughs of the city and is characterised by a high concentration of impervious areas.

Through the analysis of the land use cover raster downloadable from the New York City database, using the QGIS software, was possible to quantify the percentage of the impermeable areas that is about 76.8%.

In Table 1 are reported the specific landcover percentage.

Table 1: Land cover percentage

Value of cells	1	2	3	4	5	6	7	8
Type of land cover	Tree canopy	Tree/Grass	Bare soils	Water	Buildings	Roads	Other impervious	Rail roads
Number of pixel	3490866	531691	25287	30166	5883758	2474896	5033979	90020
Area (m^2)	3490866	531691	25287	30166	5883758	2474896	5033979	90020
%Area	20	3	0.2	0.2	33	14	29	0.6
%Impervious areas	76.8							
%Permeable areas	23.2							

The reduction of the infiltration capacities in an urban area determines an increase in the stormwater runoff volume that has to be drained by the city drainage system and by the sewer system. So according to that is important to understand how these systems are designed.

Based on the NYC TOWN+GOWN CLIMATE VULNERABILITY, IMPACT, AND ADAPTATION (VIA) ANALYSIS REPORT 2024 (NYC VIA FINAL REPORT, 2024), the first document about storm drainage designing in New York City is “Design flow calculations for storm and combined sewers” of 1973

(DEP Design Criteria and Procedures for the Preparation of Drainage Plans (Department of Water Resources Drainage Section 1973)) and it gave the directive to use the Steel formula with five-year storm coefficients in New York City. The same criteria were also adopted in the document of 2006

((DEP Criteria for Determination of Detention Facility Volume (Bureau of Water and Sewer Operations Division of Review and Construction Compliance 2006)).

Based on these documents and considering that analysing the shapefile of the building’s footprint is possible to obtain the year of construction of each building in the area, it is possible

to say that only the 15% of the constructions were built after 1973 and so is reasonable to say that the storm water management is designed using the before cited coefficients.

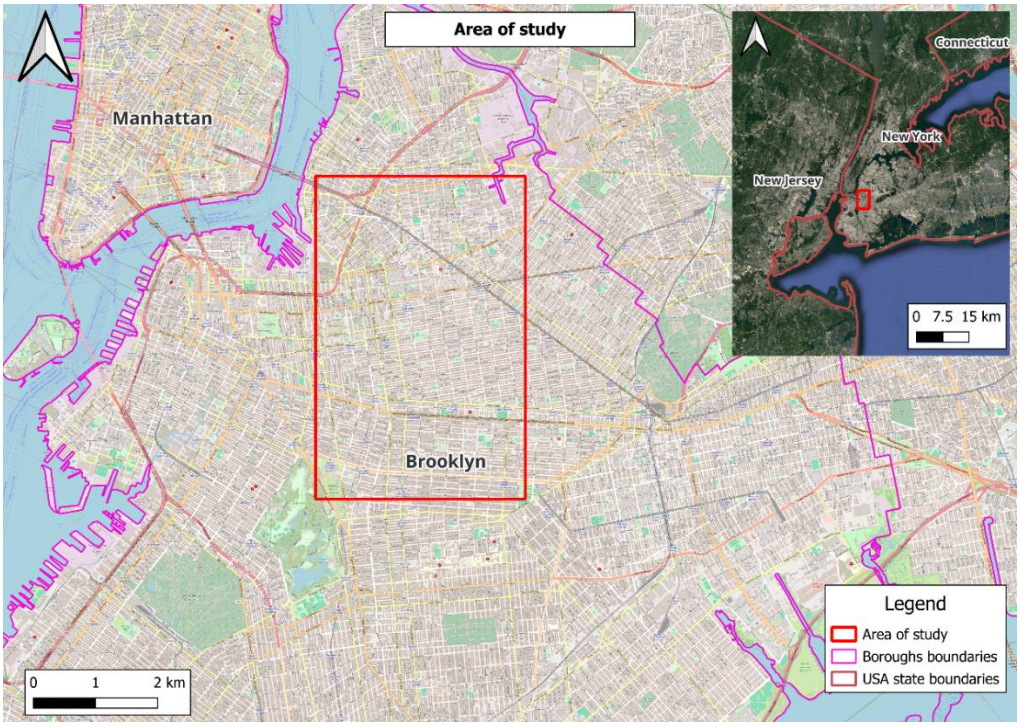

Figure 11: Area of study

To define the specific area of study, firstly was analysed the distribution of the stream gauges of the FloodNet.NYC in Brooklyn. FloodNet is a cooperative of communities, researchers, and New York City government agencies working to better understand the frequency, severity, and impacts of flooding in New York City (https://www.floodnet.nyc/).

Based on the distribution of the sensors (Figure 12), the calculation of the watershed was done, and the specific area of modeling was defined.

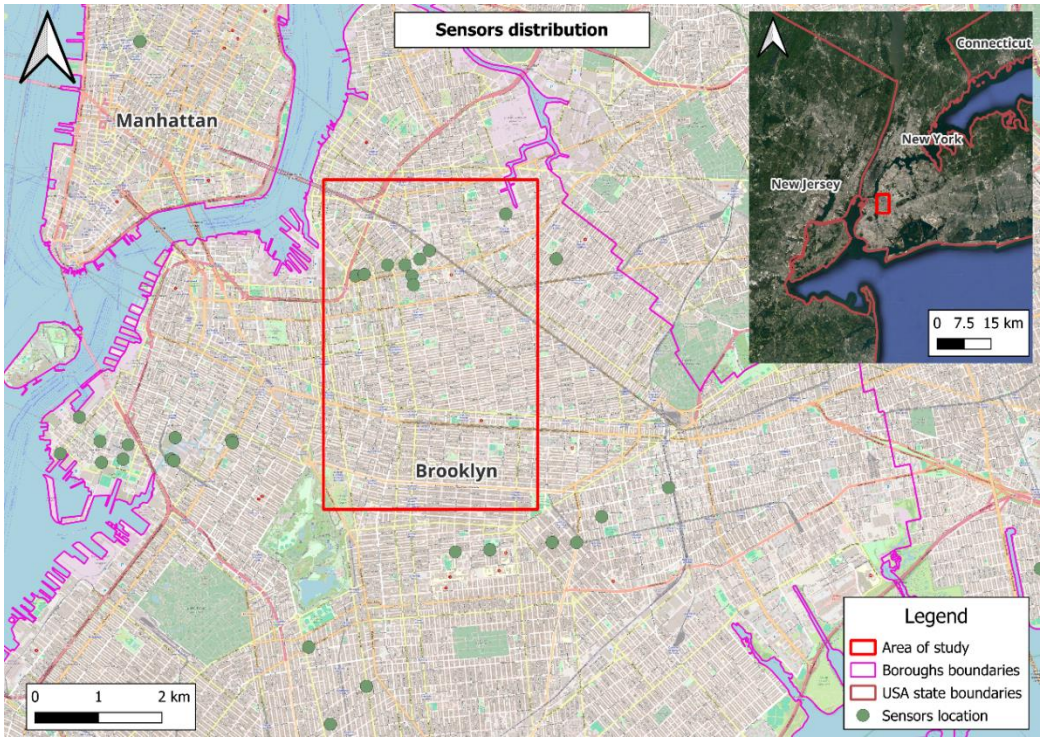

Figure 12: FloodNet sensors distribution

The watershed computation was made by the GRASS plugin on QGIS. Specifically, the procedure is below described.

The first command to use is “r.watershed” (Figure 13), where it is possible to choose many optional input parameters. The two used in this case are:

- Digital terrain model: mandatory input
- Minimum size of exterior watershed basin: optional parameter

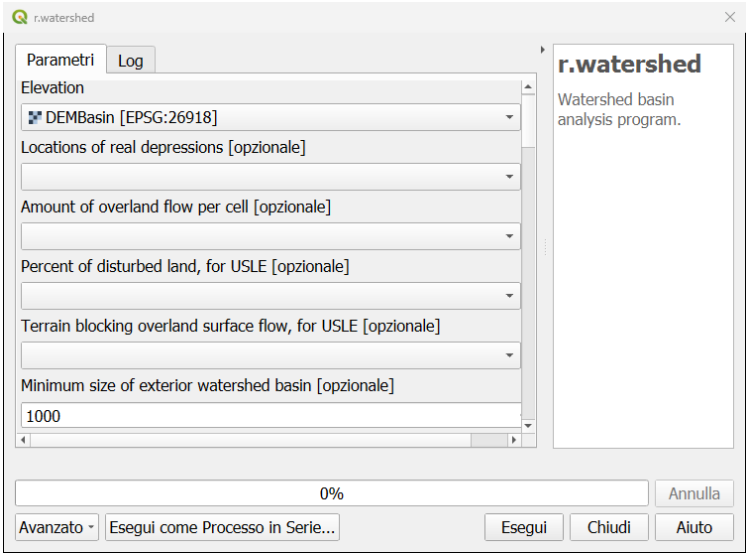

Figure 13: "r.watershed" GRASS command

With this command is possible to have many different outputs, but the two ones important for the execution of the second calculation with the command "r.water.outlet" (Figure 14) are:

- Drainage directions: mandatory for the execution of "r.water.outlet"
- Stream segments: not mandatory but useful to visualize the flow routes of the water in our basin due to the topography and the presence of obstacles

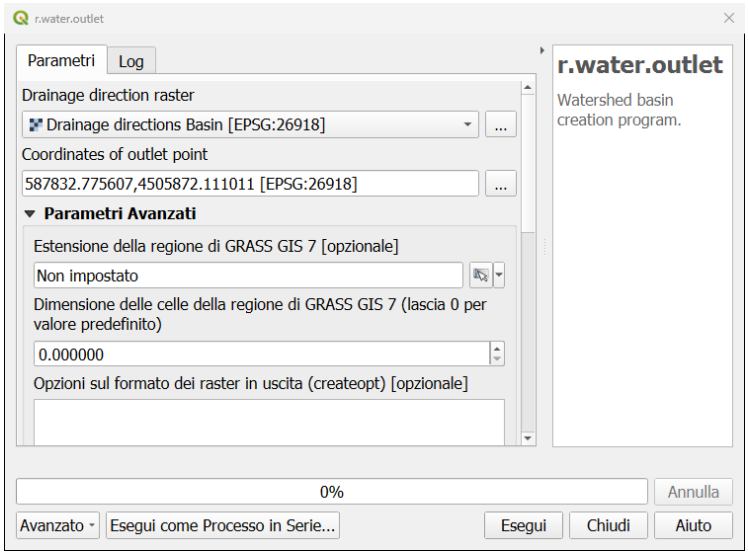

Figure 14: "r.water.outlet" GRASS command

This operator has also the necessity of the specification of the coordinates of the outlet point that in the case of this case study, according to the slope of the "DEM" and to the sensor's distribution, was chosen the same as the further west sensor.

The result that represents the drainage basin to study and so to use for the LISFLOOD-FP simulations is reported in Figure 15.

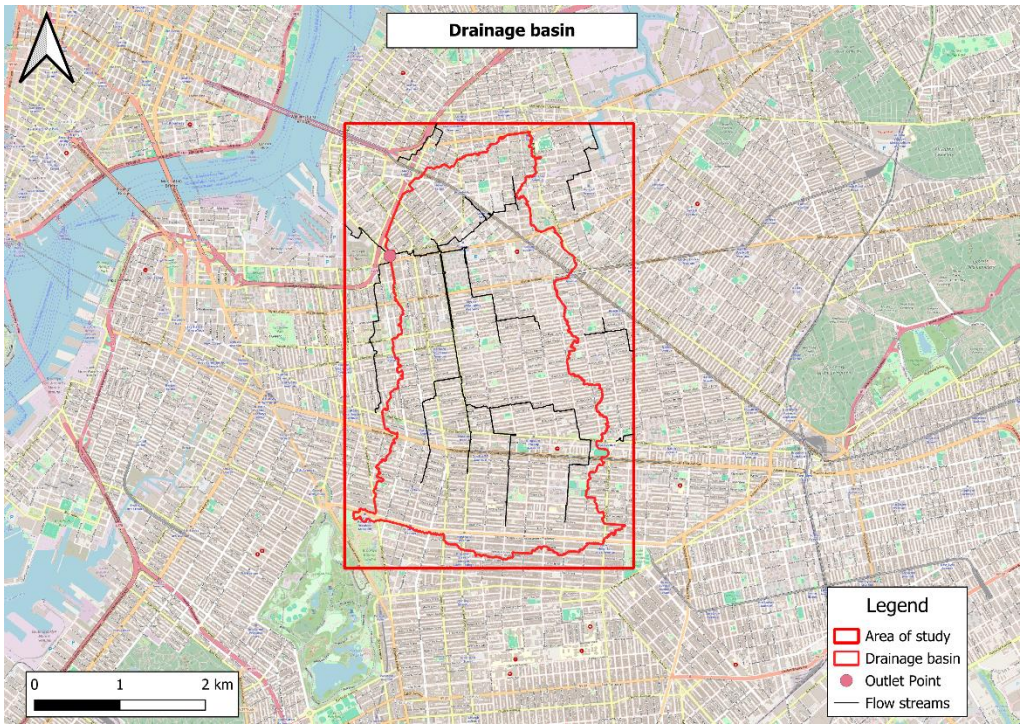

Figure 15: Drainage basin

3.3 **Hydrologic description of the event**

To better understand the urban flooding event that occurred in New York City on September 29, 2023, this section analysed the rainfall data registered during the event.

The sequent data are referred to the rain gauge positioned at the Brooklyn College, in the Brooklyn borough of New York City (Figure 16).

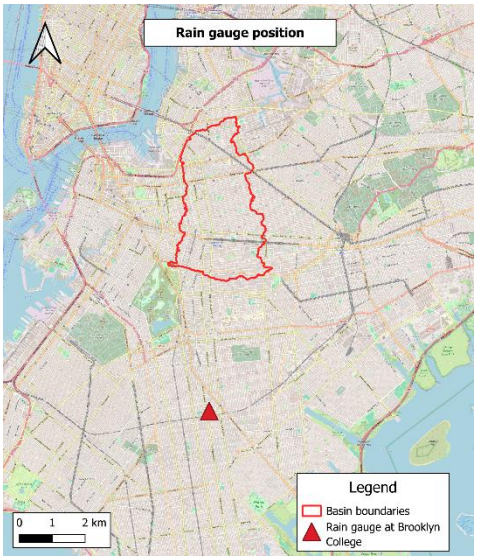

Figure 16:Rain gauge position

The precipitation data that was used as input data for this thesis is the result of the acquisition of the rainfall values every five minutes by the rain gauges. These rainfall data are represented in Figure 17 where the blue line shows the rainfall from September 28 to September 30, the red line the rainfall of September 29, and the black line, the cumulative precipitation of all three days.

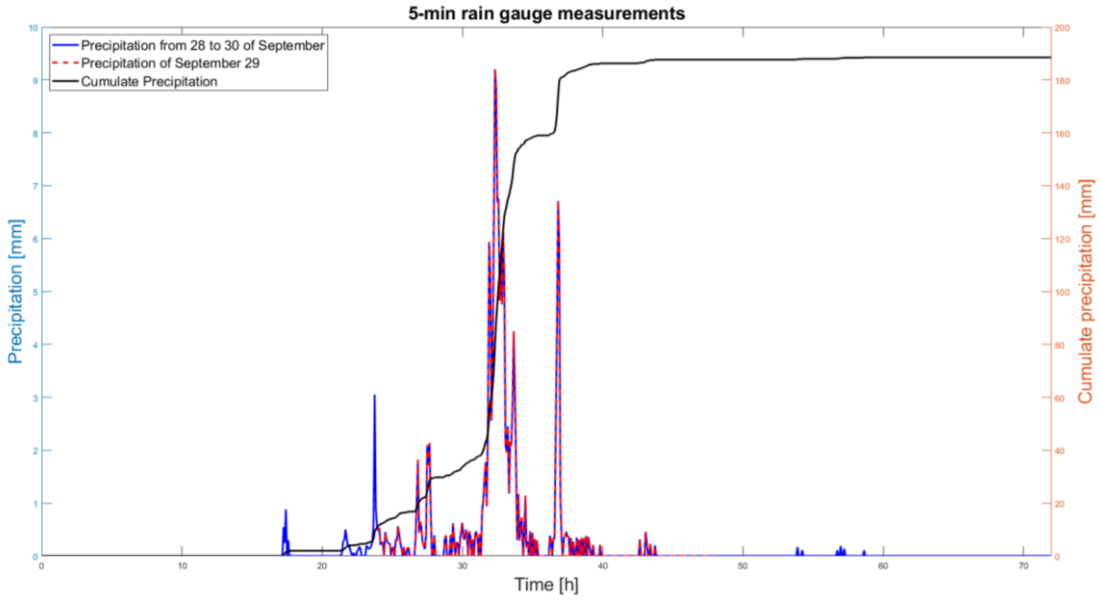

Figure 17: Precipitation and cumulative precipitation 28-30 September, 2023

The hyetograph shows that on September 29 there was the most quantity of rainfall and in one day the cumulative precipitation was about 177 mm. After having defined this information, another step to clarify the entity of the storm is to compare the data with the Intensity Duration Frequency (IDF) curves to assign a return period to the different times of precipitation that have characterized this event. In Figure 18, are represented all the curves corresponding to the return period of:

- T1= 1 year return period
- T2= 2 years return period
- T5= 5 years return period
- T25= 25 years return period
- T50= 50 years return period
- T100= 100 years return period
- T200= 200 years return period
- T500= 500 years return period
- T1000= 1000 years return period

In the same graph are shown also, with the black points, the precipitation values respectively at the time of 5', 10', 15', 30', 1h, 2h, 3h, 6h, 12h, 24h, 48h.These values were calculated using the data of precipitation of the rain gauge and applying the moving sum method using the MATLAB software.

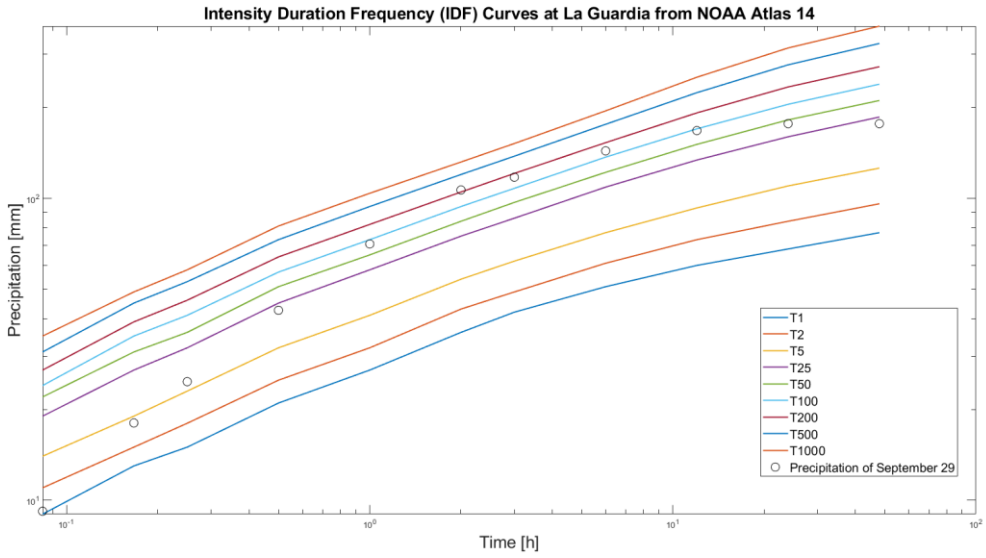

Figure 18: IDF curves with precipitation values of September 29

The analysis of the values shows that for the duration of 1h, 2h, 3h, 6h, and 12h, the return period of the storm was between 100 and 200 years, as reported in Figure 19 with the red points.

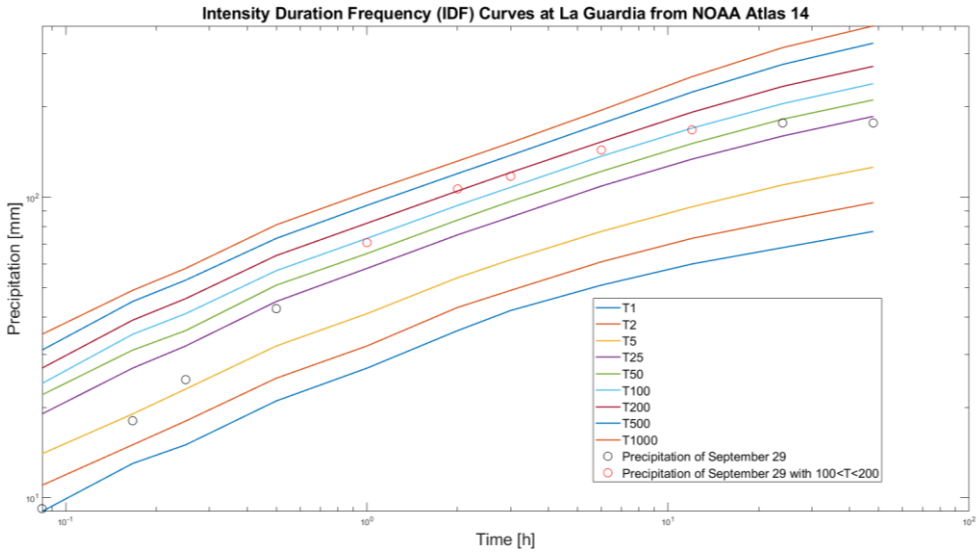

Figure 19: IDF curves with precipitation values of September 29 with red points on the critical durations

This analysis points out that the rainfall event that occurred on September 29, 2023, was unable to be drained by the drainage system considering that according to the precedent shown directive of New York City, that is designed for five years return period storm.

3.4 **Flooding water measured during the event by FloodNet system**

New York City is equipped with a distributed monitoring system for the flooding event that occurs in the urban area. For this case study the sensors used to compare the results obtained by the LISFLOOD-FP model to the acquired data during the event by the FloodNET system are represented in the below Figure 20.

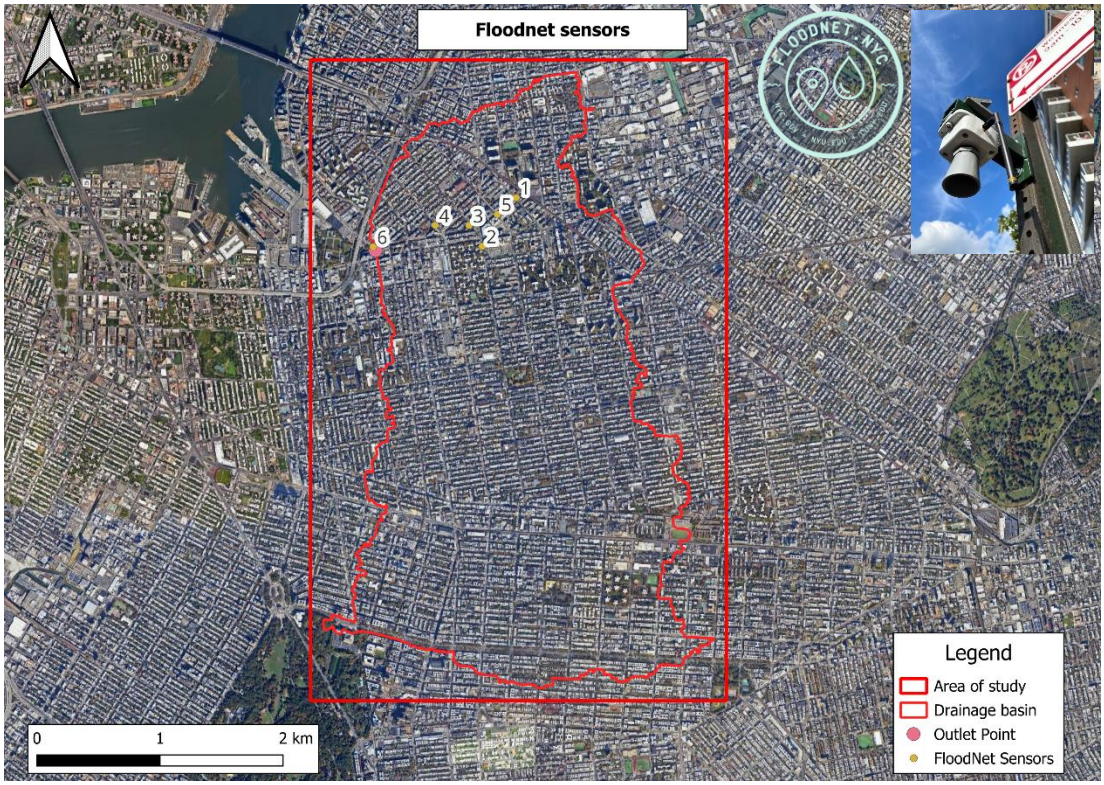

Figure 20: Floodnet sensors distribution selected to compare the results

Each of those sensors has registered during the September 29 storm event a flood depth that is reported in the graphs below (Figures 21-26). This depth is defined in inches, so to better understand the data and to compare it with the LISFLOOD-FP outputs', which are in meters, we must use the sequent conversion:

$$1\ inches = 0.0254\ m \quad \textbf{(9)}$$

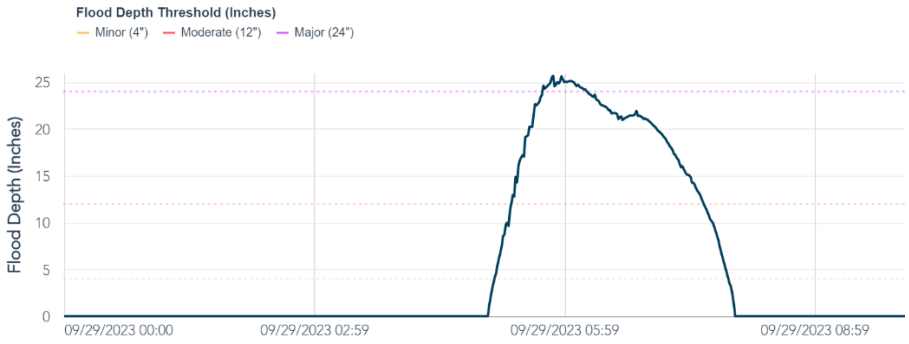

Figure 21: Sensor 1 - BK- Wallabout St/Throop Ave

Figure 22: Sensor 2 - BK - Marcy Ave/Flushing Ave

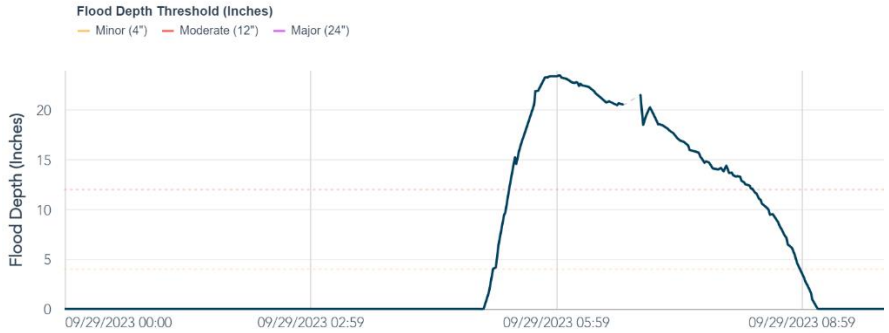

Figure 23: Sensor 3 - BK - Lee Ave/Middleton St

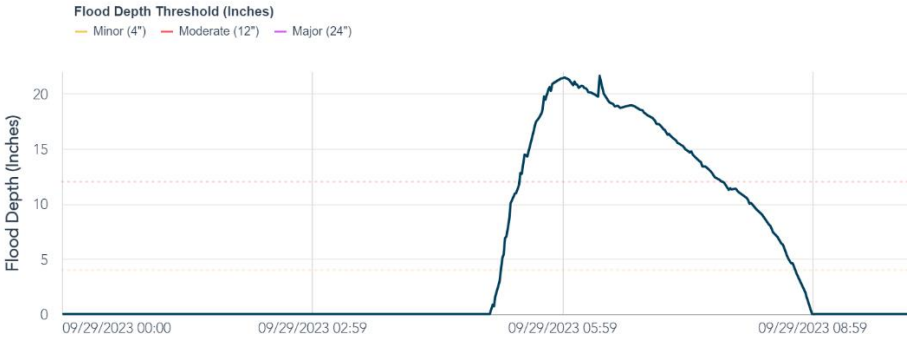

Figure 24: Sensor 4 - BK - Walton St/Marcy Ave

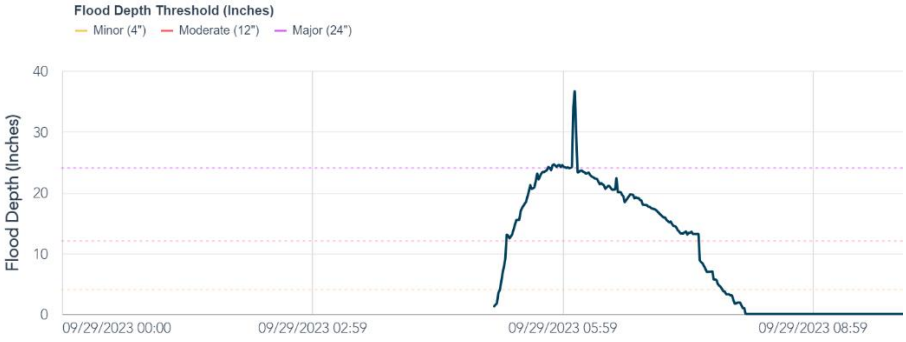

Figure 25: Sensor 5 - BK - Wallabout St/Harrison Ave

Figure 26: Sensor 6 - BK - Kent Ave/Wallabout St

CHAPTER 4
BUILDING ROOFS MODELING APPROACHES

Urban areas are characterized by the presence of many different obstacles, like buildings, roofs, or manholes that could modify the flow of the water during pluvial flooding. That means that a flooding model in this case must consider many different boundary conditions that could change drastically the results.

The focus of this thesis is to understand how the roofs, based on their geometry and construction typologies, act in modifying rainfall runoff in the streets and water accumulation dynamics. To understand the roof's behaviour, the following points were followed:

- Bibliographic research of what was previously done: research and review articles
- Selection of what were the more efficient methods to implement on LISFLOOD-FP
- Methods implementation on LISFLOOD-FP
- Results comparison with the acquired data during the event

4.1 **Bibliographic research consideration**

The bibliographic research has shown that this subject is not so studied, especially for what concerning "Non-green roofs" (Yixuan et al., 2024). Non-green roofs are made of cement, asphalt, concrete, or metal, although today they are the most frequent in the world and are also the least studied.

4.2 **Roof's runoff selected methods**

The roof's runoff selected methods are two and they were chosen considering the appliable possibility on LISFLOOD-FP model. These methods are the runoff coefficient approach (RC) (Farreny et al., 2011b) and the building induced rainfall redistribution approach (BIRR) (Xuejian et al., 2021). Both methods are described in research articles that are freely available for consultation. In this thesis are reported the main conceptual basis related to these methods.

4.2.1 *Roof selection for rainwater harvesting: Quantity and quality assessments in Spain (Farreny et al., 2011b)*

The main goal of this study is to identify the Roof Water Harvesting (RWH), so how much water could be conveyed to a rainwater storage system according to the roof characteristics.

Figure 27 represents the complete scheme of the method.

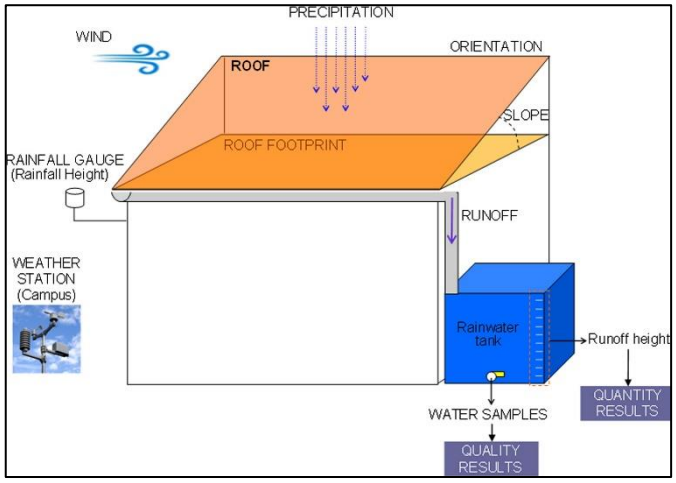

Figure 27: Diagram of the experimental design (Farreny et al., 2011)

To calculate the RWH the authors have formulated an equation (Eq. 11), taking inspiration from the rational method (Eq. 10) which is usually used to evaluate the peak runoff rate of any drainage basin, that depends on three parameters:

$$Q = k \cdot \Phi \cdot I \cdot A \qquad [L^3T^{-1}]$$

(10)

- k: Runoff coefficient adjustment factor [/]
- Φ: Runoff coefficient [\]
- I: Rainfall intensity [MT^{-1}]
- A: Catchment area [M^2]

$$RWH = P \cdot A \cdot RC \qquad [LT^{-1}]$$

(11)

- P: Precipitation [MT^{-1}]
- A: Catchment area [M^2]
- RC: Runoff coefficient [\]

For what concerns this thesis, the most important parameter is the RC, a non-dimensional coefficient that takes into consideration losses due to spillage, leakage, catchment surface wetting, and evaporation(Singh, 1992).

According to this article, the specific runoff coefficient of a roof can be estimated considering the local rainfall profile, that is the specific precipitation trend of the geographic area where the roof is situated.

Specifically, to practically calculate the RC is necessary to estimate the runoff of each rain event and then divide the total runoff per year by the annual rainfall (Farreny et al., 2011b).

The final equation is:

$$RC = \frac{R}{P} \qquad [\backslash]$$

(13)

Where:

- R: total height of runoff [M]
- P: total height of precipitations on a yearly basis for each roof [M]

Is also important to report the parameters that were studied to understand their contribution to the RC value. These are:

- Wind direction: it was demonstrated that there is not a significant relationship between RC and wind direction
- ADWP: it was demonstrated that there is a significant relationship between the antecedent dry weather period and the RC

In the articles, the authors have considered many roof typologies in different environments as summarized in Figure 28.

Roof	Roof type (slope)	Roughness	Orientation	Roof footprint (m^2)	Environment	UTM
Clay tiles	Hip sloping roof (30°)	Rather smooth	None prevailing	120.0	Surrounded by forest. A few trees overhanging the roof	424482.6 E 4594896.6 N
Metal sheet	Single pitch sloping roof (30°)	Smooth	50° NE	40.6	Urban environment (no trees nearby)	425349.6 E 4594851.4 N
Polycarbonate plastic	Single pitch sloping roof (30°)	Smooth	230° SW	40.6	Urban environment (no trees nearby)	425347.1 E 4594848.6 N
Flat gravel (particle diameter: ~5 mm, gravel depth 15–20 mm)	Flat roof (1°)	Rough	None prevailing	56.6	Urban environment (some trees nearby)	425476.6 E 4594733.4 N

Figure 28: Characteristics of the roof catchments (Farreny et al., 2011)

To understand the effective validity of the method, the authors of the articles have also done statistical analysis for each roof type using a regression model (Eq.12) between roof runoff (R) and precipitation height (P).

$$R = m \cdot P + n \quad \textit{(12)}$$

This analysis demonstrates that all the regression parameters are statistically significant (p_value<0.05 and Pearson coefficient>0.95), especially for Clay tiles and Flat gravel roofs, and so that there is a significative correlation between roof runoff and rainfall (Figure 29).

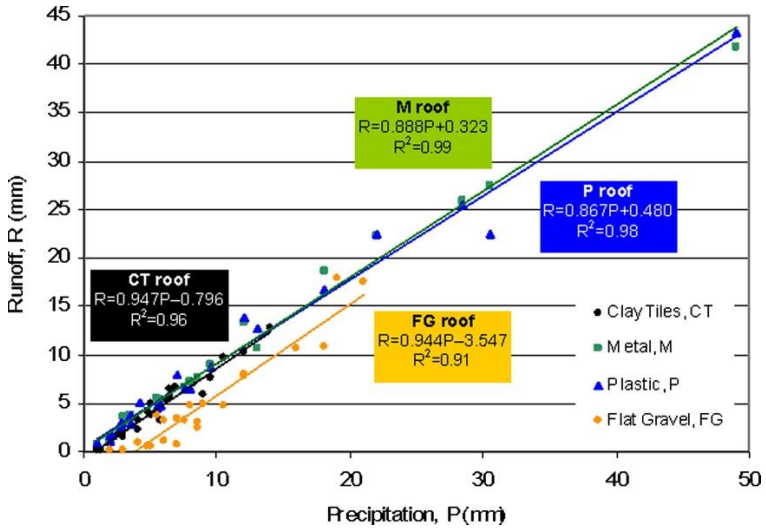

Figure 29: Regression model for roof runoff and rainfall height (Farreny et al., 2011)

Considering that the procedure that permits to estimate of a specific runoff coefficient value for each roof is strictly connected with the availability of local rainfall data, in this thesis, due to the lack of these types of data, to apply the runoff coefficient method some tables RC values reported in the article were used (Figure 30).

Roof	RC	Reference
Roofs (in general)	0.7–0.9	Pacey and Cullis (1989)
	0.75–0.95	ASCE (1969), McCuen (2004), Singh (1992), TxDOT (2009), Viessman and Lewis (2003)
	0.85	McCuen (2004), Rahman et al. (2010)
	0.8–0.9	Fewkes (2000)
	0.8	Ghisi et al. (2009)
	0.8–0.95	Lancaster (2006)
Sloping roofs		
Concrete/ asphalt	0.9	Lancaster (2006)
Metal	0.95	Lancaster (2006)
	0.81–0.84	Liaw and Tsai (2004))
Aluminium	0.7	Ward et al. (2010)
Flat roofs		
Bituminous	0.7	Ward et al. (2010)
Gravel	0.8–0.85	Lancaster (2006)
Level cement	0.81	Liaw and Tsai (2004))

Figure 30: Runoff coefficient (RC) estimates (Farreny et al., 2011)

4.2.2 *Significant Impacts of Rainfall Redistribution through the Roof of Buildings on Urban Hydrology (Xuejian et al., 2021)*

The article of Xuejian et al., 2021 reports a new method of taking into consideration the building roofs in urban hydrology dynamics. This method is called "Building induced rainfall

redistribution (BIRR)" and it is a hydrological approach particularly focused on how the drainage system of building roofs influences rainfall-runoff dynamics. The goal of this method is to better simulate the roof runoff reality, implementing the roofs redirecting of the rainfall in the downspouts of the roofs (Chang et al., 2015; Leandro et al., 2016). This redirection creates concentrated runoff patterns that can potentially affect urban hydrology (Figure 31).

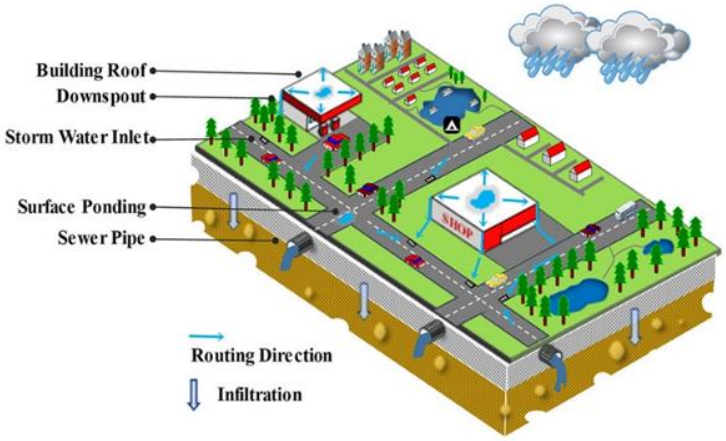

Figure 31: Scheme of BIRR method

To quantify the impacts of BIRR the methodological steps of this research were:

- Incorporating the roof layer into a grid-based urban hydrologic model (gUHM). The gUHM was validated in a typical urban catchment and designed to estimate hydrological responses in an ideal 4-hectare urban area (X. Cao, Lyu, et al., 2020; X. Cao, Ni, et al., 2020; X. J. Cao & Ni, 2019; Lyu et al., 2018). This model takes into consideration:
    - Impervious and pervious surfaces
    - Routing runoff from roads directly into a sewer network (Gangodagamage et al., 2011; Passalacqua et al., 2010)
    - Regular rectangular buildings equipped with downspouts at each corner, facilitating equal distribution of rainfall across the roof (Figure 32)
    - The overland flow on the grid is calculated using the nonlinear reservoir algorithm (Rossman and Huber 2015)
- Analysing of different land development scenarios and synthetic rainfall events:
    - Various building distributions and landscape measures, including pavement, lawns, and bioretention cells (BRC)
    - Generation of 27 types of synthetic rainfall events, varying in return periods, peak ratios, and durations

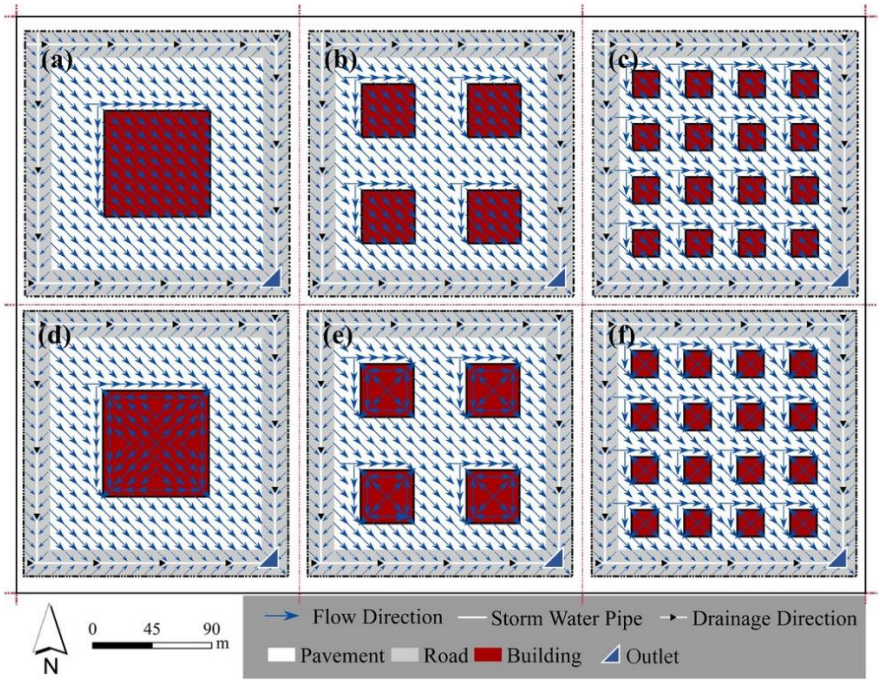

Figure 32: Grid-based urban hydrologic model (gUHM) used in the BIRR method with different configurations of buildings

What the result of this research shows is that in their case study and so with their assumption the BIRR significantly impacts urban hydrology, and it is possible to outline two main causes:

- Distribution of buildings:
    - Dispersed building arrangements tend to increase peak flow
    - Concentrated distributions reduce overall runoff volume
    - The presence of BRC and lawns also modifies the effects of BIRR, often mitigating peak flows while increasing total runoff.
- Rainfall characteristics:
    - Intense and long-duration rainfall events amplify the effects of BIRR on peak flow, while variations in rainfall duration and peak ratios exhibit varying impacts.
    - Extreme conditions during heavy rainfall led to significant increases in flow magnitude, underscoring the necessity of incorporating BIRR into urban flood prediction models.

What in this thesis was done is the application of this method but using the real different geometries of the building footprints of the area of study despite the ideal one used by Xuejian et al., 2021 and implementing a different solver equation for the overland flow.

CHAPTER 5
MODEL IMPLEMENTATION

The code of the model used to simulate the event of the case study used by LISFLOOD-FP needs multiple input parameters to be computed. All the parameters that are necessary to start the computation must stay in a single folder that has to be added to the folder of the executable file called “lisflood.exe”. The input used in this thesis to model the contribution of the buildings' roofs on the stormwater runoff dynamic during the event of September 29, 2023, are:

- Topography file
- Boundary conditions file
- Surface roughness file
- Dynamic rainfall file
- Model solver typology
- Parameter file

5.1 Topography file

The topography file is a digital elevation model (DEM) that to be used by the LISFLOOD-FP model must be converted from a “.tif” (in the case it is a GeoTIFF) to “.dem”.

The Digital Elevation Model used for both approaches are the one that was used for the applications of Professor Giuseppe Mascaro during his study. This Digital Elevation Model has a high resolution of 1 meter and was realized by subtracting by the original continuous DEM the building footprints as represented in Figure 33.

This choice was made because the LISFLOOD-FP code is not able to simulate independently what happens in the roof buildings using the DEM, but it needs a different implementation that will be later discussed. The subtraction was done using QGIS geoprocessing of the building’s shapefile to the DEM of the Brooklyn area of study.

This subtraction command in QGIS creates a unique block in the area where there are near buildings. This simplification was separately analysed for both the approaches reported in chapter 5 to understand if could affect the results of the flooding model of this thesis.

The specific analysis of the possible influence is reported in the paragraph of the dynamic rainfall implementation for each different method.

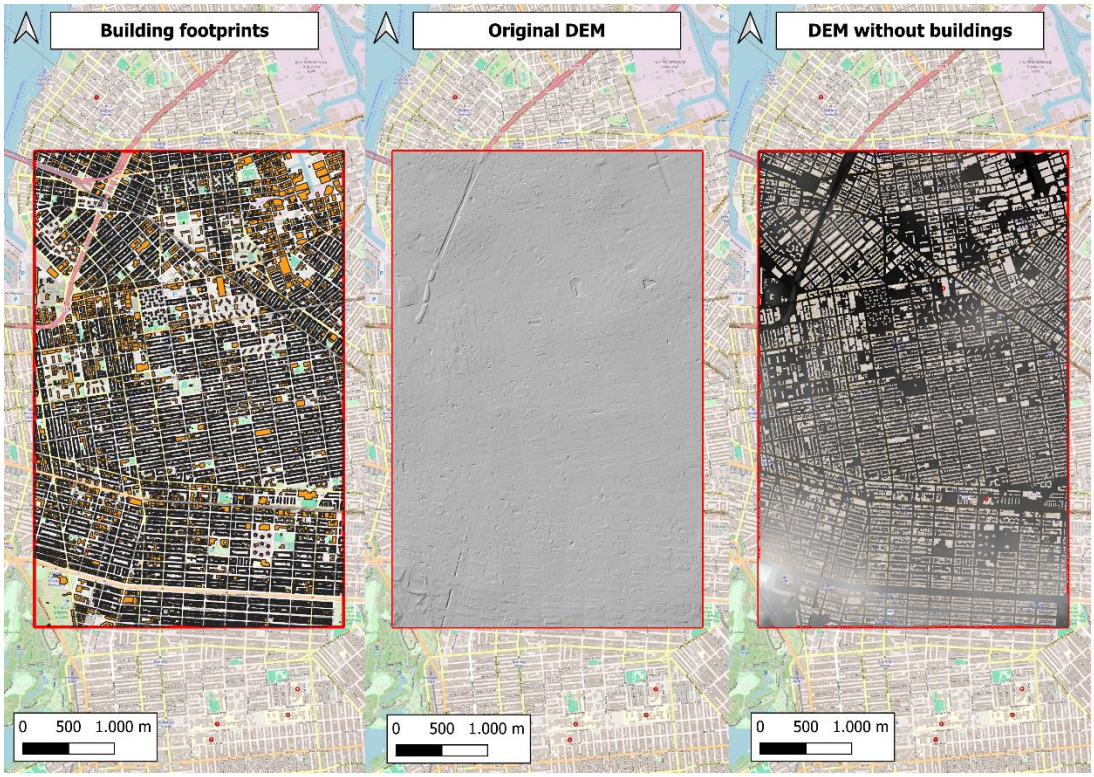

Figure 33: Dem modification procedure inputs. DEM without buildings = Original DEM – Building footprints

5.2 Boundary conditions file

The boundary conditions file has the ".bci" extension. The conditions imposed on this modelling approach are four as represented in Figure 32.

```
S     587304.4639     588762.4639     CLOSED
N     587304.4639     588762.4639     CLOSED
W     4502531.5126     4504679.5126     FREE
E     4502531.5126     4504679.5126     CLOSED
```

Figure 34: Boundary conditions file

These conditions mean that during the simulation the water can flow outside the grid only on the west side, defined with "W" in the text file, of the grid according to the natural slope profile of the digital elevation model (defined by the FREE command).

The "CLOSED" command is applied in the south (S), north (N) and east (E) sides if the grid means that the water cannot go out of the grid in those directions.

5.3 Surface roughness file

The surface roughness file is a raster file with ".n" extension of the same dimensions of the DEM file and where for each cell is specified a Manning value. The Gauckler-Manning coefficient represents the roughness of the surface, and for this case study it is defined considering the land use cover raster file (Figure 35). The land use cover raster dataset derived from the 2017 Light Detection and Ranging (LiDAR) data capture in New York City and is accessible and downloadable from the "NYC Open Data" website (https://opendata.cityofnewyork.us/).

These coefficients affect significantly the model results, influencing the stage height and the stability of the flow during the computation. In this thesis the Manning coefficients are the one used for the previous work for the seminar of Professor Giuseppe Mascaro and so the ones that give the best physical results.

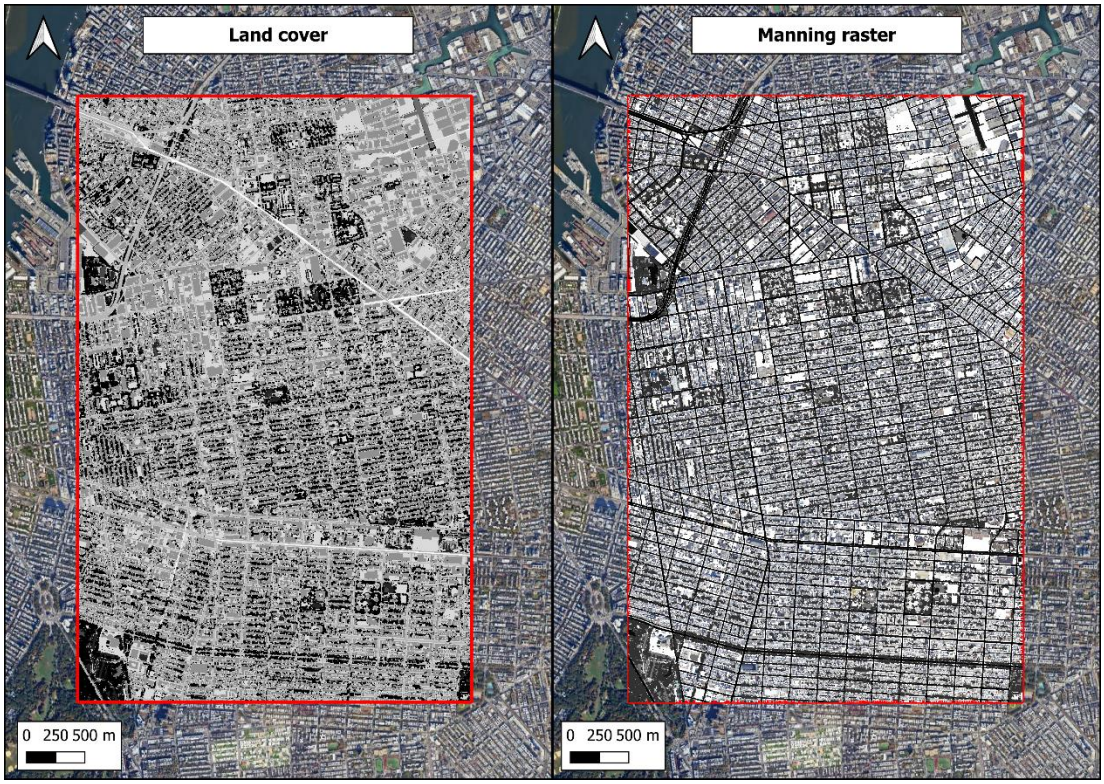

Figure 35: Land cover raster and Manning coefficients raster.

The procedure followed consists on the assignation to the cell of the manning coefficient raster, the correspondent value of roughness reported in Table 2 related to the same cell values of the land cover raster.

Table 2: Manning values

LC type	Tree Canopy	Tree/Grass	Bare soils	Water	Buildings	Roads	Other impervious	Rail roads
LC value	1	2	3	4	5	6	7	8
Manning value [$TL^{1/3}$]	0.05	0.1	0.02	0.03	NaN	0.013	0.2	0.033

The "Not a Number (NaN)" value for buildings is because also the manning raster files is characterized by the holes in correspondence of the building's footprint.

5.4 Dynamic rainfall file

The dynamic rainfall file is a NetCDF file with the extension ".nc". NetCDF (network Common Data Form) is a type of file used to store multidimensional scientific data (variables) such as rainfall depth.

In this case, the file used for the model implementation of this thesis contains the georeferenced spatial rainfall in the basin for each time step of five minutes that is acquisition time step of the data by the rain gauge.

To implement the model, this file has been modified using MATLAB to include three components in the rainfall depth values:

- Roofs implementation
- Infiltration contribution
- Sewer contribution
- Roofs contribution:
    - Runoff coefficient (RC) approach
    - Building induced rainfall redistribution (BIRR) approach

5.4.1 *First step of dynamic rainfall file creation: Roofs implementation*

The first step is the implementation of the contribution of the roofs. This procedure has been defined by the group work of Professor Giuseppe Mascaro. The code to do that was written using Python programming language.

The input files are the building's footprint raster and the rainfall time series. As said in the topography paragraph, the building's footprint raster considers the near buildings as a unique block.

For the goal of this thesis this simplification represents a conservative assumption where all the rainfall on the roofs is correctly distributed in the street's side of the building.

The conservative aspect mentioned before is because of the possibility of including in the total amount of distributed rainfall a quantity higher than the real one, caused by the presence of the internal courtyard that with the QGIS simplification are considered part of the unique block of the building.

After that the input files were defined, these are red by the calculator that for each building calculates the area. After that, for each instant of time of the rainfall series the volume of the water accumulative in each roof is computed. Then for each building, another area is defined using a buffer of one pixel around the roof footprint, and the rainfall is linearly distributed in the buffer area. In this process, all the values outside the basin boundaries have been assigned a value equal to zero. Here below in Figure 36 shows the part of the code that has been written for this thesis using MATLAB.

The complete code is visible in the appendix A.

```
%Step 4: calculation of the area and volume of the rain to redistribute in the edge of the roofs
roof_rain=zeros(size(BR,1),size(BR,2),length(dt));

roof_rain(BR==1 | BR==2)= 0;
dx=abs(R.CellExtentInWorldX); %dimension of the pixel calculation

se=strel('disk',1); %buffer calculation
Roof_buffer=imdilate(lab_roof, strel('disk', 1)) - lab_roof;

for i=2
    roof_rain_loop=roof_rain(:,:,i);
    roof_rain_loop(BR==0)=rain_roofs_depth(i);
for label = 1:num_roof
    % area of the roof
    area_roof = sum(lab_roof(:) == label) * dx * dx; % m^2

    % volume of rainfall(in mm*m^2)
    volume_rain_roof = rain_roofs_depth(i)* area_roof;

    % area of the buffer (in m^2)
    area_edge_roof = sum(Roof_buffer(:) == label) * dx * dx; % area del bordo in m^2

    % rainfall distribution on the edge area (in mm)
    if area_edge_roof > 0
        roof_rain_loop(Roof_buffer == label) = (volume_rain_roof / area_edge_roof) + rain_roofs_depth(i);
        roof_rain(:,:,i)=roof_rain_loop;
    end
  end
end
```

Figure 36: MATLAB loop to calculate the precipitation on the roofs

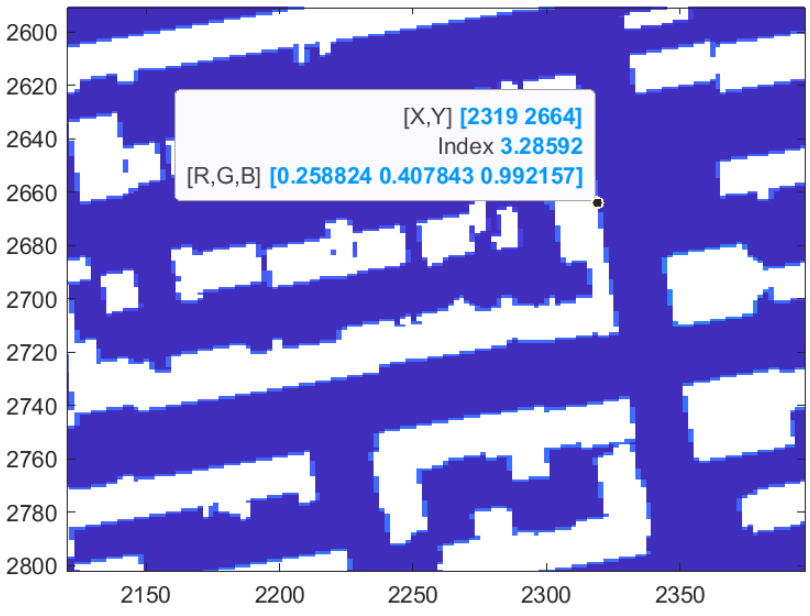

Figure 37: Example of the rainfall distribution for the instant. The pixels on the edges of the buildings (white areas) are represented in a different blue scale of colour. The value shown in the figure is an example of rainfall distributed in the building's buffer

5.4.2 *Second step of dynamic rainfall file creation: Infiltration contribution*

The second step is the modification of the rainfall values to consider the infiltration.

To consider the infiltration the Green-Ampt method was applied by the work group of Professor Mascaro.

The Green-Ampt (GA) model assumes a homogeneous soil with constant hydraulic conductivity, initial water content, and head at the wetting front. The saturated wetting front is assumed to move downwards as a single piston-like displacement (https://www-hec-usace-army-mil.translate.goog/confluence/rasdocs/ras1dtechref/6.0/overview-of-optional-capabilities/modeling-precipitation-and-infiltration/green-ampt?_x_tr_sl=en&_x_tr_tl=it&_x_tr_hl=it&_x_tr_pto=sc).

This method gives the model a small change because, as described in the 3.2 paragraph, the zone of study is characterized by a low presence of permeable areas.

5.4.3 *Third step of dynamic rainfall file creation: Sewer contribution*

The sewer contribution was taken into consideration using a fixed rate of rainfall reduction following the EA (Environment Agency) method (Environment Agency, 2019).

In this report is suggested to estimate a drainage removal value based on the critical storm duration of the territory in consideration.

For New York City storm events as reported in the NYC-VIA-Report (NYC VIA FINAL REPORT,2024) this duration is 1.75 inches per hour, so 44 mm/h.

Considering that the rain gauges have a time of acquisition of five minutes, finally, the value to subtract from the rainfall is (44*5)/60 mm/h ~ 3.6 mm every five minutes.

5.4.4 *Fourth step of dynamic rainfall file creation: Roofs contribution*

The input of this step is the NetCDF file that was written after the sewer contribution application.

5.4.4.1 *Runoff coefficient (RC) approach implementation*

The first step of this procedure is to categorize the building's shapefile, using QGIS according to roofs different characteristics.

In this case, because of the lack of data about the material of the roofs, the only distinction that was made was between flat roofs and sloping roofs. To check the roof typologies a direct analysis on Google Satellite determined that in all the analysed basin the sloping roofs are only 2% of total buildings.

To apply this information to the original NetCDF file, the edges of the building’s footprint with MATLAB follow the same procedure used in paragraph 5.4.1 (Figure 38).

```
%%Step 2: Code to find the border of the roofs
% Read the GeoTIFF
[BR, R] = geotiffread('C:\Users\Admin-VM\Desktop\Land cover\Building_raster_roof.tif');
[lab_roof, num_roof] = bwlabel(BR, 4); %here the code finds the binary image of BR with connectivity

%Calculate the dilatation of the building roofs with an r=1 using the disk
%type of extension
se=strel('disk',1);
Roof_buffer_l=imdilate(logical(lab_roof),se)&~logical(lab_roof); %l because logical
Roof_buffer=double(Roof_buffer_l);

%Loop for changing values inside Roof buffer according to the type of the roof
for ii = 1:size(BR,1)
    for jj = 1:size(BR,2)
        if Roof_buffer(ii,jj) == 1
            % This part is to control the boundaries using a control window
            row_min = max(ii-1, 1);
            row_max = min(ii+1, size(BR,1));
            col_min = max(jj-1, 1);
            col_max = min(jj+1, size(BR,2));

            % Here we control the window
            pre = BR(row_min:row_max, col_min:col_max) == 2;

            % If two of the value inside the window is 2 we update Roof_buffer(ii,jj)
            if sum(pre(:)) > 1
                Roof_buffer(ii,jj) = 2;
            end
        end
    end
end
```

Figure 38: Edge of the building's definition

To each pixel of the edge of the roof was given information about the specific roof typology. Finally, a new matrix of ones with the same dimensions as the DEM file was initialized, and each cell of the matrix was assigned the correspondent roof typology runoff coefficient value (Figure 39).

```
% % Step 5: RC matrix updating
RC(Roof_buffer==1) = 0.9; %sloping buildings, mean of all slopings
RC(Roof_buffer==2) = 0.76; %flat buildings, mean of modified
```

Figure 39: Runoff coefficient value assignment

The final step was the NetCDF file updating, which was done by multiplying the rainfall depth original variable per the RC matrix.

In this case the possible influence of the adjoining buildings considered as unique areas was studied and was determined, analysing the plot of the final dynamic rainfall NetCDF for this approach, that the simplification does not influence the rainfall variation due to the runoff coefficient.

5.4.4.2 *Building induced rainfall redistribution (BIRR) approach implementation*

The input file to implement the dynamic rainfall file for the BIRR method is the same as the RC method. As defined in paragraph 4.2.2 the main objective of the approach is the redistribution of the rainfall that falls on the roofs in the downspouts. The procedure adopted to obtain the net precipitation file for this approach is divided into two steps.

The first step of the procedure is the roof's downspout distribution design. The designing criterion that was applied is the one reported in the 2020 plumbing code of the New York State (https://codes.iccsafe.org/content/NYSPC2020P1/chapter-11-storm-drainage) where Chapter 11 reports the storm drainage designing procedures. What this code proposed is to first calculate the overall flow in gallons per minute (1 gpm = 3.785 L/min) using the following equation:

$$GPM = R \cdot A \cdot 0.0104 \quad \textbf{(14)}$$

where R is the design rainfall intensity corresponding to a rainfall of 1 hour and return period of 100 years proposed by the code, that for the city of New York is 3 inches/hour (76 mm/h) and A is the area of the roof. Then using this value of flow in this thesis, according to the data found from rainwear product manufacturers' websites in the US, a pipe size of 4 inches (0.10 m), which is one of the most common, was chosen for all the roof's downspouts. So, for each roof, the number of downspouts was calculated by dividing the specific flow of the roof per the max flow that a pipe of 4 inches could manage according to the New York State code, which is 180 gpm.

Finally, by dividing the perimeter of the roofs per the number of downspouts the distance between the drainage was calculated. To apply the procedure discussed, the AutoCAD LT 2024 software. The choice of using this software was because of the better capacity of managing geometric data and calculation coupled with the possibility of implementing automatic operation using AutoLISP (LSP) files. In fact, after having converted the building shapefile into a ".dwg" file the calculations were implemented into a ".lsp" file, reported in Appendix B, and then applied to the area of study data (Figure40).

The buildings shapefile is the same characterized by the unique blocks as well as the RC approach. In this case to understand the influence of this simplification was done an analysis on the importance of considering the height of each building that with the unique areas is neglected.

What was seen is that calculating all the retard factors for each building, so the time of delay that the water needs to flow from the roofs to the street through the downspout, the highest factor is less than one minute.

This result is representative of the fact that the times of retard are not significant considering that the time step of acquisition of the rainfall input data is five minutes.

So, is also not useful for this modeling consider the heights of each building and so the assumption of the adjoining building as a unique area is acceptable.

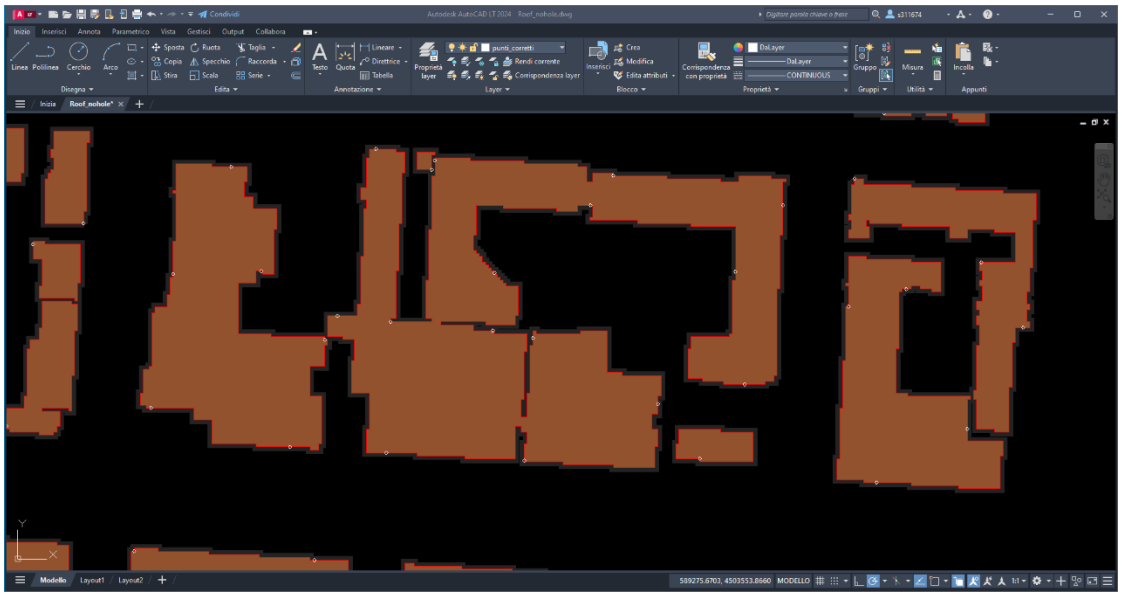

Figure 40: Downspouts distribution with AutoCAD. In orange are represented the buildings and with the white circles the calculated downspouts

The second step of the procedure is the distribution of the rainfall on the downspouts which was implemented in a MATLAB code reported in Appendix A. The codes first calculate the volume of water that falls on each roof. Then this volume is subdivided, for each roof, to the downspouts (Figure 41). The downspouts input file is the geo-raster data calculated using AutoCAD LT 2024 software. The new values of rainfall were written in a new matrix with the same dimensions as the original precipitation, and so using this matrix the NetCDF file was dated to obtain the BIRR dynamic rainfall file.

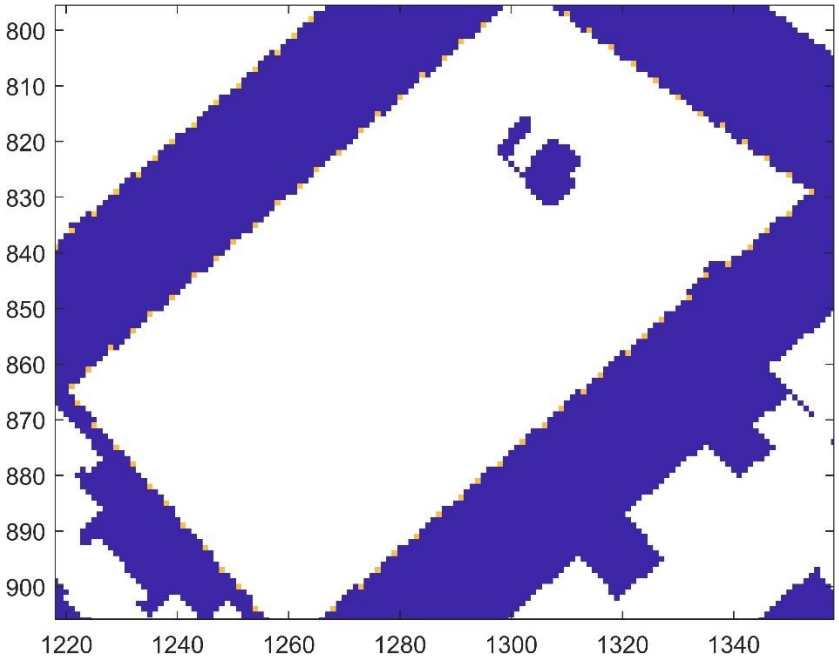

Figure 41: Rain distributed in the downspouts of a building. In orange are defined the downspouts around the white areas that are the buildings

5.6 Model solver typology

The model solver used in this model implementation is the Adaptive FV1 solver described in paragraph 2.2.

This solver was chosen based on the guidelines of LISFLOOD-FP that suggest pluvial floods modeling this type of solver. Specifically, the Adaptive FV1 GPU parallelized solver was chosen thanks to the possibility of using the "Sol Supercomputer" of the Arizona State University (Jennewein et al., 2023). The specific characteristics of the processor of the Sol supercomputer are:

- 18,000+ CPU cores using the modern AMD Epyc architecture
- Nodes with 512GB of RAM
- Over 244 GPUs (including A30s, 80GB A100s and 80GB H100s)
- Five high memory nodes with 2TiB of memory

The main setup used for the simulations in this thesis was 1 GPU, 24 cores, and 120 GB of memory. This type of configuration was defined to guarantee the repeatability of the modeling in computers with less powerful processors but without losing the capability to obtain high-resolution results in a low computational time.

5.7 Parameter file

The parameter file is a text document with ".par" extension. This file contains all the keywords that LISFLOOD-FP model reads to start the computational process. Here below in Figure 42 is an example of the parameter file for the model implementation of the case study.

```
DEMfile                 dem_big_buildings.dem
dynamicrainfile                 rain_buildings_29_september_44_mask_original.nc
bcifile                 NY.bci

dirroot                         NY_FV1_GPU_Basin_original
resroot                 NY

FV1
cuda

sim_time                        61200.0
initial_tstep                   1.0
saveint                 1800.0
massint                 1800.0

manningfile                     manning_big.n.asc

netcdf_out
elevoff
voutput
checkpoint      1800.0
```

Figure 42: Example of parameter file

The general structure of the parameter file shown in Figure 42 where are defined the main command used for the simulations of this thesis.

The commands are:

- *DEMfile: name of the DEM file*
- *dynamicrainfile: name of the NetCDF file that represents the spatial and temporal dynamic rainfall*
- *bcifile: name of the boundary conditions file*
- *diroot and resroot: name of the folder of the results and prefix of the results*
- *FV1: type of solver to use*
- *cuda: that specifies to the model to use GPU solver*
- *sim_time, initial_tstep: total simulation time and start time*
- *saveint and massint: time of saving of the results*
- *manningfile: name of the file of the surface roughness*

- *NetCDF_out, elevoff, voutput: specific optional command to create or to stop specific outputs*
- *checkpoint: time of the creation of a checkpoint file to have the possibility to restart the simulation from that file*

CHAPTER 6
RESULTS RC APPROACH

In this chapter are reported the results of the RC approach implementation using the LISFLOOD-FP 8.1 hydrologic model compared with a baseline simulation where all the buildings were modelled with a RC=1.

These results were obtained considering two values of RC coefficients, one for Sloping Roofs and one for Flat Roofs.

These coefficients are defined following the National Roofing Contractors Association guidelines (https://www.nrca.net/) which affirm that for sloping roofs the most popular roofing materials are asphalt shingles while for flat roofs the more popular roofing solutions are modified bitumen, single-ply membranes and slate.

According to what said before the RC coefficient used are:

- Flat roofs: RC=0.76
- Sloping roofs: RC=0.9

As described in Chapter four the RC method aims to obtains the water harvesting capacity of the roofs, so what is in general expected in the results is a decrease of the averaged flood water depth in all the studied urban drainage basin.

This result is correctly visible in Figure 43 and Figure 44, where it is possible to notice that the RC approach application causes a reduction of the 14% of the averaged flood water depth.

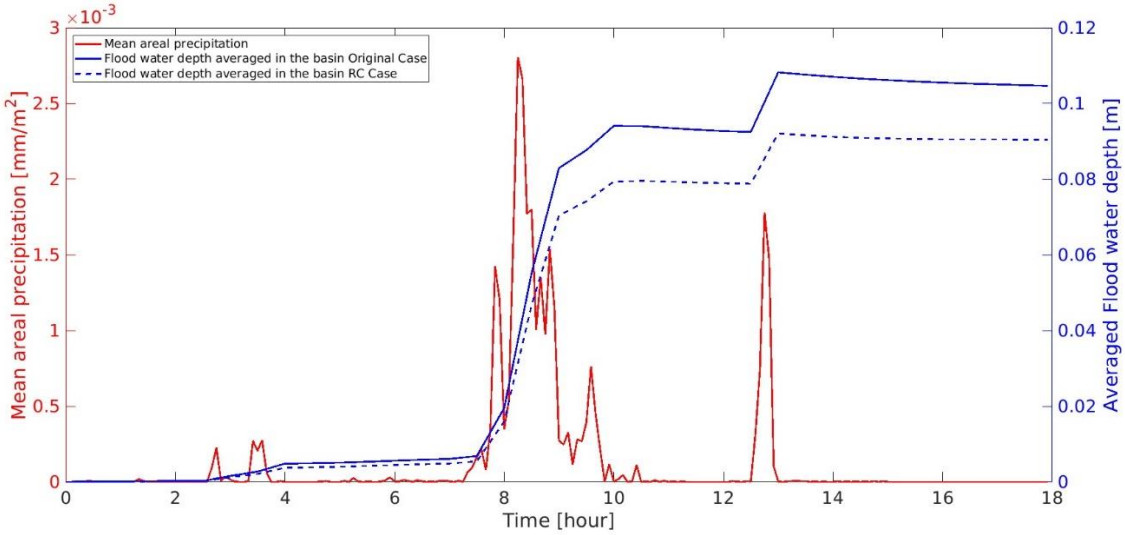

Figure 43: Mean areal precipitation and flood water depths averaged in the basin, RC approach results

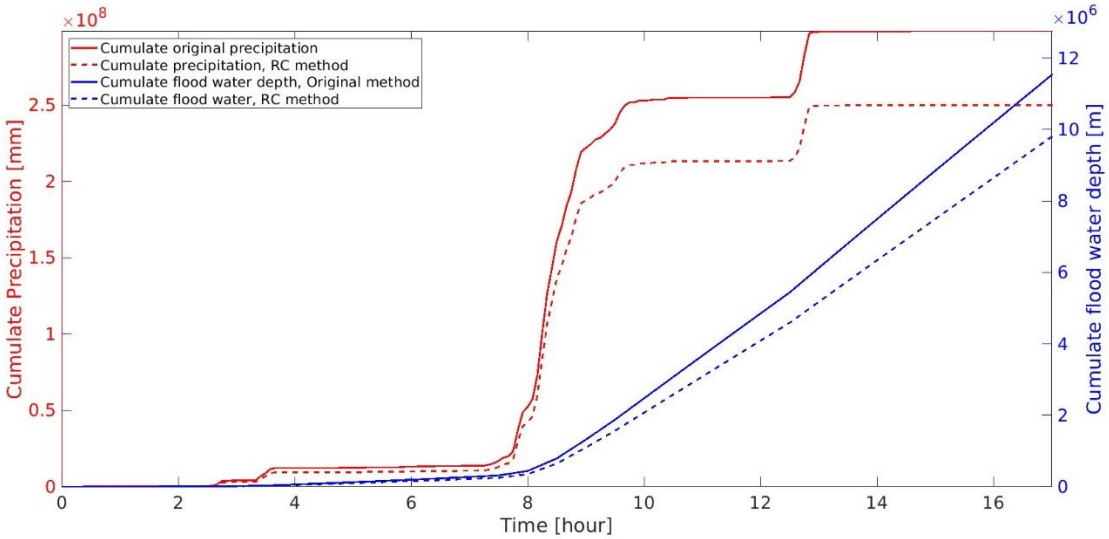

Figure 44:Cumulative precipitation and cumulative flood water depth, RC approach results

The previous graphs represent an analysis on the overall volume of flood water in the entire area of study.

To better understand and visualize the contribution of the method is necessary to analyse the results of the max flood water depth by the software represented on Figures 45-50.

These Figures represent a more accurate results of the contribution of the RC approach respect to the specific urban characteristics.

According to what said before there are areas of the basin in which the differences from the water depths value before and after the RC method application are of about 10-12 cm, and so a specific reduction of the 30% of the water depth.

These areas, that correspond to the one in Figure 47, where the variation between the values of the Baseline and of the RC is higher, are the most injured during a pluvial flood event and in fact are the one in which are positioned the monitoring instruments of the NYC FloodNET system.

In general, the RC approach, as reported by the survival function in Figure 51 furnishes a trend of this method is that there is a higher reduction of the flood water respect to the baseline case for higher water depth values.

Finally, a sensitivity analysis (Figure 52) was conducted to better understand how much the changing of these coefficients could affects the model results.

The RC coefficients used to this analysis are estimated by a research study about the quantification of the runoff retention of the extensive green roofs (Liu et al., 2020).

In this analysis all the building roofs were considered as green roofs, and two cases were taken in consideration:

- Wet Green Roof: RC=0.75
- Dry Green Roof: RC=0.58

Although these results try to show the real contribution of the roof in the storm water runoff on an urban drainage basin, it is important to underline that more detailed results could be obtained, acquiring more detailed information about the roofs characteristics.

Two sets of data very useful to implement more accurately simulations are:

- Roofs construction materials
- Total height of precipitations in a yearly basis for each roof, because in that way it will be possible to calculate a specific RC for each roof

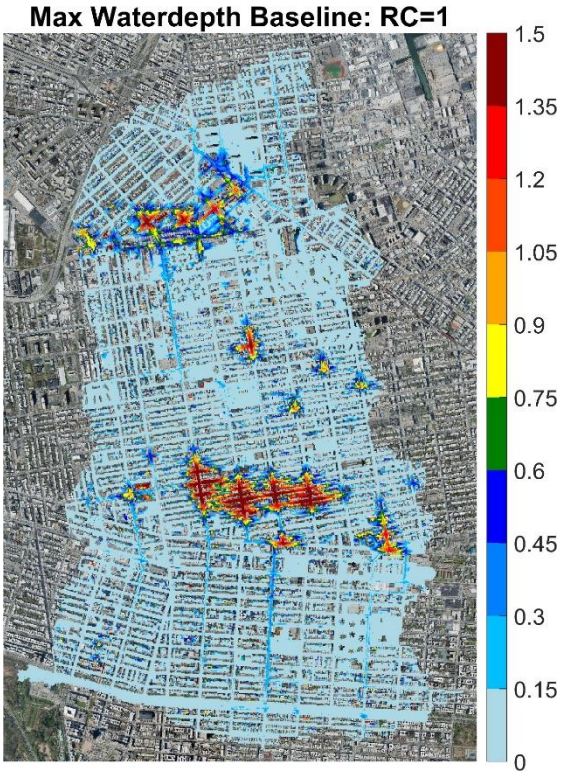

Figure 45: Water depth max: original case, RC=1

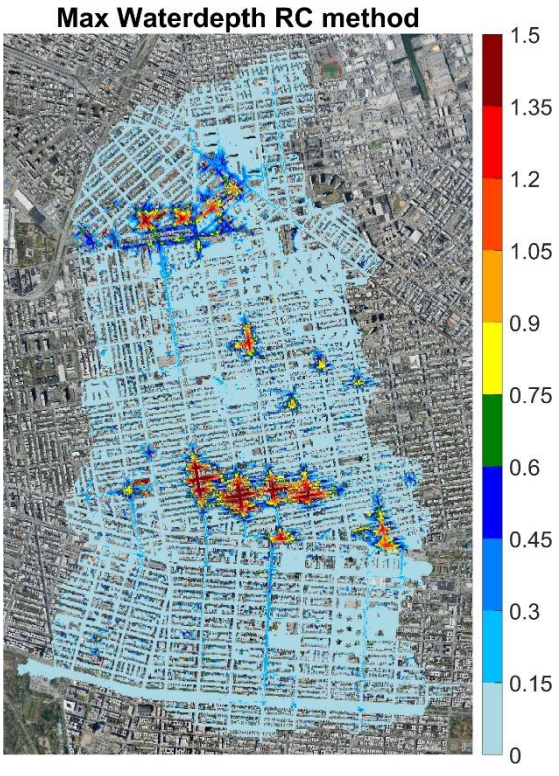

Figure 46: Water depth max: RC case, RC=0.8 (Flat roofs), RC=0.8 (Sloping roofs)

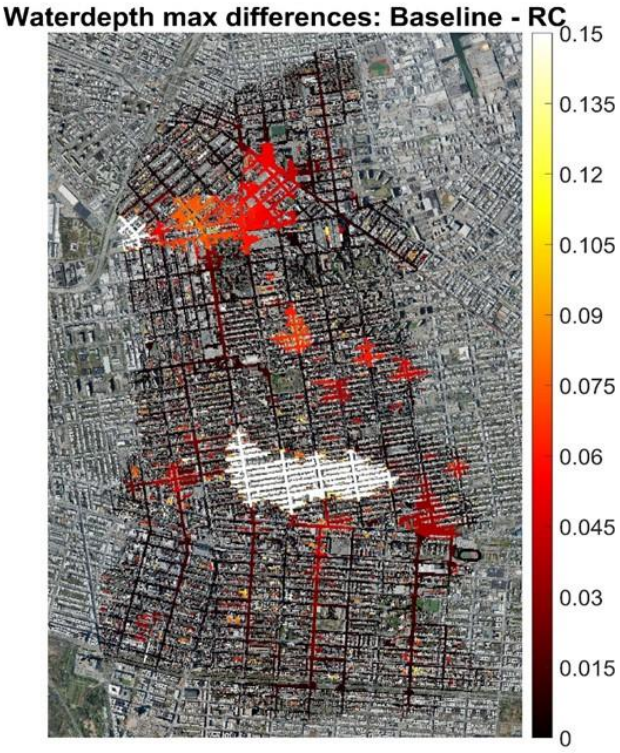

Figure 47: WD max variations: results of the subtraction of the values of the Baseline case values minus the RC case values. Positive values represent the flood water reduction.

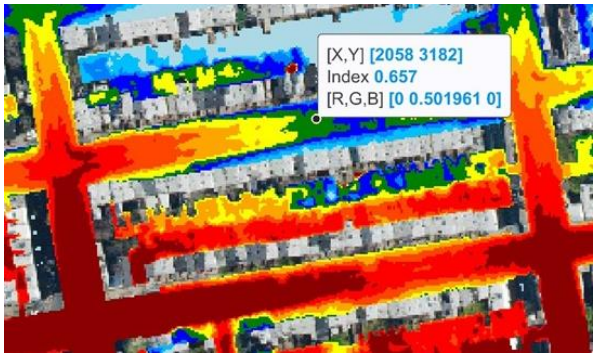

Figure 48: Detail of water depth: original case, RC=1

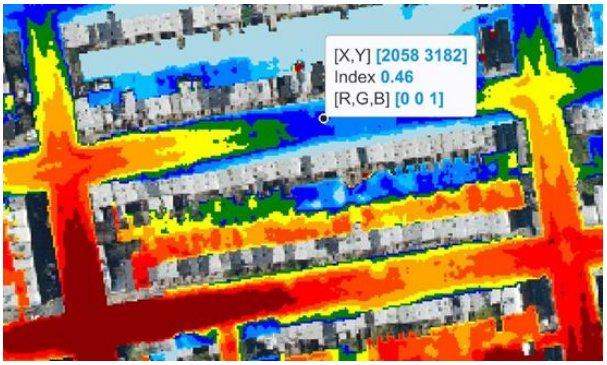

Figure 49: Detail of water depth: RC case, RC=0.76 (Flat roofs), RC=0.9 (Sloping roofs)

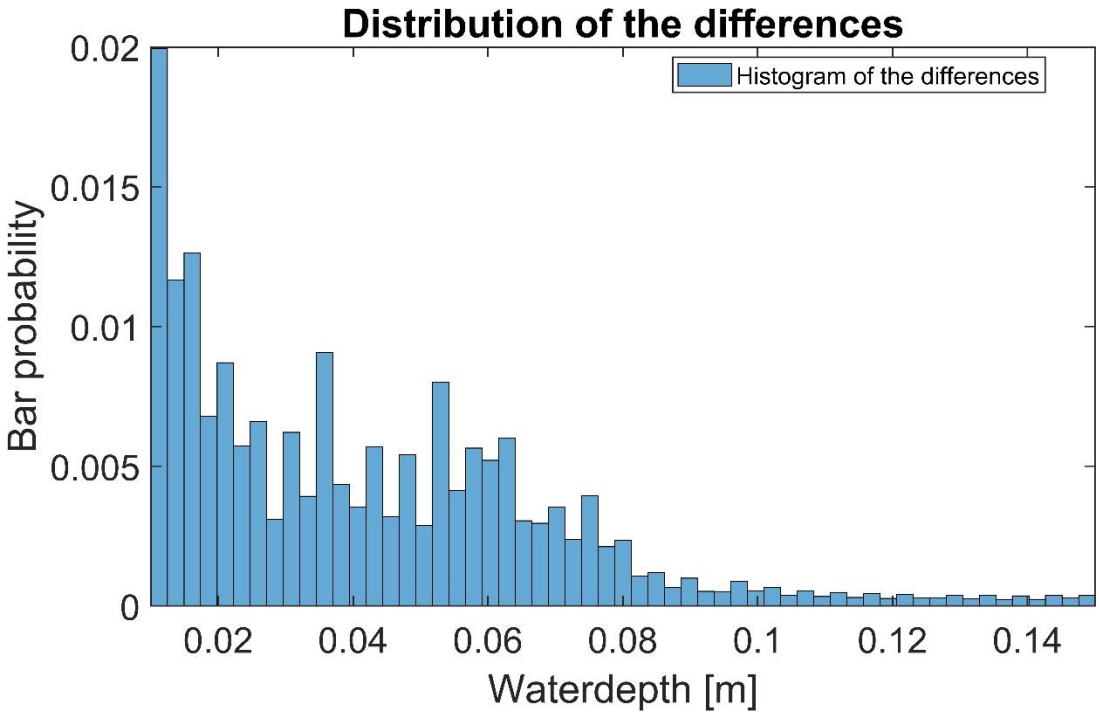

Figure 50: Histogram of the water depth differences of Baseline - RC method. Plot of the distribution of the variations. The sum of all the bar probability is equal to one.

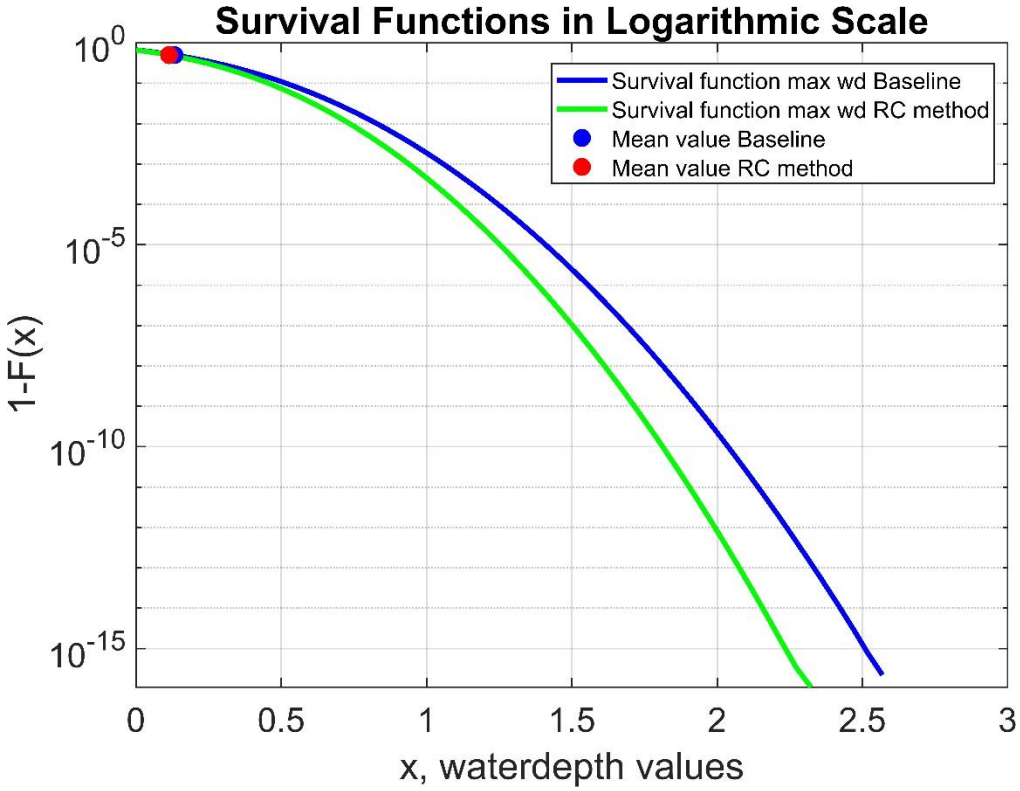

Figure 51: Survival Functions of the Baseline case and the RC case

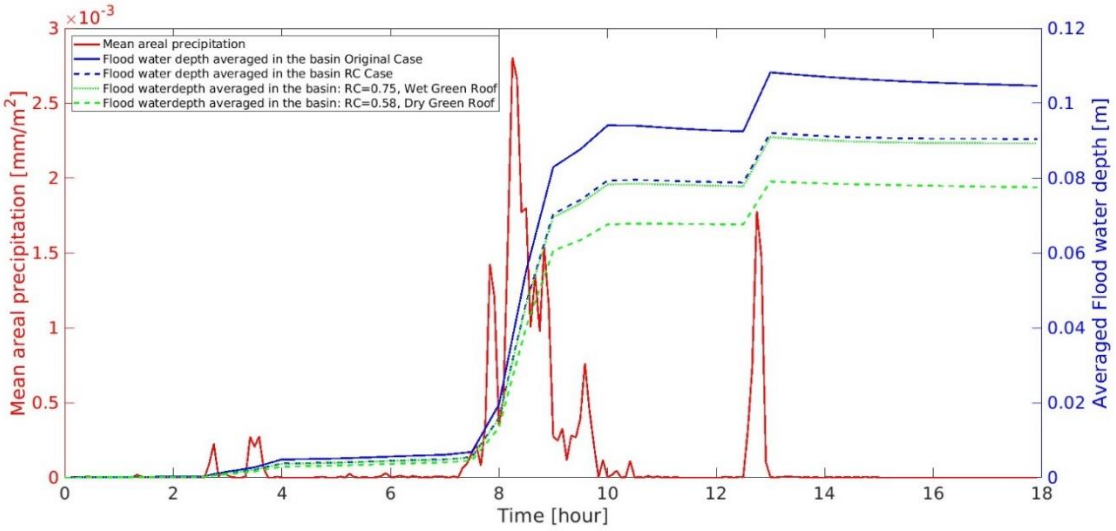

Figure 52: Sensitivity analysis of the RC approach

CHAPTER 7
RESULTS BIRR APPROACH

In this chapter are described the results of the implementation of the building induced rainfall redistribution method (BIRR) on the urban drainage basin object of this thesis using LISFLOOD-FP.

Like the results of the RC method, also for this case, was made a comparison with the same baseline data so without the redistribution of the rainfall in each downspout and with the RC coefficient equal to one.

Compared to the RC approach, the BIRR approach does not influence consistency in the overall volume of rainfall that interest the area of study as it is possible to see in Figure 54.

In this case, the goal is to understand how the distribution of the rainfall in the downspouts, and so a condition closer to reality, changes the flow dynamics of the stormwater runoff in the urban tissue of the studied area.

To comprehend better this contribution was decided to perform two different analyses, one on the simulated water depth and one on the simulated velocity, where the velocity that was studied is the vectorial sum of the velocity referred to the x axes and of the velocity referred to the y axes.

The flood water results show that the BIRR approach does not have a high influence on the overall volume of the flood water depth in the basin with respect to the baseline case.

In fact, as shown in Figures 53 and 54, there is a reduction of the water depth estimated during the flood event only of 2%.

This variation, although it is very low, is proof of a changing in the dynamics of the flow of the water.

This behaviour is interesting denoted in the max water depth variations in Figure 57. That figure was determined by the subtraction between the BIRR approach values (Figure 56) and the Baseline values (Figure 55). The values obtained from this operation show that there are two different types of variations:

- In the simulation area that corresponds to the outflow zone from the model grid there is a reduction of the flood water between 40% - 50%.
- The more diffuse variation is a low increase of water depth around 1-2% in the BIRR case, probably due to the different flow dynamics (Figure 58)

The sum of these two contributions determines the complex reduction of the overall flood water in the basin.

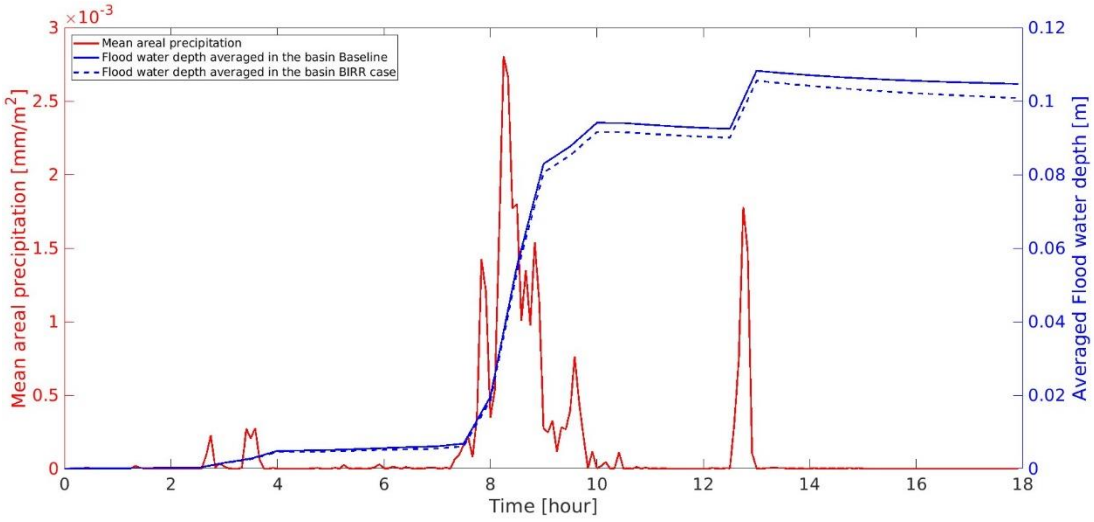

Figure 53: Mean areal precipitation and flood water depths averaged in the basin, BIRR approach results

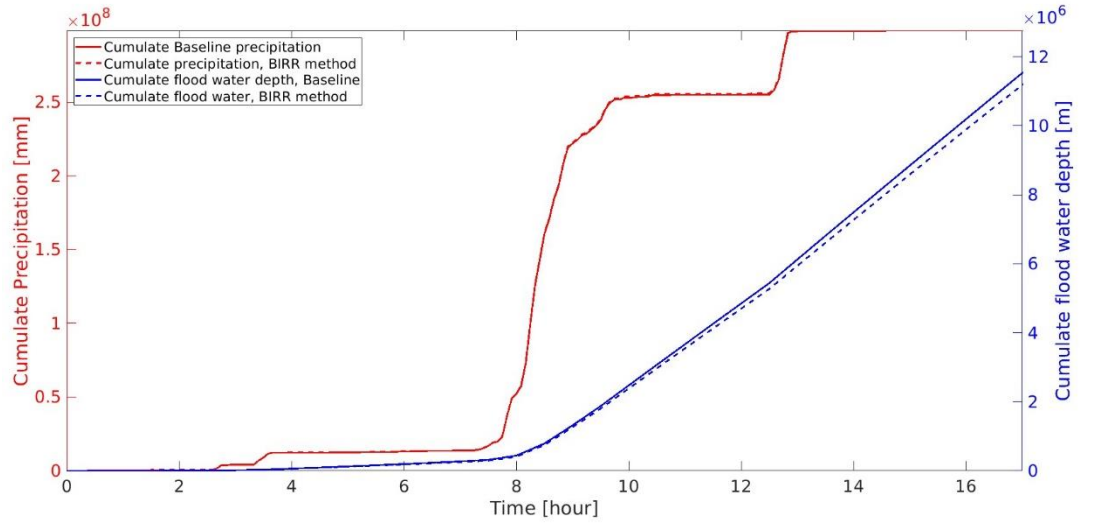

Figure 54: Cumulative precipitation and cumulative flood water depth, BIRR approach

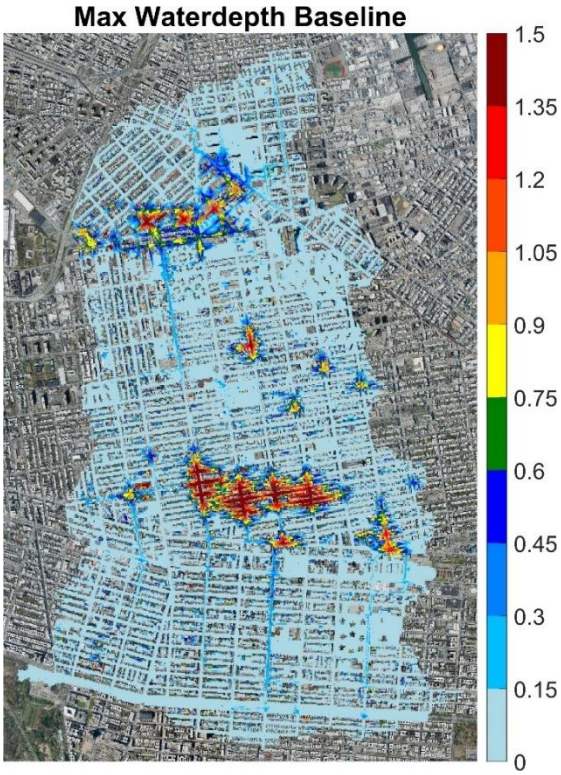

Figure 55: Water depth max [m]: Baseline

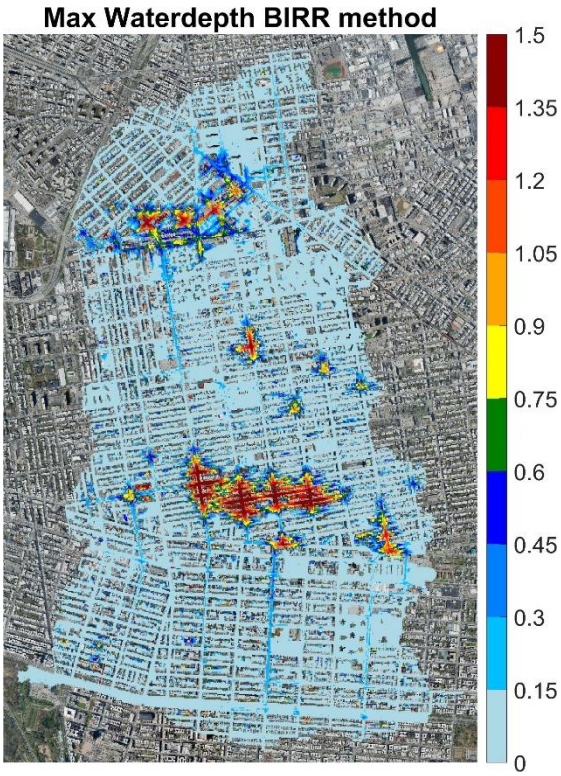

Figure 56: Water depth max [m]: BIRR case

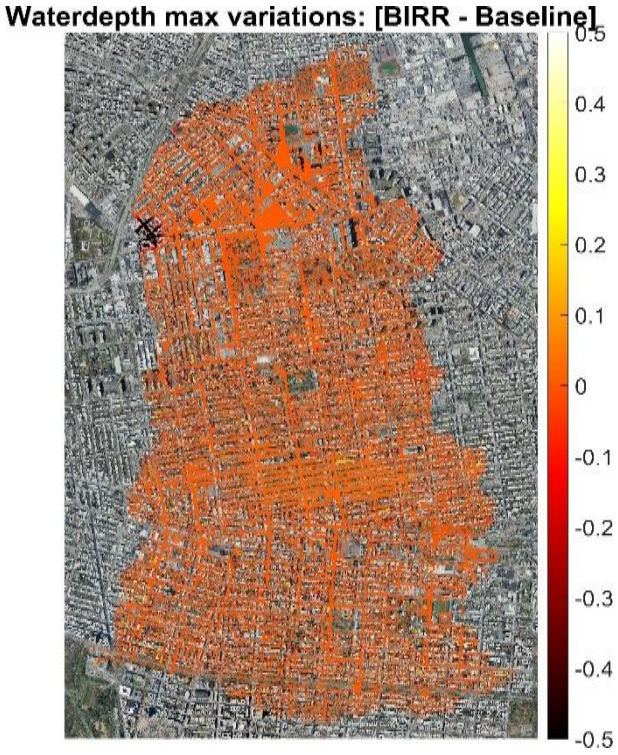

Figure 57: Water depth max variations [m]: results of the subtraction from the BIRR case values minus the Baseline case values. Positive values define an increase of water depth, and negative values a decrease of water depth.

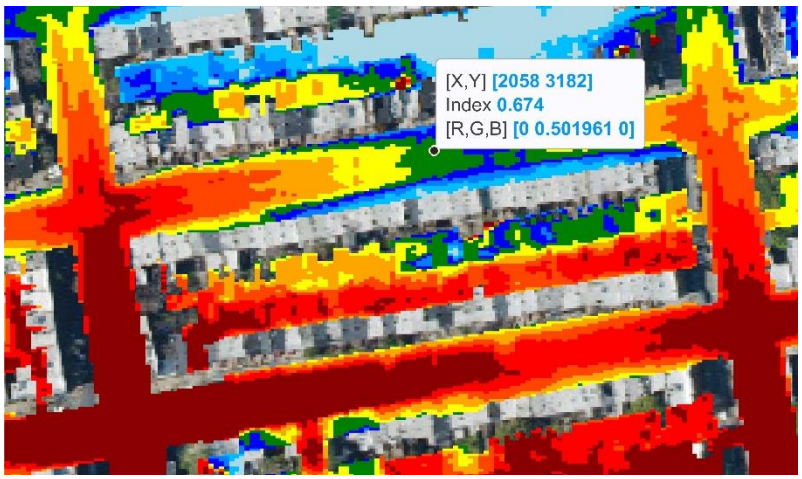

Figure 58: Detail of water depth: BIRR case. The value shown in the figure is 3% higher than the value of the Baseline case

Since the BIRR method application does not produce considerable changes in the overall flood water depth respect to the baseline case, to focus on the BIRR approach contribution, as

introduced in the first part of the chapter, was paid attention to the velocity calculated during the simulation.

This analysis aims to understand if the rainfall redistribution in the downspouts changes the velocity dynamics of the water in the studied drainage basin.

In the first step was calculated the cell velocity (V_c) for each time step, using the LISFLOOD-FP manual (Bates et al., 2013) where the sequent equation is defined, where V_i and V_j area V_x and V_y:

$$V_{c_{i,j}} = \left(\left[\left(V_{i-\frac{1}{2},j}, V_{i+\frac{1}{2},j} \right) \right]^2 + \left[\left(V_{i,j-\frac{1}{2}}, V_{i,j+\frac{1}{2}} \right) \right]^2 \right)^{0.5}$$

(15)

After calculating V_c for each time step was created a matrix where to each cell was assigned the max velocity values during the simulation to see the overall difference between BIRR and Baseline case. The result of this procedure is represented in the max velocity maps in Figures 59 and 60. These maps show that also the velocity vectors of the BIRR method are very similar to the one of the baseline cases, with maximum variations between -0.3 and 0.3 m/s (Figures 61,62,63).

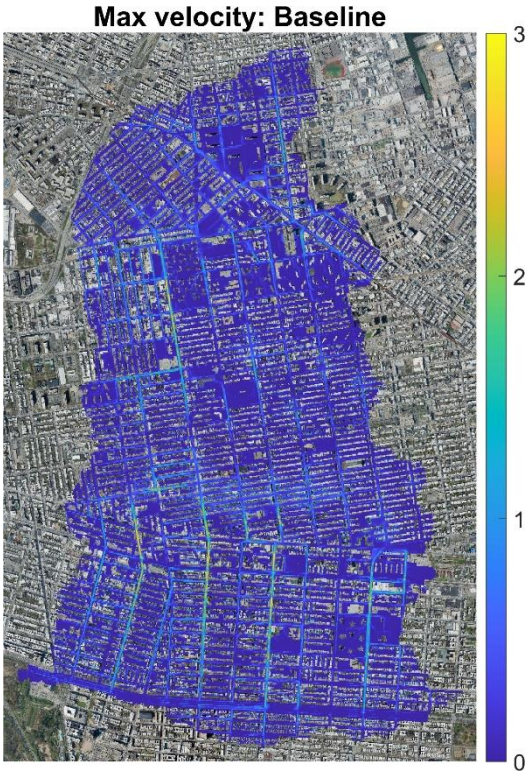

Figure 59: Max velocity map [m/s]: Baseline case

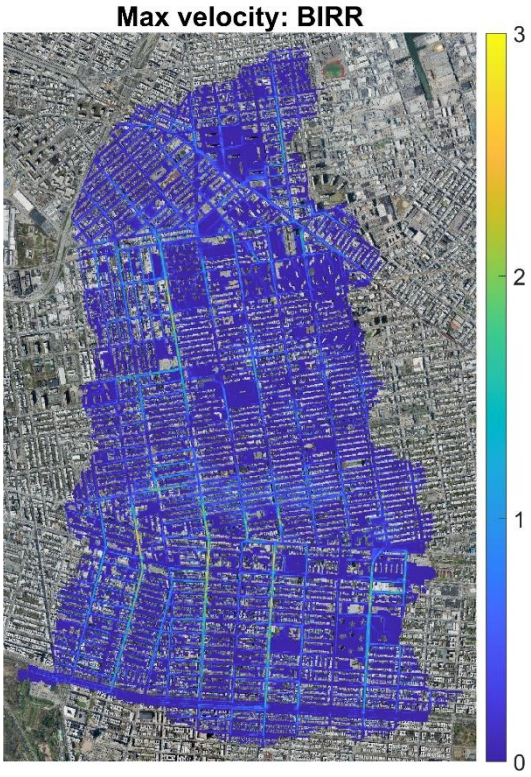

Figure 60: Max velocity map [m/s]: BIRR case

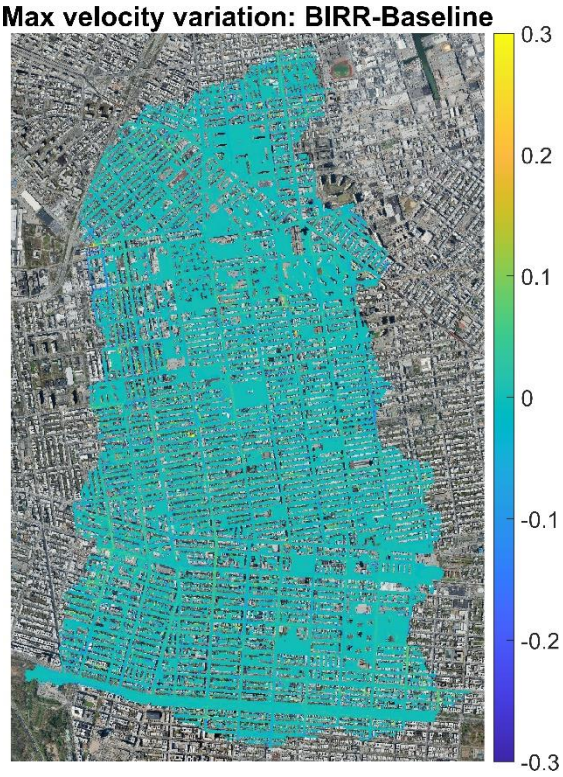

Figure 61: Max velocity variations: Baseline case - BIRR case. The map shows a general maximum variation from -0.3 to 0.3 m/s. The yellow color means that the BIRR method produces higher velocity, the blue color that produces lower velocity

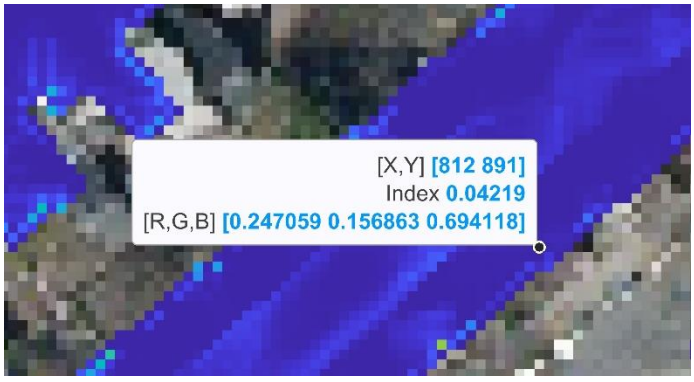

Figure 62: Focus velocity Baseline case around the downspout of a Building

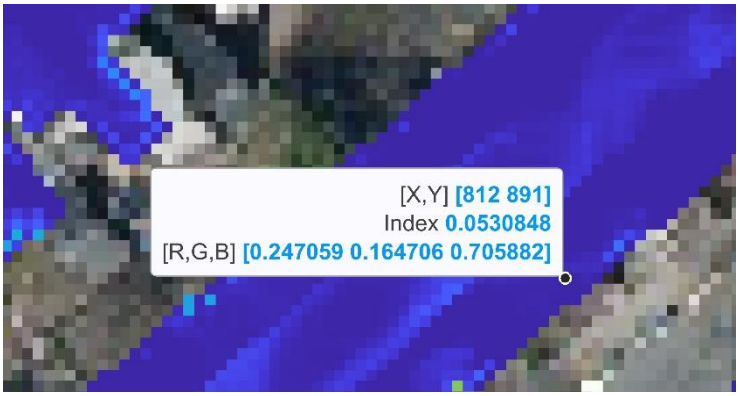

Figure 63: Focus velocity BIRR case around the downspout of a Building. The BIRR method determines an increase of 30% compared to the Baseline case

Knowing the velocities and the water depth values, it was decided to do focus on a single cell (Figure 64) around a downspout to see what is the specific contribution of the BIRR for each time step of the simulation. Figure 65 represents a clear dynamic of the storm runoff on the BIRR case, in which both water depth and velocity have higher values with respect to the Baseline case.

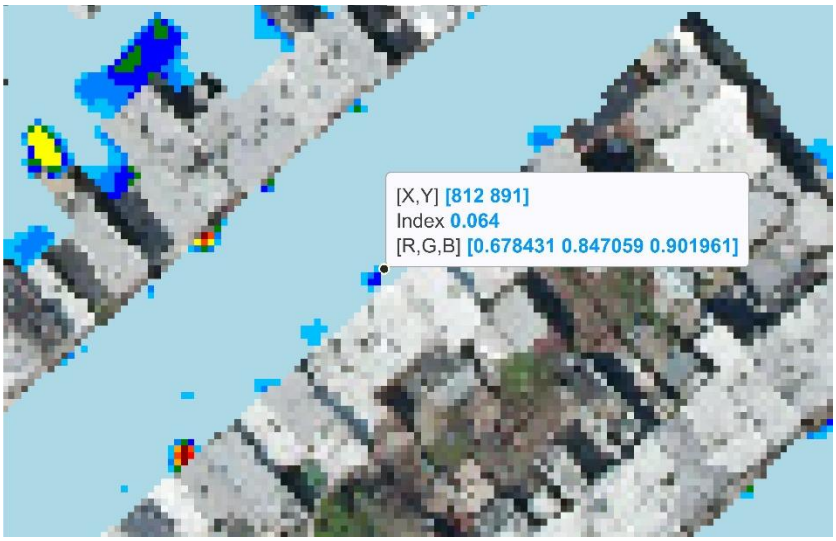

Figure 64: Focus cell value around the downspout. The downspout presence is characterized by a circular area adjacent to the edge of the area of the building.

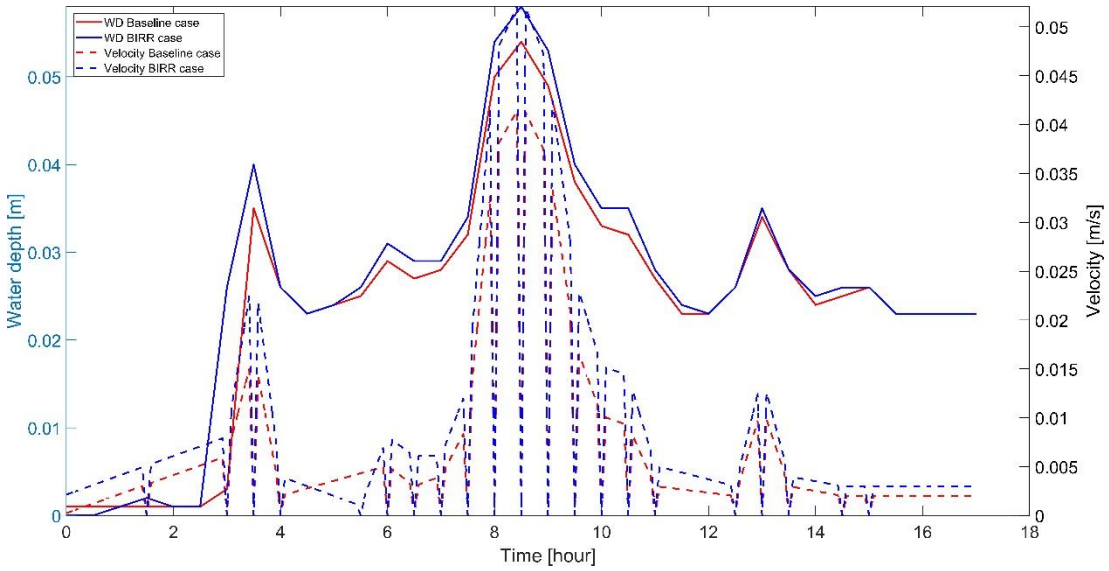

Figure 65: Water depth and Velocity trend in the cell (812,891) of Figure 64. The red lines are referred to the Baseline case, the blue lines are referred to the BIRR case

The second step of the analysis of the BIRR results, related to the study of the velocity, was the calculation of the map of the vulnerabilities or instabilities of the area of study for the vehicle and the people during the studied pluvial flood event of September 29, 2023.
The inputs to create these maps are the velocity V_c calculated before (Equation 15) and the simulated water depth obtained from LISFLOOD-FP for each time step.

These maps, which are obtained by coupling water depth and velocity with a specific procedure, are representative of the risk of instability, so the possibility of movement due to the velocity and height of the water, during the flood event and could help to analyse if the small changes of the results of the BIRR method respect to the baseline influence the final vulnerability of the studied urban system.

The specific procedure to apply the method of Arrighi et al., (2015), (2017) that permits to define the map of the area of stability and instability for people and vehicles.

The first step of the method is the calculation of the Froude number (Equation 16) in each cell of the grid using the water depth (H) and the velocity (V_c).

$$Fr = \frac{V_c}{(g \cdot H)^{1/2}} \quad \textit{(16)}$$

Where g is the gravity acceleration and is equal to 9.81 m/s^2.

Then knowing the Froude numbers, the method proposes two equations, one for the vehicles and one for the people.

The equation for the vehicles is:

$$\frac{H_{crV}}{H_V} = -0.05 \cdot Fr + 0.34$$

(17)

where H_{crV} is the critical water height that destabilizes the vehicles and H_V is the height of the vehicle that in this case was taken as 1.5 meters that is the mean height of a car in New York City according to the census.

The equation for people is:

$$\frac{H_{crP}}{H_P} = \frac{0.29}{0.24 + Fr}$$

(18)

where H_{crP} is the critical water height that destabilizes the people and H_P is the height of the people that in this case was taken as 1.77 meters is the mean height of a person in New York City according to the census.

Finally, H_{crV} and H_{crP} were compared with the max water depth calculated by the model.

The instability is defined according to the sequent criteria:

- $H_{crV} > H$: the vehicle is instable and in the map is assigned a value equal to 1
- $\frac{H}{H_{crP}} > 1$: the person is instable and in the map is assigned a value equal to 1

This procedure was implemented for each timestep. Then to can compare easily the differences between BIRR case and Baseline case, two instability maps, one for people and one for vehicles, for each method, where was assigned to the map's cells values equal to one if during the simulation at least one time that cell was characterized by $H_{crV} > H$ or $\frac{H}{H_{crP}} > 1$.

The described procedure was implemented using MATLAB software and the code is reported in Appendix A.

The application of this procedure furnishes a series of interesting results that are useful to understand better what the BIRR case causes in the dynamic of stormwater runoff.

Figure 66 illustrates the trend of the minimum critical heights calculated in the basin for both the BIRR and Baseline cases throughout the simulation time. The observed decrease in critical height corresponds to the increasing rainfall within the basin over time. As a result, the water depth and velocity values progressively increase, influencing the critical height behaviour. Based on the minimum critical height recorded at that moment in time, it appears

that the Baseline case is overall more critical, as it is where lower critical heights are observed for both vehicles and people.

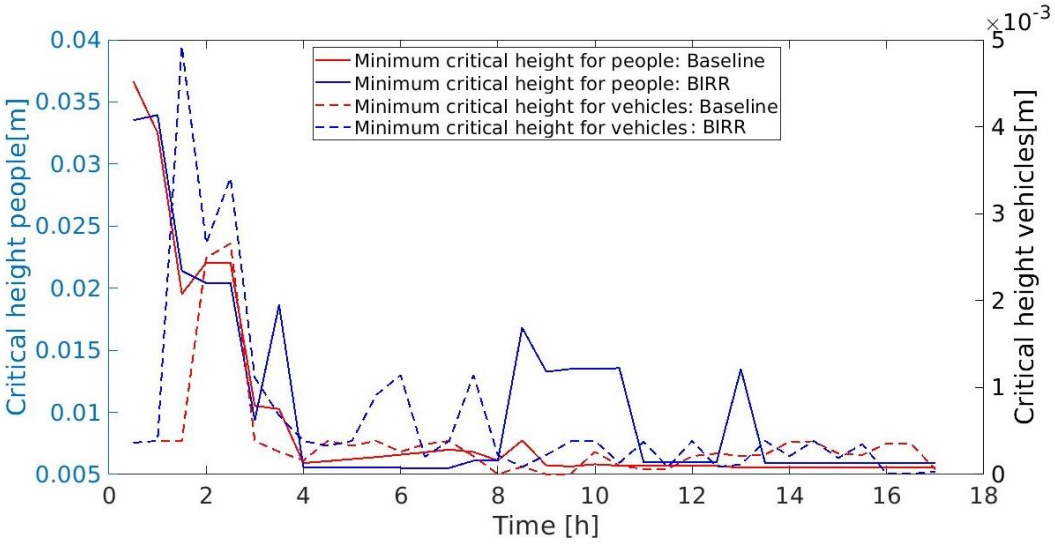

Figure 66: Trend of the critical heights for people and vehicles, for Baseline, BIRR cases

The global analysis of Figure 66 was explored better by analyzing the maps of instability (Figure 67-73) calculated using the assignation criteria of the procedure of Arrighi et al., (2015), (2017).

These maps show that the BIRR case presents greater differences from the Baseline case especially for the instability map for vehicles (Figure 68). Although the more injured areas are the same, the detailed analysis around the buildings shown in Figure 70 represents, with the black line, the pattern of unstable areas due to the presence of the downspouts.

Instead, the maps of instability for people are almost the same between the BIRR and the Baseline case with no particular differences also if focusing on the building perimeter.

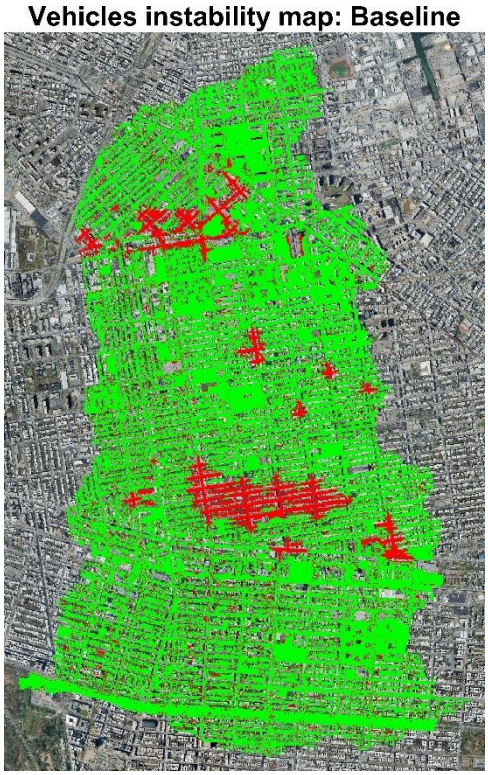

Figure 67: Map of instability Baseline case for vehicles. Red areas are zones of instability that induce the movement of the cars. Green areas are zones of stability

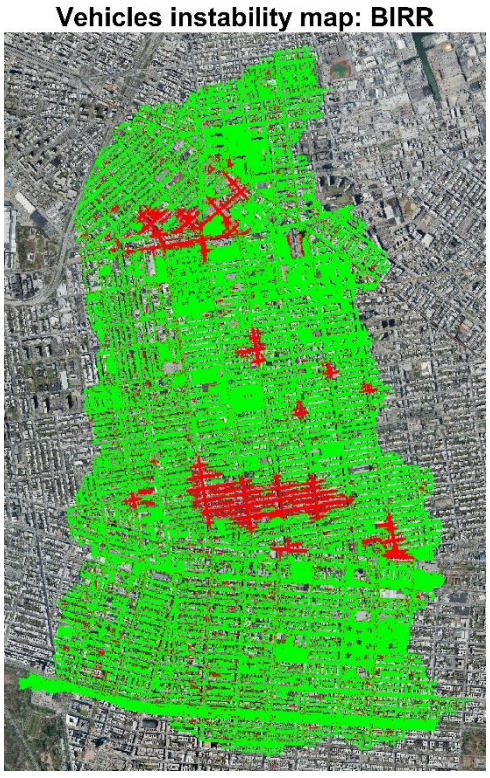

Figure 68: Map of instability BIRR case for vehicles. Red areas are zones of instability that induce the movement of the cars. Green areas are zones of stability

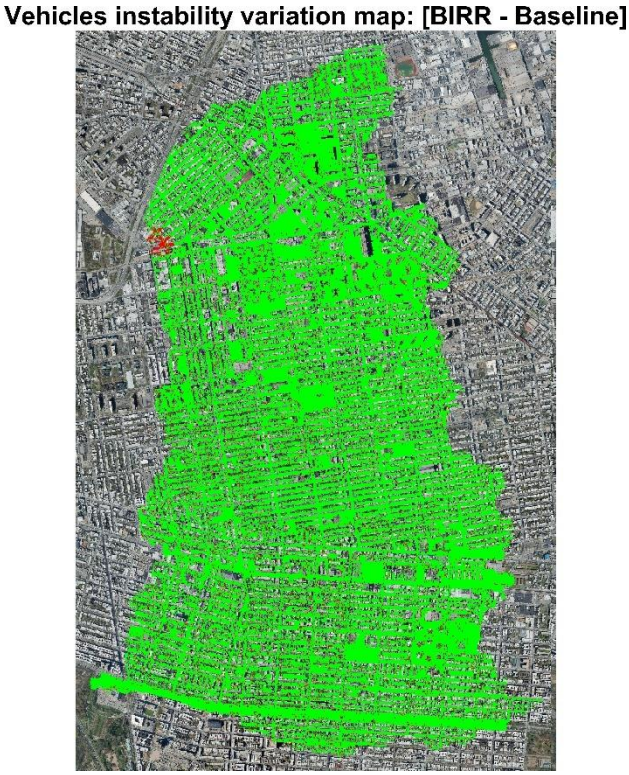

Figure 69: Map of instability area variations for vehicles: BIRR case-Baseline case. Red areas mean instability zones only in Baseline, black areas mean instability zone only BIRR, green no variations areas

Figure 70: Focus map of instability variations for vehicles, BIRR-Baseline. Black variations represent the presence of the instability zone due to the downspout rainfall redistribution

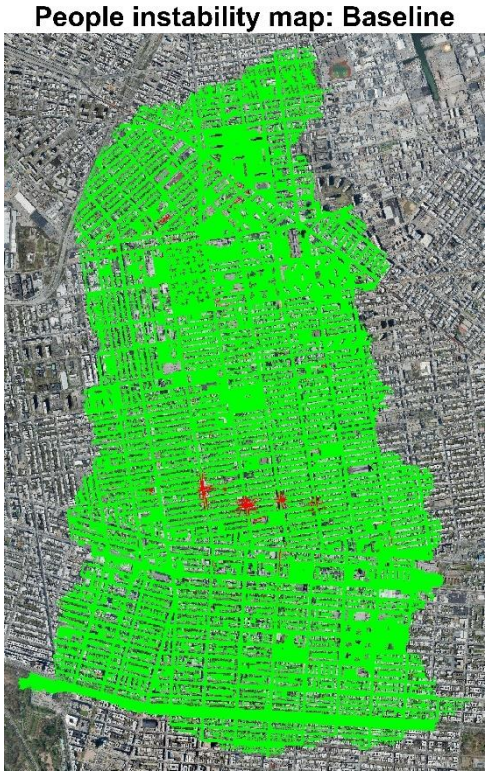

Figure 71: Map of instability Baseline case for people. Red areas are zones of instability that induce the movement of the people. Green areas are zones of stability

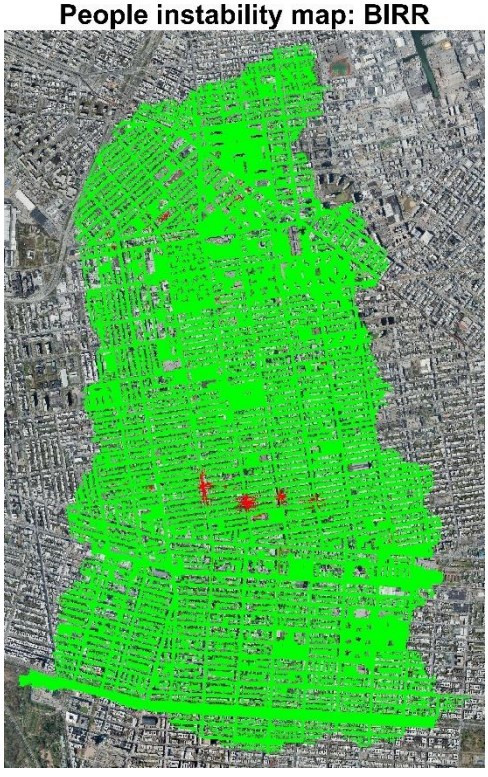

Figure 72: Map of instability BIRR case for people. Red areas are zones of instability that induce the movement of the people. Green areas are zones of stability

Figure 73: Map of instability area variations for people: BIRR case-Baseline case. In this figure there are not significant changes between the two cases and for this most of the areas are green

Furthermore, to have a complete point of view of the method was decided to combine the building induced rainfall redistribution method and the runoff coefficient approach to see if there were changes in the runoff dynamics.

This application shows that the contribution of the BIRR case is the same as that in the Baseline case because as represented by Figures 74 and 75 there is the same decreased percentage of overall water depth.

For what concerned the analysis of the critical heights in Figure 76 the BIRR+RC case is less crucial than the BIRR case for the initial time steps and then remains the same as the BIRR case. BIRR+RC is even less dangerous compared to the Baseline case.

This tendency is visible through the instability maps in Figures 77,78 and 79 where for both vehicle's and people instability map variations there a no particular changes concerning the one reported in Figures 69,70 and 73 except for a low change of extension of the major instability areas essentially due to a decrease of rainfall in the RC approach.

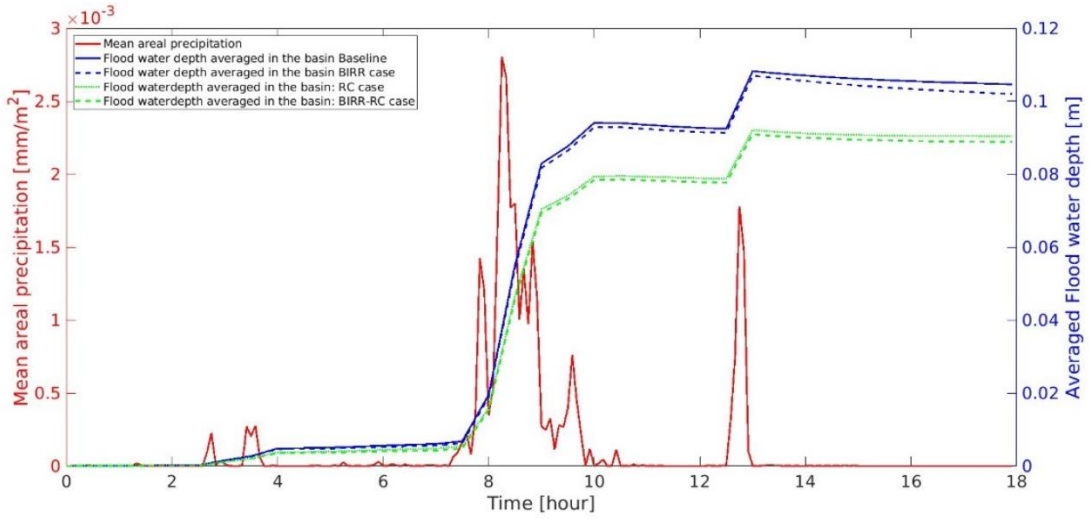

Figure 74: Mean areal precipitation and flood water depths averaged in the basin, approaches comparison

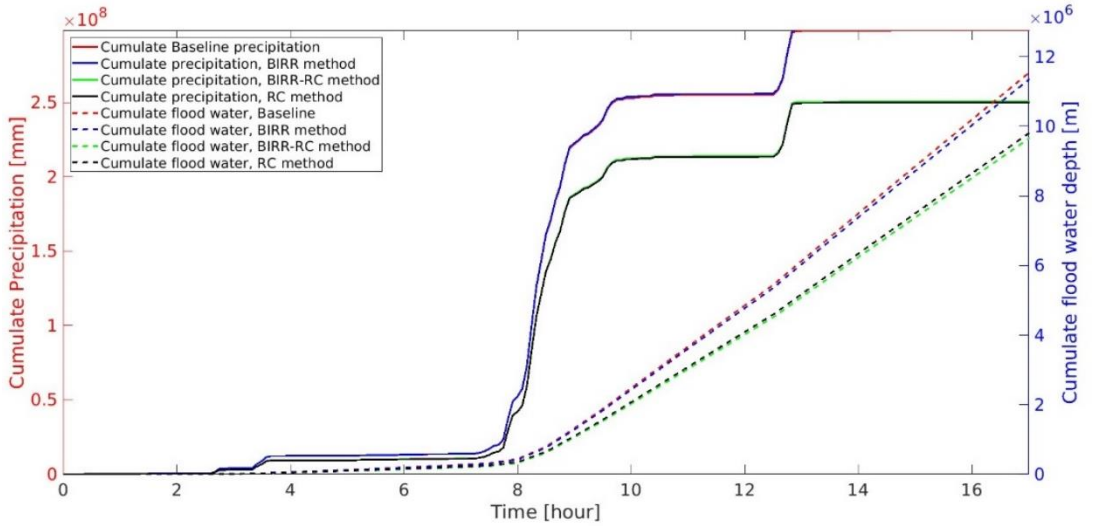

Figure 75: Cumulative precipitation and cumulative flood water depth, approaches comparison

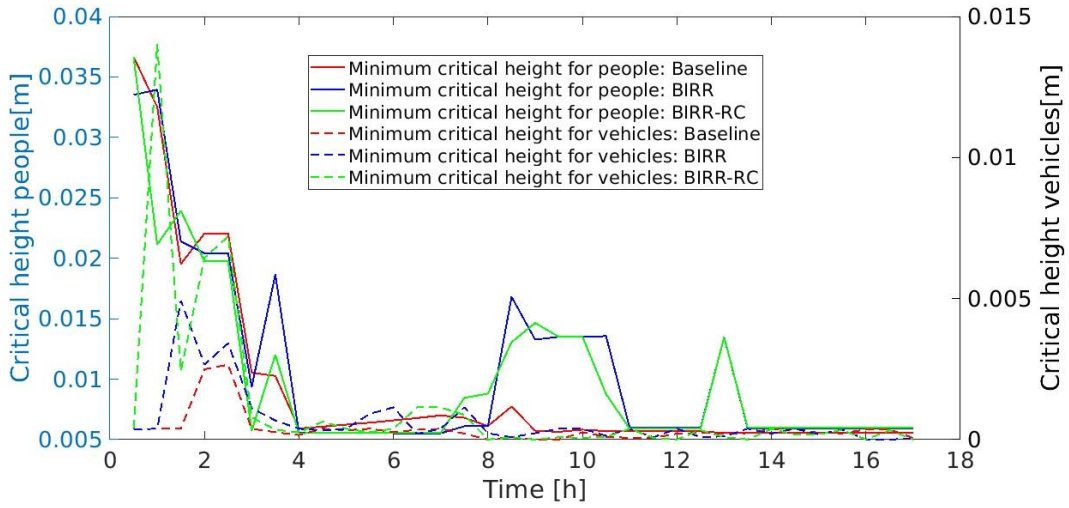

Figure 76: Trend of the critical heights for people and vehicles, for Baseline, BIRR and BIRR+RC cases

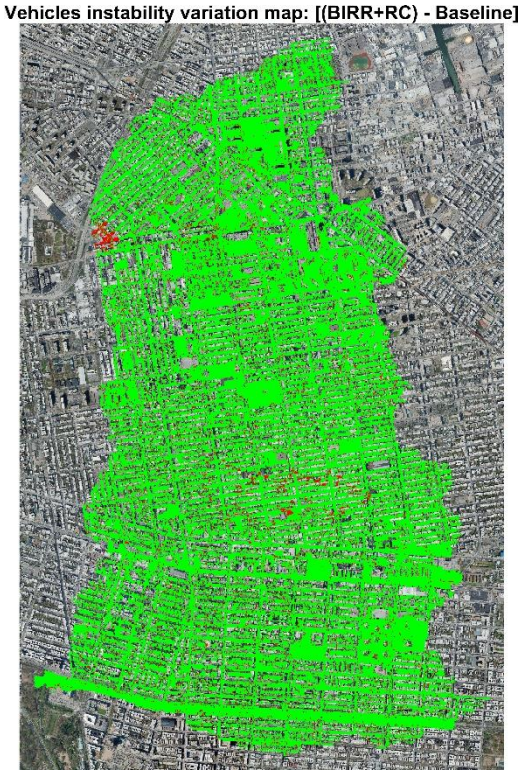

Figure 77: Map of instability area variations for vehicles: (BIRR+RC) case-Baseline case. Red areas mean instability zones only in Baseline, black areas mean instability zone only BIRR, green no variations areas

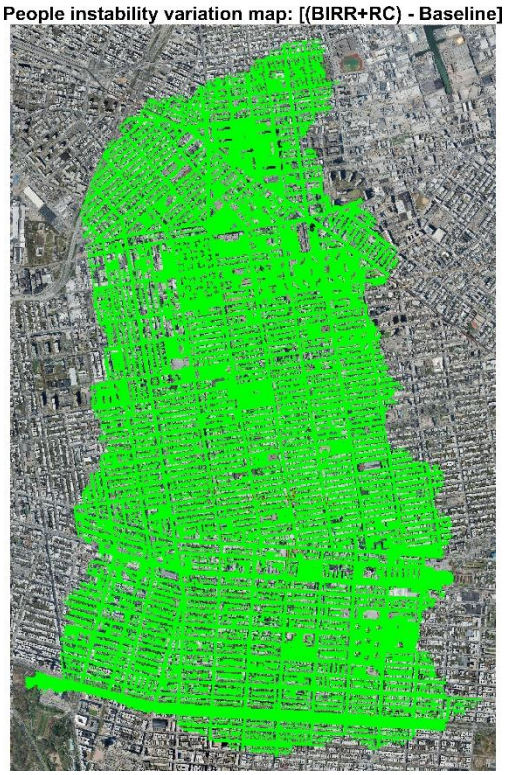

Figure 78: Map of instability area variations for people: (BIRR+RC) case-Baseline case. Red areas mean instability zones only in Baseline, black areas mean instability zone only BIRR, green no variations areas

Figure 79: Focus map of instability variations for people, (BIRR+RC)-Baseline. In this case respect to the BIRR-Baseline case for people with coupling with the RC methods there is a reduction of the vulnerability respect to the baseline as visible from the red areas.

In conclusion, from the analysis of the results of the implementation of the BIRR approach, it is evident that, despite the absence of a significant quantitative difference in water depth and velocity values, a variation in the dynamics of runoff flow can still be observed, as expected. Therefore, I believe that with even more site-specific input data, such as the actual number of downspouts per building or their connection to the sewer network, it would be possible to provide a more realistic representation of an urban flood event.

CHAPTER 8
REAL CASE COMPARISON'S

This chapter reports the comparisons (Figures 80-85) of the floodwater values between the cases simulated in this thesis and the value acquired during the event of September 29, 2023, in New York City by the FloodNET system.

These graphs show that there is a general overestimation of the floodwater amount for all the sensors, probably due to the calibration of the parameters. However, the trend of the simulated cases is like the data acquired by the monitoring system of the city of New York.

The only exception is for the sensor positioned in the outflow area from the model grid where the BIRR case and the BIRR-RC case have a trend very different from the acquired data and the Baseline and RC case.

This difference is representative of the fact that the high variation of the values in this zone using the BIRR approach, as described in Chapter 7, can be considered as an outlier.

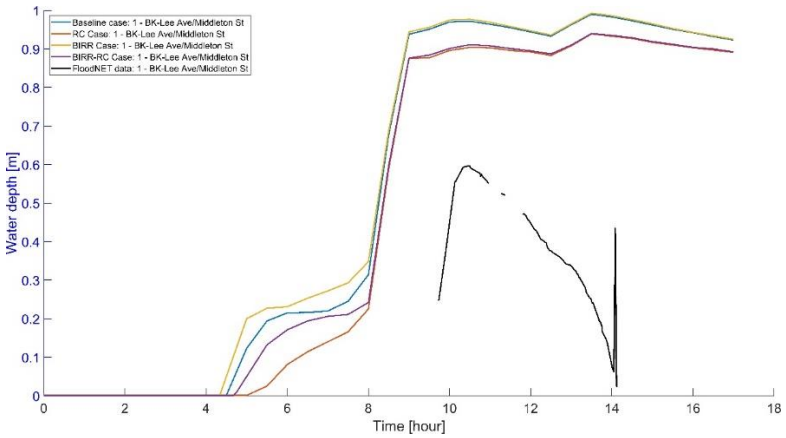

Figure 80: Comparison FloodNET data with modeling results; Sensor 1, BK-Lee Ave/Middleton St

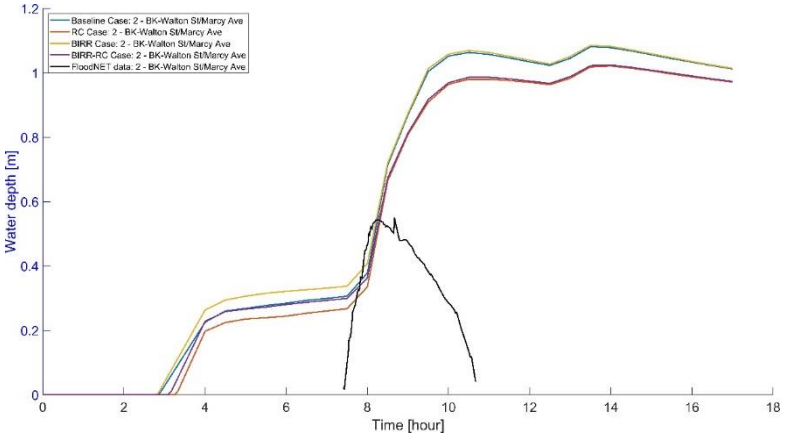

Figure 81: Comparison FloodNET data with modeling results; Sensors 2, BK-Walton St/Marcy Ave

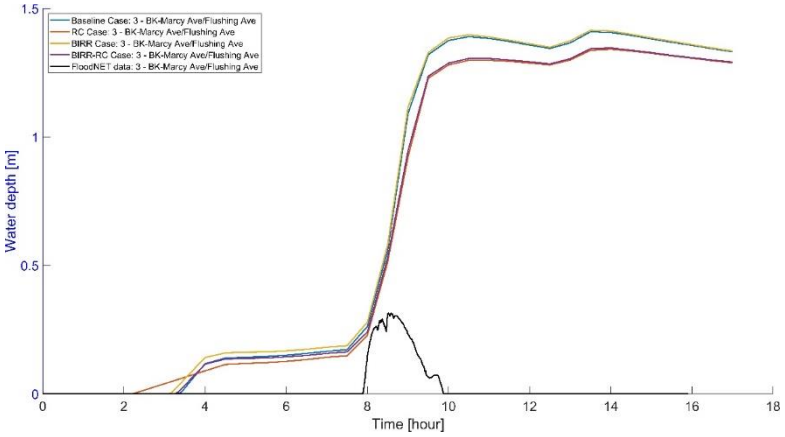

Figure 82: Comparison FloodNET data with modeling results; Sensors 3, BK-Marcy Ave/Flushing Ave

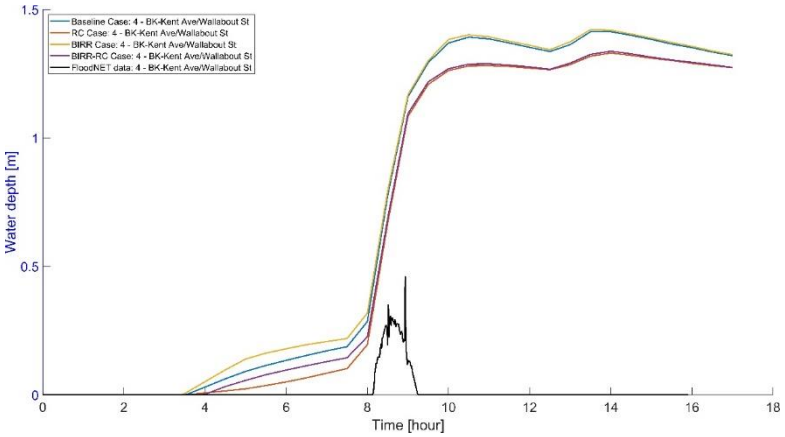

Figure 83: Comparison FloodNET data with modeling results; Sensor 4, BK-Kent Ave/Wallabout St

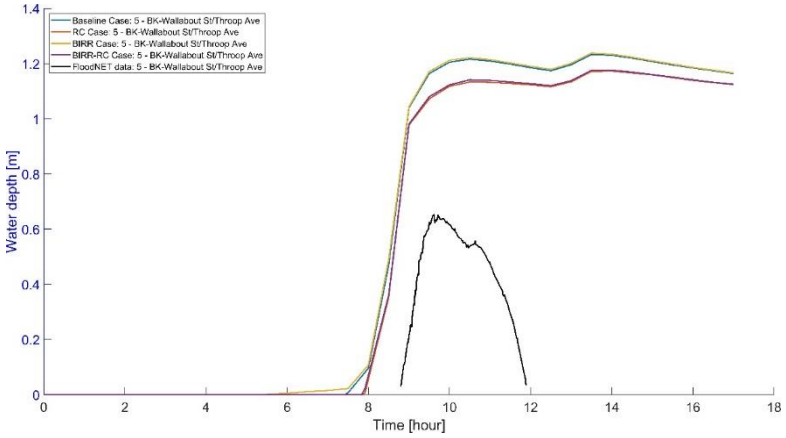

Figure 84: Comparison FloodNET data with modeling results; Sensor 4, BK-Wallabout St/Throop Ave

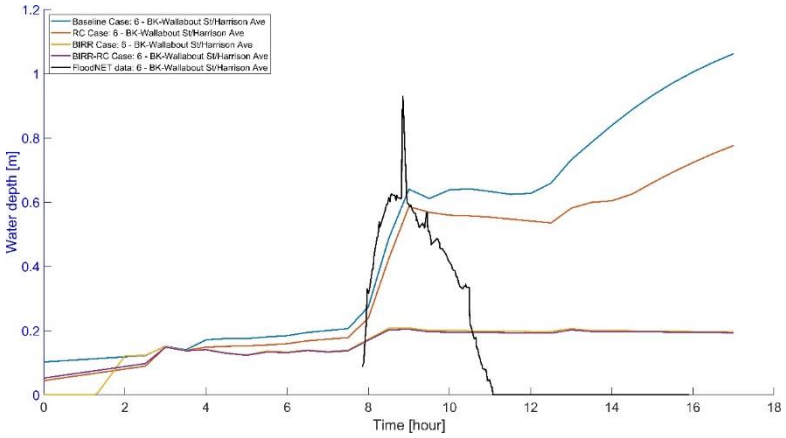

Figure 85: Comparison FloodNET data with modeling results; Sensor 4, BK-Wallabout St/Harrison Ave

CONCLUSION

This thesis analyzed the flooding event of September 29, 2023, in New York City, focusing on the role of building roofs in stormwater runoff dynamics within an urban drainage basin during a pluvial flood.

Our research began with an exploration of different approaches to incorporate these urban infrastructures into flood modeling. We then implemented several selected methods in the LISFLOOD-FP two-dimensional hydrodynamic model with the development of dedicated codes to deal with elements that were not implemented in the original version of the model. Then, the model was applied to a real pluvial flood, and results were validated using data from FloodNET, New York City's flood monitoring system, which recorded the conditions during the event.

The modeling confirmed that runoff from building roofs plays a significant role in stormwater dynamics. Comparing different modeling methods allowed us to identify which components most strongly impact pluvial flood dynamics, highlighting the most effective approaches for urban flood studies.

The approach developed in this thesis provides a valuable foundation for future research, as well as to provide support to the design of drainage infrastructures. Access to more detailed and complete data on roof and downspout characteristics could substantially enhance the accuracy and impact assessment of this methodology.

In conclusion, we believe this work offers a promising tool for evaluating pluvial flood hazards in urban areas, potentially improving mitigation strategies and emergency responses for urban flood management.

APPENDIX A
MATLAB CODES

A.1 Code to create the manning raster file from the land cover raster file

```
%Step 1: read DEM (Digital elevation model) and LC (Land cover)
[Dem,R]=readgeoraster("C:\Users\Utente\OneDrive - Politecnico di
Torino\Desktop\DEMBasinNaNBuildings.tif"); %this is for semplicity because
is a raster with the correct extension
[LC,Rlc]=readgeoraster("C:\Users\Utente\OneDrive - Politecnico di
Torino\Desktop\TESI Phoenix\Tesi_New_York\Qgis\LC_Basin.tif");

%Step 2: assign the right coefficient
Dem(LC==6)=0.013;
Dem(LC==3)=0.02;
Dem(LC==4)=0.03;
Dem(LC==8)=0.033;
Dem(LC==2)=0.1;
Dem(LC==7)=0.2;
Dem(LC==1)=0.05;
Dem(LC==5)=NaN;

%Step 3: overwrite the new geottif to the original dem
geotiffwrite("C:\Users\Utente\OneDrive - Politecnico di
Torino\Desktop\DEMBasinNaNBuildings.tif",Dem,R,"CoordRefSysCode",'EPSG:269
18');
```

A.2 Code to distribute the rainfall in the edge of the buildings

```
%Step 1: initialization of the variables
path_read = "C:\Users\Admin-VM\Desktop\";
rain_roofs_depth=load(path_read+'Pioggia_29_17h.txt');
dt=[0:5/60:17];

%Step 2: initialization of the mask to change with zero the values outside
the basin
[Mask,RM]=readgeoraster('C:\Users\Admin-
VM\Desktop\QGIS\Maschera_bigBasin.tif'); %this a mask that contains value
1 where there are data to plot and value 2 where there data to don't plot
threshold=2;
mask_= Mask<threshold;
mask=single(mask_);
plot_mask=zeros(size(Mask));
plot_mask(mask==0)=NaN;
plot_mask=~isnan(plot_mask);
```

```
%Step 3: read the GeoTIFF
[BR, R] = geotiffread('C:\Users\Admin-VM\Desktop\Land
cover\Roof_type_Bigbasin.tif');
BR(mask==0)=0;
[lab_roof, num_roof] = bwlabel(BR, 4); %here the code finds the binary
image of BR with connectivity

%Step 4: calculation of the area and volume of the rain to redistribute in
the edge of the roofs
roof_rain=zeros(size(BR,1),size(BR,2),length(dt));

roof_rain(BR==1 | BR==2)= 0;
dx=abs(R.CellExtentInWorldX); %dimension of the pixel calculation

se=strel('disk',1); %buffer calculation
Roof_buffer=imdilate(lab_roof, strel('disk', 1)) - lab_roof;

for i=2
    roof_rain_loop=roof_rain(:,:,i);
    roof_rain_loop(BR==0)=rain_roofs_depth(i);
for label = 1:num_roof
    % area of the roof
    area_roof = sum(lab_roof(:) == label) * dx * dx; % m^2

    % volume of rainfall(in mm*m^2)
    volume_rain_roof = rain_roofs_depth(i)* area_roof;

    % area of the buffer (in m^2)
    area_edge_roof = sum(Roof_buffer(:) == label) * dx * dx;

    % rainfall distribution on the edge area (in mm)
    if area_edge_roof > 0
        roof_rain_loop(Roof_buffer == label) = (volume_rain_roof /
area_edge_roof) + rain_roofs_depth(i);
        roof_rain(:,:,i)=roof_rain_loop;
    end
  end
end

%Step 5: plotting of the results
 figure;
imagesc(roof_rain(:,:,2),'Alphadata',plot_mask), title('Rainfall
distribution');
axis equal
```

A.3 Code to read the original NETCDF file and modify to apply the RC method

```
%Step 1: read the netcdf file
path_read = "C:\Users\Admin-VM\Desktop\simulation_original_44_17h\";
nc_info = ncinfo(path_read + "rain_29-Sep-2023.nc");
rainfall_depth = ncread(path_read + "rain_29-Sep-
2023.nc",'rainfall_depth');
flag=rainfall_depth(544,1535,2);
%%
```

```
%Plot
rainfall_trans=permute (rainfall_depth, [2,1,3]);
figure
imagesc(rainfall_trans(:,:,2))


%In the case you want to see the results with same cells of Qgis
% xlim([-1 1456]);
% ylim([-1 2146]);

% Change of the center of the axis
% ax = gca;
% ax.XAxisLocation = 'origin';
% ax.YAxisLocation = 'origin';
%
% axis equal;

%%Step 2: Code to find the border of the roofs
% Read the GeoTIFF
[BR, R] = geotiffread('C:\Users\Admin-VM\Desktop\Land
cover\Building_raster_roof.tif');
[lab_roof, num_roof] = bwlabel(BR, 4); %here the code finds the binary
image of BR with connectivity

%Calculate the dilatation of the building roofs with an r=1 using the disk
%type of extension
se=strel('disk',1);
Roof_buffer_l=imdilate(logical(lab_roof),se)&~logical(lab_roof); %l
because logical
Roof_buffer=double(Roof_buffer_l);

%Loop for changing values inside Roof buffer according to the type of the
roof
for ii = 1:size(BR,1)
    for jj = 1:size(BR,2)
        if Roof_buffer(ii,jj) == 1
            % This part is to control the boundaries using a control
window
            row_min = max(ii-1, 1);
            row_max = min(ii+1, size(BR,1));
            col_min = max(jj-1, 1);
            col_max = min(jj+1, size(BR,2));

            % Here we control the window
            pre = BR(row_min:row_max, col_min:col_max) == 2;

            % If two of the value inside the window is 2 we update
Roof_buffer(ii,jj)
            if sum(pre(:)) > 1
                Roof_buffer(ii,jj) = 2;
            end
        end
    end
end
```

```
%Step 3: plot of the results
figure

 % Roofs
subplot(2, 1, 1)
imshow(BR, [])
title('Buildings roofs')

% Roofs Buffer
subplot(2, 1, 2)
imshow(Roof_buffer, [])
title('Roofs buffer')

%Step 4: initialization of the RC (runoff coefficients) matrix
%Grid extension
x= size(rainfall_depth,1);
y= size(rainfall_depth,2);

%Runoff coefficients matrix initializing
RC= ones(y,x);

% Step 5: RC matrix updating
RC(Roof_buffer==1) = 0.81; %sloping buildings, mean of all slopings
RC(Roof_buffer==2) = 0.76; %flat buildings, mean of all flat

%Step 6: write the new values on the NETCDF4 file
% ncwrite(path_read+"rain_29-Sep-
2023",'rainfall_depth',rainfall_depth.*RC'); %after first running mention
this
```

A.4 Code to read and change the extension of the results of LISFLOOD-FP files

```
% Step 1: specify the path folder
path_folder = 'C:\Users\Admin-VM\Desktop\LISFLOOD-FP-v8.2\LISFLOOD-
FP\out\build\msvc-x64-Debug\Sub-basin_1_RC\NY_FV1_runoff_RC_17hour\';
new_path_folder='C:\Users\Admin-VM\Desktop\Results\NY_FV1_RC_17h\Wd\';

%Step 2: read a referement GeoTIFF, for example in this case the dem to
assign a spatial referement to our file

[L,Referement]=readgeoraster('C:\Users\Admin-VM\Desktop\Sub-
basin_1\dem_buildings.dem');

% Step 3: list all .max files (in this case max but you can also other
extensions)
fileList = dir([path_folder, '\*.max']);

% Step 4: loop through each .max file, copy it and give new extension:
.tif
for i = 1:numel(fileList)
    file = fullfile(path_folder, fileList(i).name);
    fid=fopen(file,'r'); %Open the file

%Step 5: read the header of the file
    headerLines = cell(6,1);
```

```
    for k = 1:6
        headerLines{k} = fgetl(fid); % Legge una linea dell'header
    end
        n_cols=sscanf(headerLines{1},'ncols %d\n');
        n_rows=sscanf(headerLines{2},'nrows %d\n');
        xllcorner = sscanf(headerLines{3},'xllcorner %f\n');
        yllcorner = sscanf(headerLines{4},'yllcorner %f\n');
        cellsize =sscanf(headerLines{5},'xllcorner %f\n');
        NODATA_value = sscanf(headerLines{6},'xllcorner %f\n');

%Step 6: read the results of LISFLOOD-FP like a matrix
    Lisflood_res=fscanf(fid, '%f', [n_cols, n_rows])'; %here we read the
results of Lisflood like a matrix
    fclose(fid);

    [tempDir, tempFile] = fileparts(file);
    new_file=fullfile(new_path_folder, [tempFile, '.tif']);
%Step 7: save as a GeotTIFF

geotiffwrite(new_file,Lisflood_res,Referement,"CoordRefSysCode",'EPSG:2691
8');

end
```

A.5 Code to read and plot the results to do the comparison between pre and post application RC method

```
%Step 1: read the results of LISFLOOD_FP that were changed in GeoTIFF
[Mask,RM]=readgeoraster('C:\Users\Admin-VM\Desktop\Sub-
basin_1\Temp\Maschera.tif'); %this is the mask to read only the value
inside the dem of the basin and without the building footprint
j=1;

%Step 2: read and calculate all the variables of the results without RC
method application
for j=1:2
    if j==1
        path_folder='C:\Users\Admin-VM\Desktop\Results\NY_FV1\Wd\';
        fileList = dir([path_folder, '*.tif']);
        % max_wd=[size(fileList,1)-1];
        for i = 1:numel(fileList)
            file = fullfile(path_folder, fileList(i).name);
            if strcmp(fileList(i).name,'NY.tif') %because in this case I
want to check the max
            [Results_1,R]=readgeoraster(file);
            Results_1(Mask==2)=NaN;
            Results_mask = ~isnan(Results_1(:,:,1));%here we search all
the value different from NaN to use Alphadata in the plot (1 the number, 0
the NaN)
            column_results_1=Results_1(:);
            column_results_1=column_results_1(~isnan(column_results_1));
            max_1=max(column_results_1);
            mu_1=mean(column_results_1);
            sigma_1 =std(column_results_1);
```

```
            x_1=linspace(min(column_results_1),max(column_results_1),100);
            Surv_function_1=1-normcdf(x_1,mu_1,sigma_1);
            meanS1=1 - normcdf(mu_1, mu_1, sigma_1);

    end
        end

    %Step 3: read and calculate all the variables of the results with RC
method application
    else path_folder='C:\Users\Admin-
VM\Desktop\Results\NY_FV1_RC_17h\Wd\';
        fileList = dir([path_folder, '*.tif']);
        % max_wd=[size(fileList,1)-1];
        for i = 1:numel(fileList)
            file = fullfile(path_folder, fileList(i).name);
            if strcmp(fileList(i).name,'NY.tif') %because in this case I
want to check the max
            [Results_2,R]=readgeoraster(file);
            Results_2(Mask==2)=NaN;
            Results_mask = ~isnan(Results_2(:,:,1));%here we search all
the value different from NaN to use Alphadata in the plot (1 the number, 0
the NaN)
            column_results_2=Results_2(:);
            column_results_2=column_results_2(~isnan(column_results_2));
            max_2=max(column_results_2);
            mu_2=mean(column_results_2);
            sigma_2 =std(column_results_2);
            x_2=linspace(min(column_results_2),max(column_results_2),100);
            Surv_function_2=1-normcdf(x_2,mu_2,sigma_2);
            meanS2 = 1 - normcdf(mu_2, mu_2, sigma_2);

            end
        end
    end
end

%Step 4: plot with subplot of the results, histogram calculation

%Plot
figure;

%No RC
subplot(2, 2, 1)
 Plot=imagesc(Results_1,'AlphaData',Results_mask)
    colorbar;
    caxis([0 1.5]);
title('Water depth max without the RC method application')
axis equal;

%RC
subplot(2, 2, 2)
 Plot=imagesc(Results_2,'AlphaData',Results_mask)
    colorbar;
    caxis([0, 1.5]);
title('Water depth max with the RC method application')
axis equal;
```

```
%Value distribution with histogram without RC
subplot(2, 2, 3)
histogram(column_results_1,'BinLimits',[0.01,5],'Normalization','probabili
ty');

    hold on;
    legend('Histogram','Location','Best');
    title('Water depth value distribution without RC')
    xlabel('Water depth [m]')
    ylabel('Bar probability')
    hold off

%Value distribution with histogram with RC
subplot(2, 2, 4)
histogram(column_results_2,'BinLimits',[0.01,5],'Normalization','probabili
ty');

    hold on;
    legend('Histogram','Location','Best');
    title('Water depth value distribution wit RC')
    xlabel('Water depth [m]')
    ylabel('Bar probability')
    hold off

%Step 5: plot survival function
figure;
semilogy(x_1,Surv_function_1,'b-','LineWidth',3);
hold on
semilogy(x_2,Surv_function_2,'g-','LineWidth',3);
semilogy(mu_1, meanS1, 'bo', 'MarkerSize', 10, 'MarkerFaceColor', 'b');
semilogy(mu_2, meanS2, 'ro', 'MarkerSize', 10, 'MarkerFaceColor', 'r');
legend('Survival function max WD without RC method','Survival function max
WD with RC method','Mean value','Mean value','Location','Best');
title('Survival Functions in Logarithmic Scale');
xlabel('x, water depth values');
ylabel('1-F(x)');
grid on;
hold off
%%

%Step 6: calculation and plot survival function of the differences
absolut_diff=abs([Results_2-Results_1]); %in valore assoluto
column_absolut=absolut_diff(:);
           column_absolut=column_absolut(~isnan(column_absolut));
            max_abs=max(column_absolut);
            mu_abs=mean(column_absolut);
            sigma_abs =std(column_absolut);
            x_abs=linspace(min(column_absolut),max(column_absolut),100);
            Surv_function_abs=1-normcdf(x_abs,mu_abs,sigma_abs);
            meanSabs=1 - normcdf(mu_abs, mu_abs, sigma_abs);
            Figure;
semilogy(x_abs,Surv_function_abs,'b-','LineWidth',3)

%Step 7: calculation and plot of the survival function of the relative
%differences
```

```
rel_diff=abs([Results_2-Results_1]).*100;
column_rel=rel_diff(:);
           column_rel=column_rel(~isnan(column_rel));
            max_rel=max(column_rel);
            mu_rel=mean(column_rel);
            sigma_rel =std(column_rel);
            x_rel=linspace(min(column_rel),max(column_rel),100);
            Surv_function_rel=1-normcdf(x_rel,mu_rel,sigma_rel);
            meanSrel=1 - normcdf(mu_rel, mu_rel, sigma_rel);
            figure;
semilogy(x_rel,Surv_function_rel,'b-','LineWidth',3)
```

A.6 Code to plot the MAP (mean areal precipitation) and the water depth averaged in the basin during simulation and to plot the cumulative precipitation and the cumulative flood water.

```
%Step 1: read the netcdf variable
path_read = "C:\Users\Admin-VM\Desktop\";
nc_info = ncinfo(path_read + "rain_29-Sep-2023_original.nc");
rainfall_depth = ncread(path_read + "rain_29-Sep-
2023_original.nc",'rainfall_depth');
path_RC="C:\Users\Admin-VM\Desktop\LISFLOOD-FP-v8.2\LISFLOOD-
FP\out\build\msvc-x64-Debug\Sub-basin_1_RC\rain_29-Sep-2023_RC.nc";
rainfall_depth_RC=ncread(path_RC,'rainfall_depth');
time = ncread(path_read + "rain_29-Sep-2023_original.nc",'time');
rainfall_mean=zeros(1,size(time,1));

%Step 2: initialize the variable that will be used in the loop
matrix_original=zeros(size(rainfall_depth,1),size(rainfall_depth,2));
area=9718*10^6; %m^2
%Initializing cumulative precipitation vectors
P_original_cum=zeros(1,size(time,1));
P_RC_cum=zeros(1,size(time,1));

%Step 3: Initialization of the mask
[Mask,RM]=readgeoraster('C:\Users\Admin-VM\Desktop\Sub-
basin_1\Temp\Maschera.tif'); %this a mask that contains value 1 where
there are data to plot and value 2 where there data to don't plot
threshold=2;
mask= Mask<threshold;

%Step 4: Loop to calculate the cumulative and the mean areal precipitation
for i=1:size(time)
    matrix_original=rainfall_depth(:,:,i);
    matrix_original_mask=matrix_original(mask);
    matrix_RC=rainfall_depth_RC(:,:,i);
    matrix_RC_mask=matrix_RC(mask);
    sum_rainfall=sum(matrix_original_mask(:));
    sum_rainfall_RC=sum(matrix_RC_mask(:));
    if i==1
    P_original_cum(i)=sum_rainfall;
    P_RC_cum(i)=sum_rainfall_RC;
    else
    P_original_cum(i)=sum_rainfall+P_original_cum(i-1);
```

```
    P_RC_cum(i)=sum_rainfall_RC+P_RC_cum(i-1);
    end
    rainfall_mean(i)=sum_rainfall/area;
end

%Step 5: Loop to calculate the averaged areal water depth
j=1;
for j=1:2
    if j==1
       new_path_folder='C:\Users\Admin-
VM\Desktop\Results\NY_FV1_RC_17h\Wd\';
       water depth_1=zeros(1,size(time,1));
       wd_cum_1=zeros(1,size(time,1));
       fileList = dir([new_path_folder, '*.tif']);
       k=1;
       for i = 1:numel(fileList)-1
        file = fullfile(new_path_folder, fileList(i).name);
        [Wd,R]=readgeoraster(file);
        wd_mask=Wd(mask);
        num_elements=numel(wd_mask);
        water depth_1(k)=sum(wd_mask)/num_elements;
        if i==1
        wd_cum_1(k)=sum(wd_mask);
        else wd_cum_1(k)=sum(wd_mask)+wd_cum_1(k-12);
        end
        k=k+12;
       end
    elseif j==2
       new_path_folder='C:\Users\Admin-VM\Desktop\Results\NY_FV1\Wd\';
       water depth_2=zeros(1,size(time,1));
       wd_cum_2=zeros(1,size(time,1));
       fileList = dir([new_path_folder, '*.tif']);
       k=1;
       for i = 1:numel(fileList)-1
        file = fullfile(new_path_folder, fileList(i).name);
        [Wd,R]=readgeoraster(file);
        wd_mask=Wd(mask);
        num_elements=numel(wd_mask);
        water depth_2(k)=sum(wd_mask)/num_elements;
        if i==1
            wd_cum_2(k)=sum(wd_mask);
        else wd_cum_2(k)=sum(wd_mask)+wd_cum_2(k-12);
        end
        k=k+12;
       end
    end
end

%Step 6: Interpolation of the water depth value to obtain a linear
%distribution

%Wd averaged interpolation New result
index=find(water depth_1~= 0);
values=water depth_1(index);
xq = 1:length(water depth_1);
wd_interp_1=interp1(index,values,xq,'linear','extrap');
```

```
%Wd averaged interpolation original
index=find(water depth_2~= 0);
values=water depth_2(index);
xq = 1:length(water depth_2);
wd_interp_2=interp1(index,values,xq,'linear','extrap');

%Step 7: cumulative water depth calculation

%Wd cumsum interpolation New result
index=find(wd_cum_1~= 0);
values=wd_cum_1(index);
xq = 1:length(wd_cum_1);
wd_intcum_1=interp1(index,values,xq,'linear','extrap');

%Wd cumsum interpolation original
index=find(wd_cum_2 ~= 0);
values=wd_cum_2(index);
xq = 1:length(wd_cum_2);
wd_intcum_2=interp1(index,values,xq,'linear','extrap');


%Step 8: Plot of the results
yyaxis left
plot(time,rainfall_mean,'k','LineWidth',1.5)
xlabel('Time [hour]')
ylabel('Mean areal precipitation [mm]')

yyaxis right
plot(time,wd_interp_2,'b','LineWidth',1.5)
hold on
plot(time,wd_interp_1,'r','LineWidth',1.5)
ylabel('Averaged Flood water depth [m]')

legend('Mean areal precipitation','Flood water depth averaged in the
basin, Original Case','Flood water depth averaged in the basin, RC
Case','Location','Best');

hold off
%%
%Plot cumulative precipitation and water depth
figure;
yyaxis left
plot(time,P_original_cum,'g','LineWidth',1.5)
xlabel('Time [hour]')
ylabel('Cumulative Precipitation')
hold on
plot(time,P_RC_cum,'k','LineWidth',1.5)

yyaxis right
plot(time,wd_intcum_2,'b','LineWidth',1.5)
ylim([0 max(wd_intcum_2)])
xlim([0 17])
hold on

p=plot(time,wd_intcum_1,'r','LineWidth',1.5)
```

```
ylim([0 max(wd_intcum_1)])
ylabel('Cumulative flood water depth [m]')

legend('Cumulative original precipitation','Cumulative precipitation, RC
method','Cumulative flood water depth, Original method','Cumulative flood
water, RC method','Location','northwest');
```

A.7 Code to the downspout's rainfall redistribution

```
% Step 1: Data input
% Mask
%[mask_data, R_mask] = geotiffread('C:\Users\Admin-
VM\Desktop\QGIS\Maschera.tif');
[mask_data, R_mask] =
geotiffread('/home/gparadi1/Desktop/Maschera_bigBasin.tif');
mask = mask_data < 2; % logical mask

% NetCDF
path_read = "/home/gparadi1/netcdf/";
rain_roofs = ncread(path_read +
"rain_buildings_29_september_44_mask_original.nc", 'rainfall_depth');
rain_roofs = permute(rain_roofs, [2, 1, 3]);
rain_roofs(~mask) = NaN;
time = ncread(path_read +
"rain_buildings_29_september_44_mask_original.nc", 'time');

% Roof Buffer
%[BR, R] = geotiffread("C:\Users\Admin-VM\Desktop\Land
cover\Building_raster_roof.tif");
[BR, R] =
geotiffread('/home/gparadi1/Desktop/Building_clipped_bigbasin.tif');
BR(~mask) = NaN;
[lab_roof, num_roof] = bwlabel(BR, 4); % Binary image of BR with
connectivity
Roof_buffer = imdilate(lab_roof, strel('disk', 1)) - lab_roof;
unique_roofs = unique(Roof_buffer); % Find unique roofs
dx = abs(R.CellExtentInWorldX); % Pixel dimension calculation

% Vector of the sum of the rain per roof
rain_per_roof = zeros(length(num_roof), length(time));

% Downspout distribution
[Downspout, Rd] =
geotiffread('/home/gparadi1/Desktop/Downspout_corretto_final.tif');
mask_down = Downspout > 0;
Downspout(~mask | ~mask_down) = NaN;
rain_downspouts = zeros(size(rain_roofs));


% Step 2: Loop to change the value in the Downspouts
for t = 1:length(time)
    rain_mask = rain_roofs(:, :, t);
    x = rain_roofs(955, 1162, t);
    for r = 1:num_roof
        % Extract the pixels of the current roof
```

```
        roof_buffer_pixels = Roof_buffer == r;

        num_pixels = sum(roof_buffer_pixels(:) ~= 0);

        % Sum the rain on roof pixels for time t
        rain_per_roof(r, t) = sum(rain_mask(roof_buffer_pixels)) - x *
num_pixels;
    end
end

for t = 1:length(time)
    for r = 1:num_roof
        % Extract the pixels of the buffer around the current roof
        buffer_pixels = Roof_buffer == r;

        % Extract the downspout pixels associated with this roof
        downspout_pixels = Downspout > 0 & buffer_pixels;

        % Number of downspouts in the buffer
        num_downspout_pixels = sum(downspout_pixels(:));

        if num_downspout_pixels > 0
            % Find linear indices of downspout pixels
            [row_idx, col_idx] = find(downspout_pixels);

            % Redistribute the rain pixel by pixel
            for i = 1:length(row_idx)
                rain_downspouts(row_idx(i), col_idx(i), t) =
rain_per_roof(r, t) / num_downspout_pixels;
            end
        end
    end
end

save("rain_downspouts.mat", "rain_downspouts", "-v7.3");

% Step 3: Loop to change the value of the roof_buffer
modified_rain_roofs_buffer = rain_roofs;

for t = 1:length(time)
    x = rain_roofs(955, 1162, t);
    A = rain_roofs(:, :, t);
    A(Roof_buffer == 1 | Roof_buffer == 2) = x;
    modified_rain_roofs_buffer(:, :, t) = A;
end
save("modified_rain_roofs.mat", "modified_rain_roofs_buffer", "-v7.3");

RC_BIRR_data = load('/home/gparadi1/netcdf/RC_BIRR.mat');
RC_BIRR = RC_BIRR_data.E;

% final_rain_downspout_distributed = (modified_rain_roofs_buffer +
rain_downspouts) .* RC_BIRR; % Case BIRR & RC
final_rain_downspout_distributed = (modified_rain_roofs_buffer +
rain_downspouts); % Case BIRR
save('rain_downspout_red.mat', "final_rain_downspout_distributed", '-
v7.3');
```

```
%Step 4: NetCDF writing
ncwrite(path_read + "rain_buildings_29_september_44_mask_original.nc",
'rainfall_depth', rain_roofs .* 0 +
permute(final_rain_downspout_distributed, [2, 1, 3])); %Case BIRR_RC
ncwrite(path_read + "rain_buildings_29_september_44_mask_original.nc",
'rainfall_depth', rain_roofs ./ RC_BIRR'); %Case BIRR
```

A.8 Code to make the video of the simulation starting from the .tif files

```
%Step 1: Data initialization
folderPath = "C:\Users\Admin-VM\Desktop\Results\FV1_RC_BASIN\Wd_tif\";
tifFiles = dir(fullfile(folderPath, '*.tif'));
numFrames = length(tifFiles);
base=imread("C:\Users\Admin-VM\Desktop\Results\Base_map.jpg");
[Mask,RM]=readgeoraster('C:\Users\Admin-
VM\Desktop\Results\Maschera_bigBasin.tif'); %this a mask that contains
value 1 where there are data to plot and value 2 where there data to don't
plot
threshold=2;
mask_= Mask<threshold;
mask=single(mask_);
plot_mask=zeros(size(Mask));
plot_mask(mask==0)=NaN;
plot_mask=~isnan(plot_mask);

%Step 2: colorbar definition
cmap = [
    173, 216, 230;
    0, 191, 255;
    0, 128, 255;
    0, 0, 255;
    0, 128, 0;
    255, 255, 0;
    255, 165, 0;
    255, 69, 0;
    255, 0, 0;
    139, 0, 0
] /255; %normalization in [0 1]
figure;
% Array to save frames
frames(numFrames) = struct('cdata', [], 'colormap', []);

%Step 3: loop over all the tiff files
for k = 1:numFrames
    fileName = fullfile(folderPath, tifFiles(k).name);
    img = imread(fileName);
    imshow(base)
    hold on
    imagesc(img,'AlphaData',plot_mask);
    colormap(cmap)
    colorbar;
    cbt=colorbar;
    set(cbt,'YTick',[0:0.15:1.5])
    caxis([0 1.5]);
```

```
    axis image;
    hold off
    title(['Frame: ', num2str(k), ' / ', num2str(numFrames)]);
    frames(k) = getframe(gcf);
end

%Step 4: plot the animation to see the result
figure;
movie(frames, 1, 2); % 1 is the number of the repetition, 2 is the fps

%Step 5: Save
v = VideoWriter('Animation_RC_Basin.mp4','MPEG-4');
v.FrameRate = 2; % fps
open(v);
writeVideo(v, frames);
close(v);
```

A.9 Code to calculate the max cell's velocity of the simulation

```
% Step 1: Define folder paths
% Specify the paths to folders containing vx and vy data
folder_vx_original =
'/home/gparadi1/Results/NY_FV1_original_Basin/Vx_tif/';
folder_vy_original =
'/home/gparadi1/Results/NY_FV1_original_Basin/Vy_tif/';
folder_vx_BIRR = '/home/gparadi1/Results/NY_FV1_BIRR_Basin/Vx_tif/';
folder_vy_BIRR = '/home/gparadi1/Results/NY_FV1_BIRR_Basin/Vy_tif/';
folder_vx_BIRR_RC = '/home/gparadi1/Results/NY_FV1_BIRR_RC/Vx_tif/';
folder_vy_BIRR_RC = '/home/gparadi1/Results/NY_FV1_BIRR_RC/Vy_tif/';

% Step 2: List files in folders
% Retrieve lists of files in the specified folders
files_vx_original = dir(fullfile(folder_vx_original, '*.tif'));
files_vy_original = dir(fullfile(folder_vy_original, '*.tif'));
files_vx_BIRR = dir(fullfile(folder_vx_BIRR, '*.tif'));
files_vy_BIRR = dir(fullfile(folder_vy_BIRR, '*.tif'));
files_vx_BIRR_RC = dir(fullfile(folder_vx_BIRR_RC, '*.tif'));
files_vy_BIRR_RC = dir(fullfile(folder_vy_BIRR_RC, '*.tif'));

% Step 3: Determine the number of matrices
% Get the total number of files/matrices to process
num_matrices = min(length(files_vx_original), length(files_vy_original));

% Step 4: Initialize cell arrays for results
% Create empty cell arrays to store the computed vc results
Vc_original = cell(1, num_matrices);
Vc_BIRR = Vc_original;
Vc_BIRR_RC = Vc_original;

% Step 5: Process original matrices
% Loop through and process original vx and vy matrices
for k = 1:num_matrices
    % Load the k-th vx and vy matrices
    [vx_data, Rx] = geotiffread(fullfile(folder_vx_original,
files_vx_original(k).name));
```

```
    [vy_data, Ry] = geotiffread(fullfile(folder_vy_original,
files_vy_original(k).name));
    % Get the size of the matrices
    [m, n] = size(vx_data);
    % Initialize the vc matrix
    Vc_original{k} = zeros(m, n);
    for i = 2:m-1
        for j = 2:n-1
            % Compute maximum values among neighbors
            max_vx = max(vx_data(i-1, j), vx_data(i+1, j));
            max_vy = max(vy_data(i, j-1), vy_data(i, j+1));
            % Compute vc value
            Vc_original{k}(i, j) = sqrt((max_vx)^2 + (max_vy)^2);
        end
    end
end

% Step 6: Process BIRR matrices
% Loop through and process BIRR vx and vy matrices
for k = 1:num_matrices
    % Load the k-th vx and vy matrices
    [vx_data, Rx] = geotiffread(fullfile(folder_vx_BIRR,
files_vx_BIRR(k).name));
    [vy_data, Ry] = geotiffread(fullfile(folder_vy_BIRR,
files_vy_BIRR(k).name));
    % Get the size of the matrices
    [m, n] = size(vx_data);
    % Initialize the vc matrix
    Vc_BIRR{k} = zeros(m, n);
    for i = 2:m-1
        for j = 2:n-1
            % Compute maximum values among neighbors
            max_vx = max(vx_data(i-1, j), vx_data(i+1, j));
            max_vy = max(vy_data(i, j-1), vy_data(i, j+1));
            % Compute vc value
            Vc_BIRR{k}(i, j) = sqrt((max_vx)^2 + (max_vy)^2);
        end
    end
end

% Step 7: Process BIRR_RC matrices
% Loop through and process BIRR_RC vx and vy matrices
for k = 1:num_matrices
    % Load the k-th vx and vy matrices
    [vx_data, Rx] = geotiffread(fullfile(folder_vx_BIRR_RC,
files_vx_BIRR_RC(k).name));
    [vy_data, Ry] = geotiffread(fullfile(folder_vy_BIRR_RC,
files_vy_BIRR_RC(k).name));
    % Get the size of the matrices
    [m, n] = size(vx_data);
    % Initialize the vc matrix
    Vc_BIRR_RC{k} = zeros(m, n);
    for i = 2:m-1
        for j = 2:n-1
            % Compute maximum values among neighbors
            max_vx = max(vx_data(i-1, j), vx_data(i+1, j));
```

```
            max_vy = max(vy_data(i, j-1), vy_data(i, j+1));
            % Compute vc value
            Vc_BIRR_RC{k}(i, j) = sqrt((max_vx)^2 + (max_vy)^2);
        end
    end
end

% Step 8: Save results to .mat files
% Save the computed vc results to .mat files
save("Vc_original.mat", "Vc_original", '-v7.3');
save("Vc_BIRR.mat", "Vc_BIRR", '-v7.3');
save("Vc_BIRR_RC.mat", "Vc_BIRR_RC", '-v7.3');
```

A.10 Code to obtain the vulnerability/instability map of vehicles and people

```
% Define folders containing the water depth (Wd) GeoTIFF files
folder_wd_original =
'/home/gparadi1/Results/NY_FV1_original_Basin/Wd_tif/';
folder_wd_BIRR = '/home/gparadi1/Results/NY_FV1_BIRR_Basin/Wd_tif/';
folder_wd_BIRR_RC = '/home/gparadi1/Results/NY_FV1_BIRR_RC/Wd_tif/';

% Step 1: Retrieve file lists from the folders
files_wd_original = dir(fullfile(folder_wd_original, '*.tif')); % Original
water depth files
files_wd_BIRR = dir(fullfile(folder_wd_BIRR, '*.tif')); % BIRR water depth
files
files_wd_BIRR_RC = dir(fullfile(folder_wd_BIRR_RC, '*.tif')); % BIRR_RC
water depth files

% Step 2: Define the total number of matrices based on the smallest file
count
num_matrices = min(length(files_wd_original), length(files_wd_BIRR));

% Step 3: Initialize cell arrays to store water depth data
Hmax_original = cell(1, num_matrices);
Hmax_BIRR = Hmax_original;
Hmax_BIRR_RC = Hmax_original;

% Step 4: Loop through each matrix and read GeoTIFF files
for k = 1:num_matrices
    % Read the k-th water depth file for each folder
    [H_original, R1] = geotiffread(fullfile(folder_wd_original,
files_wd_original(k).name));
    [H_BIRR, R2] = geotiffread(fullfile(folder_wd_BIRR,
files_wd_BIRR(k).name));
    [H_BIRR_RC, R3] = geotiffread(fullfile(folder_wd_BIRR_RC,
files_wd_BIRR_RC(k).name));

    % Store the water depth matrices in the respective cells
    Hmax_original{k} = H_original;
    Hmax_BIRR{k} = H_BIRR;
    Hmax_BIRR_RC{k} = H_BIRR_RC;
end

% Step 5: Define constants and load additional data
```

```
g = 9.81; % Gravitational acceleration (m/s^2)
H_veicolo = 1.5; % Average vehicle height (m)
H_persona = 1.77; % Average person height (m)
[H_max, R_wdmax] =
geotiffread('/home/gparadi1/Results/NY_FV1_BIRR_Basin/NY.tif');

% Step 6: Compute Froude number maps
Fr_original = cell(1, num_matrices);
Fr_BIRR = cell(1, num_matrices);
Fr_BIRR_RC = cell(1, num_matrices);

for k = 1:num_matrices
    % Calculate Froude number for each matrix
    Fr_original{k} = Vc_original{k} ./ sqrt(g .* Hmax_original{k});
    Fr_BIRR{k} = Vc_BIRR{k} ./ sqrt(g .* Hmax_BIRR{k});
    Fr_BIRR_RC{k} = Vc_BIRR_RC{k} ./ sqrt(g .* Hmax_BIRR_RC{k});
end

% Save Froude number data to .mat files
save("Fr_original.mat", "Fr_original", '-v7.3');
save("Fr_BIRR.mat", "Fr_BIRR", '-v7.3');
save("Fr_BIRR_RC.mat", "Fr_BIRR_RC", '-v7.3');

% Step 7: Calculate critical height for vehicles
Hcr_v_original = cell(1, num_matrices);
Hcr_v_BIRR = cell(1, num_matrices);
Hcr_v_BIRR_RC = cell(1, num_matrices);

for k = 1:num_matrices
    % Compute critical height for vehicles
    Hcr_v_original{k} = (-0.05 .* Fr_original{k} + 0.34) .* H_veicolo;
    Hcr_v_BIRR{k} = (-0.05 .* Fr_BIRR{k} + 0.34) .* H_veicolo;
    Hcr_v_BIRR_RC{k} = (-0.05 .* Fr_BIRR_RC{k} + 0.34) .* H_veicolo;
end

% Step 8: Save critical height for vehicles to .mat files
save("Hcr_v_original.mat", "Hcr_v_original", '-v7.3');
save("Hcr_v_BIRR.mat", "Hcr_v_BIRR", '-v7.3');
save("Hcr_v_BIRR_RC.mat", "Hcr_v_BIRR_RC", '-v7.3');

% Step 9: Calculate critical height for people
Hcr_p_original = cell(1, num_matrices);
Hcr_p_BIRR = cell(1, num_matrices);
Hcr_p_BIRR_RC = cell(1, num_matrices);

for k = 1:num_matrices
    % Compute critical height for people
    Hcr_p_original{k} = (0.29 ./ (0.24 + Fr_original{k})) .* H_persona;
    Hcr_p_BIRR{k} = (0.29 ./ (0.24 + Fr_BIRR{k})) .* H_persona;
    Hcr_p_BIRR_RC{k} = (0.29 ./ (0.24 + Fr_BIRR_RC{k})) .* H_persona;
end

% Save critical height for people to .mat files
save("Hcr_p_original.mat", "Hcr_p_original", '-v7.3');
save("Hcr_p_BIRR.mat", "Hcr_p_BIRR", '-v7.3');
save("Hcr_p_BIRR_RC.mat", "Hcr_p_BIRR_RC", '-v7.3');
```

```
% Step 10: Initialize vulnerability maps for vehicles and people
Vuln_v_original = cell(1, num_matrices);
Vuln_p_original = cell(1, num_matrices);
Vuln_v_BIRR = cell(1, num_matrices);
Vuln_p_BIRR = cell(1, num_matrices);
Vuln_v_BIRR_RC = cell(1, num_matrices);
Vuln_p_BIRR_RC = cell(1, num_matrices);

for k = 1:num_matrices
    % Assign vulnerability based on thresholds
    Vuln_v_original{k} = Hcr_v_original{k} < Hmax_original{k};
    Vuln_p_original{k} = (Hmax_original{k} ./ Hcr_p_original{k}) > 1;
    Vuln_v_BIRR{k} = Hcr_v_BIRR{k} < Hmax_BIRR{k};
    Vuln_p_BIRR{k} = (Hmax_BIRR{k} ./ Hcr_p_BIRR{k}) > 1;
    Vuln_v_BIRR_RC{k} = Hcr_v_BIRR_RC{k} < Hmax_BIRR_RC{k};
    Vuln_p_BIRR_RC{k} = (Hmax_BIRR_RC{k} ./ Hcr_p_BIRR_RC{k}) > 1;
end

% Save vulnerability maps to .mat files
save("Vuln_v_original.mat", "Vuln_v_original", '-v7.3');
save("Vuln_v_BIRR.mat", "Vuln_v_BIRR", '-v7.3');
save("Vuln_v_BIRR_RC.mat", "Vuln_v_BIRR_RC", '-v7.3');
save("Vuln_p_original.mat", "Vuln_p_original", '-v7.3');
save("Vuln_p_BIRR.mat", "Vuln_p_BIRR", '-v7.3');
save("Vuln_p_BIRR_RC.mat", "Vuln_p_BIRR_RC", '-v7.3');
```

APPENDIX B
AUTOLISP CODES

B.1 Code to the downspout's roof distribution

```
(defun c:DistribuisciPuntiPerAreaPerimetro (/ ss ent area perimeter gpm number-downspouts distance-points list-points length-point j point)
  ;; Select all polylines or polygons in the drawing
  (setq ss (ssget "X" '((0 . "LWPOLYLINE,POLYLINE"))))
;; "X" selects everything, the filter selects only polylines
  ;; Check if any polylines were selected
  (if ss
    (progn
      ;; Iterate through all the polylines in the selection set
      (repeat (setq i (sslength ss)) ;; Number of elements in the selection set
        ;; Get the current polyline
        (setq ent (ssname ss (setq i (1- i))))
        ;; Calculate the area and perimeter of the polyline
        (setq area (vlax-curve-getarea ent))
        (setq perimeter (vlax-curve-getdistatparam ent (vlax-curve-getendparam ent)))
        ;; Calculate gpm and the number of downspouts
        (setq gpm (* area 3 0.0104 10.764)) ;; Calculate gpm
        (setq number-downspouts (max 1 (fix (/ gpm 180))))
;; Set number of downspouts to 1 if zero or negative
        (setq distance-points (/ perimeter number-downspouts))
;; Distance between points = perimeter / number of downspouts
        ;; Initialize the list of points and the current segment length
        (setq list-points nil
              length-point 0
              j 0)
```

```
        ;; Loop to position the points along the perimeter
        (repeat number-downspouts
          ;; Calculate the point on the curve based on the current segment length
          (setq length-point (* j distance-points))
          (setq point (vlax-curve-getpointatdist ent length-point))
          ;; Add the point to the list of points
          (setq list-points (cons point list-points))
          (setq j (1+ j)))
        ;; Insert the points into the drawing
        (foreach pt list-points
          (entmake
            (list (cons 0 "POINT")
                  (cons 10 pt))))
      )
    )
  )
)
```

BIBLIOGRAPHY

Agency, E. (2019). *Title here in 8pt Arial (change text colour to black) i What is the Risk of Flooding from Surface Water map?* http://publications.environmen

Aksoy, H., Kirca, V. S. O., Burgan, H. I., & Kellecioglu, D. (2016). Hydrological and hydraulic models for determination of flood-prone and flood inundation areas. *Proceedings of the International Association of Hydrological Sciences*, *373*, 137–141. https://doi.org/10.5194/piahs-373-137-2016

Arrighi, C., Alcèrreca-Huerta, J. C., Oumeraci, H., & Castelli, F. (2015). Drag and lift contribution to the incipient motion of partly submerged flooded vehicles. *Journal of Fluids and Structures*, *57*, 170–184. https://doi.org/10.1016/j.jfluidstructs.2015.06.010

Arrighi, C., Oumeraci, H., & Castelli, F. (2017). Hydrodynamics of pedestrians' instability in floodwaters. *Hydrology and Earth System Sciences*, *21*(1), 515–531. https://doi.org/10.5194/hess-21-515-2017

Bates, P., Trigg, M., Neal, J., & Dabrowa, A. (2013). *LISFLOOD-FP User manual Code release 6.1.1*. https://svn.ggy.bris.ac.uk/subversion/lisflood/

Bisht, D. S., Chatterjee, C., Kalakoti, S., Upadhyay, P., Sahoo, M., & Panda, A. (2016). Modeling urban floods and drainage using SWMM and MIKE URBAN: a case study. *Natural Hazards*, *84*(2), 749–776. https://doi.org/10.1007/s11069-016-2455-1

Bulti, D. T., & Abebe, B. G. (2020). A review of flood modeling methods for urban pluvial flood application. In *Modeling Earth Systems and Environment* (Vol. 6, Issue 3, pp. 1293–1302). Springer Science and Business Media Deutschland GmbH. https://doi.org/10.1007/s40808-020-00803-z

Cao, X. J., & Ni, G. H. (2019). Effect of storm network simplification on flooding prediction with varying rainfall conditions. *IOP Conference Series: Earth and Environmental Science*, *344*(1), 012093. https://doi.org/10.1088/1755-1315/344/1/012093

Cao, X., Lyu, H., Ni, G., Tian, F., Ma, Y., & Grimmond, C. S. B. (2020). Spatial Scale Effect of Surface Routing and Its Parameter Upscaling for Urban Flood Simulation Using a Grid-Based Model. *Water Resources Research*, *56*(2). https://doi.org/10.1029/2019WR025468

Cao, X., Ni, G., Qi, Y., & Liu, B. (2020). Does Subgrid Routing Information Matter for Urban Flood Forecasting? A Multiscenario Analysis at the Land Parcel Scale. *Journal of Hydrometeorology*, *21*(9), 2083–2099. https://doi.org/10.1175/JHM-D-20-0075.1

Chang, T.-J., Wang, C.-H., & Chen, A. S. (2015). A novel approach to model dynamic flow interactions between storm sewer system and overland surface for different land covers in urban areas. *Journal of Hydrology*, *524*, 662–679. https://doi.org/10.1016/j.jhydrol.2015.03.014

CITY OF NEW YORK DEPARTMENT OF ENVIRONMENTAL PROTECTION BUREAU OF WATER AND SEWER OPERATIONS DIVISION OF REVIEW AND CONSTRUCTION COMPLIANCE CRITERIA FOR DETERMINATION OF DETENTION FACILITY VOLUME. (n.d.).

Farreny, R., Morales-Pinzón, T., Guisasola, A., Tayà, C., Rieradevall, J., & Gabarrell, X. (2011a). Roof selection for rainwater harvesting: Quantity and quality assessments in Spain. *Water Research*, *45*(10), 3245–3254. https://doi.org/10.1016/j.watres.2011.03.036

Farreny, R., Morales-Pinzón, T., Guisasola, A., Tayà, C., Rieradevall, J., & Gabarrell, X. (2011b). Roof selection for rainwater harvesting: Quantity and quality assessments in Spain. *Water Research*, *45*(10), 3245–3254. https://doi.org/10.1016/j.watres.2011.03.036

Fewtrell, T. J., Bates, P. D., Horritt, M., & Hunter, N. M. (2008). Evaluating the effect of scale in flood inundation modelling in urban environments. *Hydrological Processes*, *22*(26), 5107–5118. https://doi.org/10.1002/hyp.7148

Gangodagamage, C., Belmont, P., & Foufoula-Georgiou, E. (2011). Revisiting scaling laws in river basins: New considerations across hillslope and fluvial regimes. *Water Resources Research*, *47*(7). https://doi.org/10.1029/2010WR009252

Gharbi, M., Soualmia, A., Dartus, D., & Masbernat, L. (2016). *Comparison of 1D and 2D hydraulic models for floods simulation on the medjerda riverin tunisia*. *7*, 3017–3026.

Hammond, M. J., Chen, A. S., Djordjević, S., Butler, D., & Mark, O. (2015). Urban flood impact assessment: A state-of-the-art review. *Urban Water Journal*, *12*(1), 14–29. https://doi.org/10.1080/1573062X.2013.857421

Hankin, B., Waller, S., Astle, G., & Kellagher, R. (2008). Mapping space for water: screening for urban flash flooding. *Journal of Flood Risk Management*, *1*(1), 13–22. https://doi.org/10.1111/j.1753-318X.2008.00003.x

Hénonin, J., Hongtao, M., Zheng-Yu, Y., Hartnack, J., Havnø, K., Gourbesville, P., & Mark, O. (2015). Citywide multi-grid urban flood modelling: the July 2012 flood in Beijing. *Urban Water Journal*, *12*(1), 52–66. https://doi.org/10.1080/1573062X.2013.851710

Henonin, J., Russo, B., Mark, O., & Gourbesville, P. (2013). Real-time urban flood forecasting and modelling – a state of the art. *Journal of Hydroinformatics*, *15*(3), 717–736. https://doi.org/10.2166/hydro.2013.132

Jahanbazi, M., & Egger, U. (2014). Application and comparison of two different dual drainage models to assess urban flooding. *Urban Water Journal*, *11*(7), 584–595. https://doi.org/10.1080/1573062X.2013.871041

Jennewein, D. M., Lee, J., Kurtz, C., Dizon, W., Shaeffer, I., Chapman, A., Chiquete, A., Burks, J., Carlson, A., Mason, N., Kobawala, A., Jagadeesan, T., Basani, P. B., Battelle, T., Belshe, R., McCaffrey, D., Brazil, M., Inumella, C., Kuznia, K., … Yalim, J. (2023). The Sol Supercomputer at Arizona State University. *Practice and Experience in Advanced Research Computing*, 296–301. https://doi.org/10.1145/3569951.3597573

Jiang, L., Chen, Y., & Wang, H. (2015). Urban flood simulation based on the SWMM model. *Proceedings of the International Association of Hydrological Sciences*, *368*, 186–191. https://doi.org/10.5194/piahs-368-186-2015

Kesserwani, G., Ayog, J. L., & Bau, D. (2018). Discontinuous Galerkin formulation for 2D hydrodynamic modelling: Trade-offs between theoretical complexity and practical convenience. *Computer Methods in Applied Mechanics and Engineering*, *342*, 710–741. https://doi.org/10.1016/j.cma.2018.08.003

Kesserwani, G., & Liang, Q. (2012). Locally Limited and Fully Conserved RKDG2 Shallow Water Solutions with Wetting and Drying. *Journal of Scientific Computing*, *50*(1), 120–144. https://doi.org/10.1007/s10915-011-9476-4

Kim, B., Sanders, B. F., Schubert, J. E., & Famiglietti, J. S. (2014). Mesh type tradeoffs in 2D hydrodynamic modeling of flooding with a Godunov-based flow solver.

Advances in Water Resources, *68*, 42–61. https://doi.org/10.1016/j.advwatres.2014.02.013

Kourtis, I. M., Bellos, V., & Tsihrintzis, V. A. (2017). *Comparison of 1D-1D and 1D-2D urban flood models*.

Leandro, J., Chen, A. S., Djordjević, S., & Savić, D. A. (2009). Comparison of 1D/1D and 1D/2D Coupled (Sewer/Surface) Hydraulic Models for Urban Flood Simulation. *Journal of Hydraulic Engineering*, *135*(6), 495–504. https://doi.org/10.1061/(ASCE)HY.1943-7900.0000037

Leandro, J., Schumann, A., & Pfister, A. (2016). A step towards considering the spatial heterogeneity of urban key features in urban hydrology flood modelling. *Journal of Hydrology*, *535*, 356–365. https://doi.org/10.1016/j.jhydrol.2016.01.060

Liang, Q., & Marche, F. (2009). Numerical resolution of well-balanced shallow water equations with complex source terms. *Advances in Water Resources*, *32*(6), 873–884. https://doi.org/10.1016/j.advwatres.2009.02.010

Liu, Y., & Pender, G. (2013). Carlisle 2005 urban flood event simulation using cellular automata-based rapid flood spreading model. *Soft Computing*, *17*(1), 29–37. https://doi.org/10.1007/s00500-012-0898-1

Lyu, H., Ni, G., Cao, X., Ma, Y., & Tian, F. (2018). Effect of Temporal Resolution of Rainfall on Simulation of Urban Flood Processes. *Water*, *10*(7), 880. https://doi.org/10.3390/w10070880

Mark, O., Weesakul, S., Apirumanekul, C., Aroonnet, S. B., & Djordjević, S. (2004). Potential and limitations of 1D modelling of urban flooding. *Journal of Hydrology*, *299*(3–4), 284–299. https://doi.org/10.1016/j.jhydrol.2004.08.014

Miele, J. A., & Gaffoglio, R. (n.d.). *DEPARTMENT OF ENVIRONMENTAL PROTECTION BUREAU OF ENVIRONMENTAL ENGINEERING*.

Nations Office for Disaster Risk Reduction, U. (n.d.). *Sendai Framework for Disaster Risk Reduction 2015 - 2030*.

Nkwunonwo, U. C., Whitworth, M., & Baily, B. (2020). A review of the current status of flood modelling for urban flood risk management in the developing countries. *Scientific African*, *7*, e00269. https://doi.org/10.1016/j.sciaf.2020.e00269

NYC TOWN+GOWN CLIMATE VULNERABILITY, IMPACT, AND ADAPTATION (VIA) ANALYSIS New York City Town+Gown Climate Vulnerability, Impact, and Adaptation Analysis Final Report. (2024).

Ochoa-Rodríguez, S., Onof, C., Maksimović, Č., Wang, L.-P., Willems, P., Assel, J. Van, Gires, A., Ichiba, A., Bruni, G., & Ten Veldhuis, M.-C. (2013). *URBAN PLUVIAL FLOOD MODELLING: CURRENT THEORY AND PRACTICE Review document related to Work Package 3-Action 13 With contributions from: RainGain WP3 Review Document Urban pluvial flood modelling: Current theory and practice*.

Passalacqua, P., Tarolli, P., & Foufoula-Georgiou, E. (2010). Testing space-scale methodologies for automatic geomorphic feature extraction from lidar in a complex mountainous landscape. *Water Resources Research*, *46*(11). https://doi.org/10.1029/2009WR008812

Pina, R. D., Ochoa-Rodriguez, S., Simões, N. E., Mijic, A., Marques, A. S., & Maksimović, Č. (2016). Semi- vs. Fully-distributed urban stormwater models: Model set up and comparison with two real case studies. *Water (Switzerland)*, *8*(2). https://doi.org/10.3390/w8020058

Sañudo, E., Cea, L., & Puertas, J. (2022). Comparison of three different numerical implementations to model rainfall-runoff transformation on roofs. *Hydrological Processes*, *36*(5). https://doi.org/10.1002/hyp.14588

Schlauß, S., & Grottker, M. (2016). *Coupling Process for 1D-2D Numerical Flash Flood Simulation: A Parameter Study of Involved Variables for Gullies and Manholes*. https://doi.org/10.15142/T3759N

Shaik, F., & Agarwal, S. (2019). *Urban Flood Modeling and Management using SWMM for New R.R. Pet Region, Vijayawada, India*.

Sharifian, M. K., Kesserwani, G., Chowdhury, A. A., Neal, J., & Bates, P. (2023). LISFLOOD-FP 8.1: New GPU-Accelerated solvers for faster fluvial/pluvial flood simulations. *Geoscientific Model Development*, *16*(9), 2391–2413. https://doi.org/10.5194/gmd-16-2391-2023

Shaw, J., Kesserwani, G., Neal, J., Bates, P., & Sharifian, M. K. (2021). LISFLOOD-FP 8.0: The new discontinuous Galerkin shallow-water solver for multi-core CPUs and GPUs. *Geoscientific Model Development*, *14*(6), 3577–3602. https://doi.org/10.5194/gmd-14-3577-2021

Shen, D., Wang, J., Cheng, X., Rui, Y., & Ye, S. (2015). Integration of 2-D hydraulic model and high-resolution lidar-derived DEM for floodplain flow modeling. *Hydrology and Earth System Sciences*, *19*(8), 3605–3616. https://doi.org/10.5194/hess-19-3605-2015

Singh, V. P. (Vijay P.). (1992). *Elementary hydrology*. Prentice Hall. https://cir.nii.ac.jp/crid/1130000795217606272.bib?lang=ja

Supply, W., & Resources Division, W. (n.d.). *Storm Water Management Model Reference Manual Volume I-Hydrology (Revised) Office of Research and Development Water Supply and Water Resources Division*.

The_Courant_Friedrichs_Lewy_CFL_Conditio. (n.d.).

Urban Drainage, Third Edition. (2010). CRC Press. https://doi.org/10.1201/9781315272535

Walsh, T. C., Pomeroy, C. A., & Burian, S. J. (2014). Hydrologic modeling analysis of a passive, residential rainwater harvesting program in an urbanized, semi-arid watershed. *Journal of Hydrology*, *508*, 240–253. https://doi.org/10.1016/j.jhydrol.2013.10.038

Xuejian, C., Youcun, Q., & Guangheng, N. (2021). Significant impacts of rainfall redistribution through the roof of buildings on urban hydrology. *Journal of Hydrometeorology*, *22*(4), 1007–1023. https://doi.org/10.1175/JHM-D-20-0220.1

Yixuan, W., Jiayu, W., & Tian, C. (2024). Multi-Scenario analysis of rooftop greening regulation on runoff effects based on adaptive Evaluation: A case study of Macau, China. *Ecological Indicators*, *163*. https://doi.org/10.1016/j.ecolind.2024.111856

Zhu, Z., Chen, Z., Chen, X., & He, P. (2016). Approach for evaluating inundation risks in urban drainage systems. *Science of The Total Environment*, *553*, 1–12. https://doi.org/10.1016/j.scitotenv.2016.02.025

ACKNOLEDGEMENTS

Oggi giunge al termine un percorso che è iniziato ben cinque anni fa e pertanto mi sembra doveroso fare un ringraziamento a chi in questi anni mi ha supportato e ha contributo a rendere questi anni indimenticabili.

Innanzitutto, ringrazio il mio relatore, il prof. Daniele Ganora per avermi permesso di rendere la stesura di questi tesi una vera e propria esperienza di vita che non scorderò.

Ringrazio anche il mio correlatore Giuseppe Mascaro che in questi mesi è stato sempre disponibile ad ascoltare e a discutere i miei dubbi.

Ora tocca a loro, Liliana e Vincenzo, che mi hanno sempre sostenuto e che per primi hanno creduto nelle mie capacità, non stancandosi mai di dirmi "Vai ma stai attento".

Grazie a mia sorella Chiara, pronta ad ascoltarmi e capace di capire con uno sguardo se qualcosa non stesse andando nel verso giusto.

Grazie a Zia Daniela, Zio Ciccio e Sofia per essersi sempre informati sui miei progressi e grazie a Zio Peppe e Loredana per le chiamate per assicurarsi del mio stato mentale.

E per completare tutta la famiglia, come non ringraziare i miei nonni, sempre stati in prima linea, tra un "Bravo", un "Come sono i Torinesi" ed un "Non rifiutare mai nessun voto".

Per concludere, sperando che nessuno si sia annoiato, devo ringraziare tutti i miei amici, quelli nuovi e quelli vecchi, che tra birre, mojito fatti in casa, arancini e pizze hanno reso tutto più leggero.

Amici siciliani, i Davide, Luca, Marco, Carla, Sofia, Sonia e Vittoria, vi voglio bene.

Grazie Thomas che in questi anni sei stato un coinquilino e un fratello.

Grazie Matteo per essere stato sin da subito un amico di università ma anche di vita, che più volte mi hai fatto sentire a casa con la tua disponibilità e nella tua famiglia, sono contentissimo che oggi festeggiamo insieme.

Un grazie speciale va anche a chi in questi tre mesi mi ha ricordato che ovunque vai, anche in mezzo al deserto dell'Arizona puoi sempre trovare delle bellissime persone, quindi grazie a voi Sara, Jhonny, Raquel, Filippo e ai miei affettuosi coinquilini.

Un ringraziamento speciale infine va a Francesca, come da tuo suggerimento mi rifaccio a quanto detto per la tua laurea; in questi due anni sei stata prima di tutto un'amica, oltre che una fidanzata, una guida che mi ha spinto ad andare avanti e sono onorato di aver condiviso questo percorso con te.

Detto questo, carusi, da domani chiamatemi Ingegnere, un bacio a tutti.